

Durham E-Theses

Boundary related enhancements in spatial firing of grid cells

CLAUSEN-DITCH, SALLY,MAE

How to cite:

CLAUSEN-DITCH, SALLY,MAE (2019) *Boundary related enhancements in spatial firing of grid cells*, Durham theses, Durham University. Available at Durham E-Theses Online:
<http://etheses.dur.ac.uk/13780/>

Use policy

The full-text may be used and/or reproduced, and given to third parties in any format or medium, without prior permission or charge, for personal research or study, educational, or not-for-profit purposes provided that:

- a full bibliographic reference is made to the original source
- a [link](#) is made to the metadata record in Durham E-Theses
- the full-text is not changed in any way

The full-text must not be sold in any format or medium without the formal permission of the copyright holders.

Please consult the [full Durham E-Theses policy](#) for further details.

Boundary related enhancements in spatial firing of grid cells

Sally Mae Clausen-Ditch

Submitted in accordance with the requirements for the degree of
Doctor of Philosophy

Durham University
Department of Psychology

June 2019

Declaration

I, Sally Mae Clausen-Ditch, confirm that the work presented in this thesis is my own.

Where information has been derived from other sources, I confirm that this has been indicated in this thesis.

Acknowledgments

First and foremost, I would like to give a huge thank you to my husband, Antony, for being a rock and for being understanding when I had to repeatedly cancel plans. I think he may have been looking forward to my submission deadline more than I was.

To my supervisor, Colin Lever, thank you for agreeing to supervise my PhD and for supporting and inspiring my research. I would also like to thank everyone in the Lever lab for being supportive and taking the time to show me, someone who did not have a background in behavioural neuroscience, the electrophys ropes.

Lastly, I would like to acknowledge everyone in the psychology department for being so supportive and understanding while I carried on working 6 weeks after giving birth to my daughter.

Abstract

It has been established that environmental boundaries influence the firing of grid cells. However, whether they can enhance grid cell firing, and how this might occur, is not known. One possibility is that they reduce environmental uncertainty. The aim of Experiment 1 was to investigate how a wall versus a drop-edge might enhance grid cell firing at distal locations. The results showed that the 4th wall increased gridness, not just at locations proximal to the manipulated boundary, but at locations distal to the manipulated boundary. Additionally, the 4th wall, which was initially novel, increased gridness relative to the drop-edge, which was highly familiar. This is in contrast to previous research that has shown that novelty causes gridness to decrease (Barry et al., 2012). This suggests that walls provide more certainty about the environment compared to drop-edges, and this immediately counteracts the relatively subtle environmental novelty. In Experiment 2, the key hypothesis was that a barrier inserted into the environment would reduce spatial uncertainty, and that, according to Towse et al. (2014), this would reduce spatial scale. The results confirmed this hypothesis. They also demonstrated that the same manipulation can bidirectionally modify grid scale: the presence of the barrier caused grid scale to initially expand, becoming larger than grid scale recorded on the baseline day (no barrier present) occurring immediately before the first manipulation day, then contract, becoming smaller than grid scale recorded on the baseline day immediately following the last manipulation day. Considering these findings together, this thesis presents novel research showing that boundaries can have an enhancing effect upon established grid patterns. It also, at least partially, teased apart the two factors of boundariness and familiarity, and shows that enhancement effects were not simply driven by familiarity.

Table of Contents

Acknowledgments.....	ii
Abstract.....	iii
Table of contents.....	iv
List of figures.....	x
List of tables.....	xiii

Figure 1.1.....	x
Figure 1.2.....	x
Figure 1.3.....	x
Figure 2.1.....	x
Figure 2.2.....	x
Figure 2.4 Firing fields of subicular BVCs in different environments.....	x
Figure 2.5 BVCs produce additional firing fields along additional boundaries.....	x
Figure 2.6.....	x
Figure 2.8.....	x
Figure 2.9.....	x
Figure 3.1.....	x
Figure 3.2.....	x
Figure 3.3.....	x
Figure 3.4.....	x
Figure 3.5.....	x
Figure 3.7.....	xi
Figure 3.8.....	xi
Figure 3.9.....	xi
Figure 3.10.....	xi
Figure 4.1.....	xi
Figure 4.3 An increase in gridness does not occur on middle trials BCDE vs early/late trials AF on BaselinePOST when the drop-edge is present during all 6 trials.....	xi
Figure 4.4 Gridness is higher in the stable half of the arena.	xi
Figure 4.5 The 4 th wall increased gridness across the whole arena.	xi
Figure 4.6 Gridness is higher in the stable half of the arena compared to the manipulated half during both DROP-EDGE trials (AF) and WALL-ATTACHED trials (BCDE) on manipulation days 1-8.	xi
Figure 4.8 Grid scale was larger in the manipulated half of the arena.....	xi

Figure 4.9 Grid scale is smaller in the stable half of the arena during the DROP-EDGE trials, but not during the WALL-ATTACHED trials.	xi
Figure 5.2 The gridness reducing effect of the barrier is time-limited.....	xi
Figure 5.3 Gridness.....	xi
Figure 5.5.....	xi
Figure 5.6.....	xi
Figure 5.7.....	xii
Figure 5.8 Grid scale decreased when the barrier was present.	xii
Figure 5.9 The.....	xii
Figure 5.10.....	xii
Figure 5.11.....	xii
Figure 5.12 Grid scale expands when first introduced to the barrier.....	xii
Figure 5.13 The.....	xii
1 Chapter 1 Introduction part 1: Anatomy of the hippocampal formation	4
1.1 Nomenclature.....	4
1.2 Gross Morphology	5
1.3 Organization of the hippocampal formation and the parahippocampal region	6
1.4 Cytoarchitectonic organisation	8
1.4.1 Laminar organization of the CA fields.....	8
1.4.2 Laminar organization of the Dentate Gyrus (DG)	9
1.4.3 Laminar organization of the Subiculum	10
1.4.4 Laminar organization of the Entorhinal cortex (EC)	10
1.4.5 Laminar organization of the pre- and parasubiculum	11
1.5 General connectivity	12
1.5.1 Intrinsic connectivity of the hippocampal formation	12
1.5.2 Parahippocampal afferents to the hippocampal formation	13
1.5.3 Subcortical afferents to the hippocampal formation	14
1.5.4 Efferents from the hippocampal formation.....	17
1.6 The subiculum	17
1.6.1 Intrinsic connections	17
1.6.2 Intrahippocampal connections	17
1.6.3 Neocortical connections	19
1.6.4 Connections to other regions.....	19
1.7 The entorhinal cortex	19
1.7.1 Intrinsic connections	20

1.7.2	Commissural connections	20
1.7.3	Intrahippocampal connections	20
1.7.4	Subcortical connections	21
1.7.5	Neocortical connections	22
1.8	The presubiculum and parasubiculum	23
1.8.1	Intrinsic pre- and parasubicular connections	23
1.8.2	Commissural connections	23
1.8.3	Intrahippocampal connections	24
1.8.4	Subcortical inputs	25
1.8.5	Neocortical connections	26
1.8.6	Other connections.....	27
2	Chapter 2 Introduction part 2: Spatial Cells.....	28
2.1	Brief Overview: spatial information	28
2.2	Head-direction cells.....	30
2.2.1	Anatomical locations of Head-direction cells	30
2.2.2	Manipulating Head-direction cells with allothetic and idiothetic cues	32
2.2.3	Head direction input is crucial for other spatial cells	34
2.3	Place cells	35
2.3.1	Allocentric & idiothetic input.....	35
2.3.2	Size and Shape.....	36
2.3.3	Remapping	36
2.3.4	The influence of boundaries on place cells.....	37
2.4	Boundary cells	40
2.4.1	Boundary vector cells.....	40
2.4.2	BVC characteristics.....	41
2.4.3	BVCs respond to various boundary types	44
2.4.4	Border cells.....	45
2.5	Grid cells	46
2.5.1	Grid cell properties.....	46
2.5.2	Grid cells in novel environments.....	50
2.5.3	Grid scale expansion: a response to spatial uncertainty	52
2.5.4	Grid patterns and cue integration.....	54
2.5.5	Grids and boundary geometry	55
2.5.6	Grids as a spatial metric	60

2.5.7	Anatomical locations of grid cells	61
2.5.8	Grid cells as place cell input	62
2.6	Speed cells	63
2.7	Aims of this thesis.....	64
3	Chapter 3 Methods	67
3.1	Ethics	67
3.2	Subjects	67
3.3	Recording apparatus	67
3.3.1	Electrodes.....	67
3.3.2	Microdrives	68
3.4	Surgery.....	69
3.5	Data recording.....	72
3.5.1	Head position and orientation and running speed.....	72
3.5.2	Single-unit recording.....	72
3.6	Materials.....	73
3.6.1	Laboratory layout.....	73
3.6.2	Test environment and materials.....	74
3.7	Experimental procedure.....	78
3.7.1	Screening and training	78
3.7.2	General procedure	79
3.7.3	Task	80
3.8	Experiments.....	80
3.8.1	Experiment 1	80
3.8.2	Experiment 2	81
3.9	Data Processing	84
3.9.1	Cluster-cutting.....	84
3.9.2	Recording stability.....	85
3.10	Data Analysis	86
3.10.1	Waveform analysis	86
3.10.2	Figures of spatial firing.....	87
3.11	Grid cell analysis	88
3.11.1	Spatial autocorrelogram	88
3.12	The number of grid cells recorded	91
4	Experiment 1: Grid cell responses to a drop-edge and wall attachment	92

4.1	Gridness analysis	92
4.1.1	Gridness increases when the 4th wall is attached.....	92
4.1.2	Split arena analysis: Gridness.....	97
4.1.2.1	The 4 th wall increases gridness not only in the manipulated (proximal) half, but also in the stable (distal) half.....	98
4.1.2.2	Stable half vs manipulated half: Gridness.....	100
4.1.2.3	Non-bistable interference effects gridness.....	102
4.1.3	Gridness increases with familiarization	103
4.2	Grid scale	105
4.2.1	Split arena analysis: Manipulated half vs Stable half: Grid scale.....	105
4.2.1.1	Grid scale between arena-halves becomes similar when the 4 th wall is present.....	106
4.2.1.2	Grid scale between arena-halves becomes similar with increased familiarization	107
4.2.2	Initial exposure to the 4 th wall, despite its relative novelty, did not cause grid scale to expand	108
4.3	Firing rates	109
4.3.1	Mean rate.....	109
4.3.2	Peak rate	110
4.4	Experiment 1 specific Discussion.....	113
4.4.1	Boundaries confer enhancements in spatial firing of grid cells both distally and proximally	113
4.4.2	Grid cell function: extending boundary-based spatial certainty into open space.....	117
4.4.3	Grid scale – lack of expansion	121
5	Experiment 2: Grid cell responses to an inserted barrier, which partially divided the environment.....	123
5.1	Gridness.....	124
5.1.1	The presence of the inserted barrier initially reduced gridness in the Early days, but in the Late days, gridness was similar across both environmental configurations	125
5.1.2	Gridness increased with increasing familiarization	130
5.1.3	Gridness increased in the BARRIER-IN condition with increasing familiarization	131
5.1.4	Gridness increases to baseline levels following barrier induced reduction.....	132
5.2	Grid scale	134

5.2.1	As hypothesized, the barrier reduced grid scale	134
5.2.2	The barrier interacted with familiarization to further reduce the grid scale 135	
5.2.3	First exposure to barrier insertion caused grid scale to expand	138
5.2.4	The barrier, not just familiarity/repetition causes a reduction in grid scale 140	
5.3	Firing rates.....	142
5.3.1	Mean Rate	142
5.3.2	Peak Rate.....	143
5.4	Experiment 2 specific discussion	145
5.4.1	Summary of Results of Experiment 2.....	145
5.4.2	Models of spatial uncertainty and grid scale: grid scale is adaptive	146
5.4.3	Previous literature regarding grid scale and uncertainty	148
5.4.4	Grid scale can be bidirectionally modified by the same manipulation ..	149
5.4.5	Gridness returns to baseline levels following an initial novelty induced reduction	151
5.4.6	Peak rates might be linked to grid plasticity.....	152
5.4.7	Conclusion	152
6	General discussion	153
6.1	Results overview.....	153
6.2	Similarities and differences in Experiments 1 & 2; how boundary cues enhance spatiality in the grid signal	154
6.3	Relationship with previous work: manipulating spatial uncertainty in Experiments 1 and 2.....	155
6.4	Relationship with previous work: how boundary cues enhance grid spatiality in distal space in Experiment 1	157
6.5	Interference.....	158
6.6	Limitations	160

List of figures

Figure 1.1 An illustration of the position of the rodent hippocampal formation from a lateral viewpoint	5
Figure 1.2 A horizontal section through the rodent hippocampal formation and parahippocampal region	7
Figure 1.3 The 20 Hippocampal Gene Expression Atlas (HGEA) subregions of the hippocampal and subicular long axis	8
Figure 1.4 A diagram of the internal connections of the hippocampal-parahippocampal regions along with cortical input and output to and from these regions	14
Figure 2.1 The five types of fundamental of spatial cells	29
Figure 2.2 Place fields respond different to boundary insertion	39
Figure 2.3 A BVC fires maximally when a boundary is located at the cell's preferred distance and allocentric direction from the rat.	41
Figure 2.4 Firing fields of subicular BVCs in different environments.....	43
Figure 2.5 BVCs produce additional firing fields along additional boundaries.....	44
Figure 2.6 Grid scale increases along the dorsoventral axis	48
Figure 2.7 Spatial autocorrelation is used to determine the parameters of the grid pattern.....	50
Figure 2.8 Grid cell firing patterns transition from local to global representation with increasing experience.	57
Figure 2.9 Grid patterns are not always homogenous	59
Figure 3.1 Illustration of microdrive frame.....	69
Figure 3.2 An Illustration of the testing arena; a square, walled open field	73
Figure 3.3 Bird's eye view of laboratory	74
Figure 3.4 "To-scale" drawing of Environmental configurations during baseline trials (A) and manipulation trials (B) of Expt 1 to show box-to-walls ratio more accurately.....	76
Figure 3.5 "To-scale" drawing of Environmental configurations during baseline trials (A) and manipulation trials (B) of Expt 2 to show box-to-walls ratio more accurately.....	77
Figure 3.6 Illustration of environmental manipulations.	83

Figure 3.7 Examples of cell clusters and waveforms in Tint	85
Figure 3.8 Waveform illustration	87
Figure 3.9 Example rate map of a grid cell.....	88
Figure 3.10 Spatial autocorrelation is used to determine the gridness score and grid scale of the grid pattern.....	90
Figure 4.1 Gridness increases when the 4 th wall is attached and can be seen during early as well as later exposure	94
Figure 4.2 Gridness increases when the 4 th wall is attached.....	95
Figure 4.3 An increase in gridness does not occur on middle trials BCDE vs early/late trials AF on BaselinePOST when the drop-edge is present during all 6 trials.....	97
Figure 4.4 Gridness is higher in the stable half of the arena.	98
Figure 4.5 The 4 th wall increased gridness across the whole arena.	99
Figure 4.6 Gridness is higher in the stable half of the arena compared to the manipulated half during both DROP-EDGE trials (AF) and WALL-ATTACHED trials (BCDE) on manipulation days 1-8.	101
Figure 4.7 Gridness increases with increasing familiarization.....	104
Figure 4.8 Grid scale was larger in the manipulated half of the arena.....	105
Figure 4.9 Grid scale is smaller in the stable half of the arena during the DROP-EDGE trials, but not during the WALL-ATTACHED trials.	107
Figure 4.10 Grid scale is significantly smaller in the stable half of the arena during the EARLY time-block, but not during the LATE time-block.....	108
Figure 5.1 Gridness decreases when the barrier is present.	126
Figure 5.2 The gridness reducing effect of the barrier is time-limited.....	127
Figure 5.3 Gridness was significantly reduced in the barrier-in condition during early manipulation days (days 1-4) when the barrier was present, but not during late manipulation days (days 5-8).....	128
Figure 5.4 Gridness on trials AF and trials BCDE are not significantly different when the barrier is absent across all six trials... ..	130
Figure 5.5 Gridness is higher in the late manipulation days (days 5-8) compared to the early manipulation days (days 1-4).....	131
Figure 5.6 Gridness in the BARRIER-IN condition increases with familiarization	132

Figure 5.7 Gridness to baseline levels as the barrier becomes more familiar.....	133
Figure 5.8 Grid scale decreased when the barrier was present.	135
Figure 5.9 The barrier caused a reduction in grid scale during the late time-block, not the early time-block.	136
Figure 5.10 Grid scale becomes smaller when the barrier is present	137
Figure 5.11 Grid scale does not decrease during trials BCDE when the barrier is absent in baseline trials before (A) and after (B) the manipulation period (days 1-8).	138
Figure 5.12 Grid scale expands when first introduced to the barrier.....	138
Figure 5.13 The presence of the barrier, not just familiarisation, causes grid scale to decrease.	141

List of tables

Table 3.1 Target implant co-ordinates for each rat	71
Table 3.2 Each rat's experience of the wall-off wall-on manipulation	81
Table 3.3 Each rat's experience of the barrier-in barrier-out manipulation	82
Table 3.4 Grid cell numbers in each experiment	91
Table 4.1 There were no significant main effects of wall-state or time-block on mean rate	110
Table 4.2 There were no significant main effects of wall-state or time-block on peak rate	111
Table 4.3 There was a significant interaction between wall-state and time-block.....	112
Table 5.1 There were no significant main effects of barrier-state or time-block during manipulation days (days 1-8).....	142
Table 5.2 Barrier-state, but not time-block, had a significant main effect on peak rate	143

Introduction

The ability to navigate through an environment is essential for the survival of freely-moving animals (finding food and shelter and evading predators). There are two sets of cues that animals use to perform this process: allothetic cues and idiothetic cues. Allothetic cues exist outside the animal's body (external landmarks) and are processed by the sensory systems (visual, somatosensory, olfactory) (Wiebe et al., 1997; Wills et al., 2005). Idiothetic cues are generated internally and depend on a set of senses that perceive the body's movements (vestibular, proprioceptive, motor efference copy etc) (McNaughton et al, 2006a). The ability to integrate these two cue types results in optimal navigation. The problems that can arise when relying on one cue type or the other is discussed below.

When a rodent is introduced to a new environment they form a 'home-base.' This is a highly visited location to which they repeatedly return throughout the exploration period, and in which the rodent executes various investigatory activities (head scans and rearing), presumably to provide allothetic spatial information. The rodent leaves the home base in a somewhat meandering pattern but returns fairly directly. This is likely accomplished using path integration— the ability to keep track of the distance and direction travelled by integrating idiothetic cues (McNaughton et al, 2006a). The problem with relying on idiothetic cues alone is that they accumulate error over time, resulting in poor estimates about the animal's location (McNaughton et al., 1996; 2006a; Burak and Fiete, 2009). Allocentric cues help correct this by resetting the animal's position estimate. It is also possible to navigate using only allocentric cues, but as with the sole use of idiothetic cues, it comes with a problem: allocentric cues are not always available (e.g. darkness) or stable (e.g. changes to the environment).

Idiothetic cues can help fill in this gap by allowing an animal to keep track of their location within the environment using senses that perceive the bodies movements. Though, this only works for a period of time. As mentioned above, idiothetic cues accumulate error over time. However, they could help long enough for an animal to reach a familiar landmark, which then corrects any error in the estimated position.

What mechanisms underlie this behaviour? It is a question that scientists were not able to address until the development of in vivo electrophysiology. Since then, scientists have discovered a network of cells within the hippocampal formation that code for different types of spatial information within the environment.

One such cell is the grid cell, which makes use of both allothetic (Hafting et al, 2005; Krupic et al, 2015) and idiothetic cues (Hardcastle et al, 2015; Winter et al, 2015; Chen et al, 2016) and is believed to perform path integration (Hafting et al, 2005; Gil et al, 2018). These cells are able to function using primarily idiothetic cues, however they accumulate error over time and require allothetic cues to correct this error (Hardcastle et al, 2015; Cheng et al, 2016). One example of this comes from Hardcastle et al. (2015) who observed that grid cells accumulate error relative to time and distance traveled since the animal last had contact with a wall-boundary (a prominent allothetic cue). This caused grid patterns to become distorted— grid scale increases and gridness decreases. When the animal reencountered a wall-boundary, the distortion in the grid pattern was corrected. This suggests that boundaries act as an error correction mechanism for grid cells.

It has been established that environmental boundaries influence the firing of grid cells. However, whether they can enhance grid cell firing, and how this might occur, is not known. One possibility is that they reduce environmental uncertainty. A

computational study by Towse et al (2014) demonstrated that an increase in grid scale may be the optimal response to spatial uncertainty, resulting from a trade-off between maximizing precision of location within an environment (requiring small scales) and minimizing uncertainty of location within an environment (requiring large scales). To my knowledge, there is relatively little work speaking directly to the relationship between grid scale and uncertainty, and all such work uses environmental novelty to elicit uncertainty (Barry 2007; 2012).

Much of the work previously conducted on environmental boundaries and grids cells has focused on the global or proximal effects (e.g. distortion or recalibration) boundaries have upon grid cells (Carpenter et al, 2015; Hardcastle et al, 2015; Krupic et al, 2015; Stensola et al, 2015). To my knowledge, previous work has not specifically addressed the question of how boundaries in given locations effect the spatial firing of grid cells in distal locations or if they can have enhancing effects on grid cells.

The general aim of this thesis was to investigate the enhancing effects that environmental boundaries have on grid cells. More specifically, in Experiment 1, I tested the hypothesis that due to lower uncertainty of spatial localization associated with a vertical wall (vs a drop-edge), gridness would be higher when the wall was attached compared to when it was not attached, and that gridness-enhancing effects might also apply to distal space, not just that space immediately adjacent to the boundary in question.

In Experiment 2, the key hypothesis was that a barrier within the environment would reduce spatial uncertainty, and that this would reduce grid scale. Spatial uncertainty would be reduced because of the addition of an extra space-defining cue,

(both visual and somatosensory) to guide distance judgements.

Before diving into the methodology and results of these experiments, the two following introductory chapters offer an overview of the relevant literature.

1 Chapter 1 Introduction part 1: Anatomy of the hippocampal formation

1.1 Nomenclature

This thesis adopts the nomenclature whereby the *hippocampus* includes the cornu ammonis (CA) fields (CA1, CA2 & CA3) and the dentate gyrus (DG). The *hippocampal formation* includes the hippocampus and the subiculum. The *parahippocampal region* includes the entorhinal cortex and the pre- and parasubiculum (Scharfman et al., 2000).

The above definitions are based on connectivity and laminar organisation. The hippocampal formation is distinctive in having a trilaminar (three-layered) organization, which defines the allocortex. The parahippocampal region has a multilaminar (six-layered) organization similar to the neocortex. This region can therefore be viewed as the transition from allocortex to neocortex (Amaral & Lavenex, 2007). Another difference between the hippocampal formation and the parahippocampal region can be found in their connectivity. Hippocampal connectivity is largely unidirectional, whereas the parahippocampal region has at least two sets of reciprocal connections; one between peri- and postrhinal cortices and the entorhinal cortex, and the other between the pre- and parasubiculum and entorhinal cortex.

1.2 Gross Morphology

Figure 1.1 illustrates the position of the hippocampal formation (the 'C' shaped structure) within the rat brain. The long axis (often referred to as the dorso-ventral axis) of the hippocampal formation is oriented septal-to-temporal (posterior-to-anterior in primates) (Strange et al., 2014). It stretches from the midline of the brain near the septal nuclei over and behind the thalamus into the temporal lobe. Orthogonal to this is the transverse axis running mediolaterally. The proximo-distal axis is used to differentiate between opposite ends of each anatomical region of the hippocampus on a plane perpendicular to the long axis. It follows the S-like curvature seen within the hippocampal formation with the proximal end lying closer to the dentate gyrus (Figure 1.2). These axes are important landmarks in the structural connectivity of the hippocampal formation.

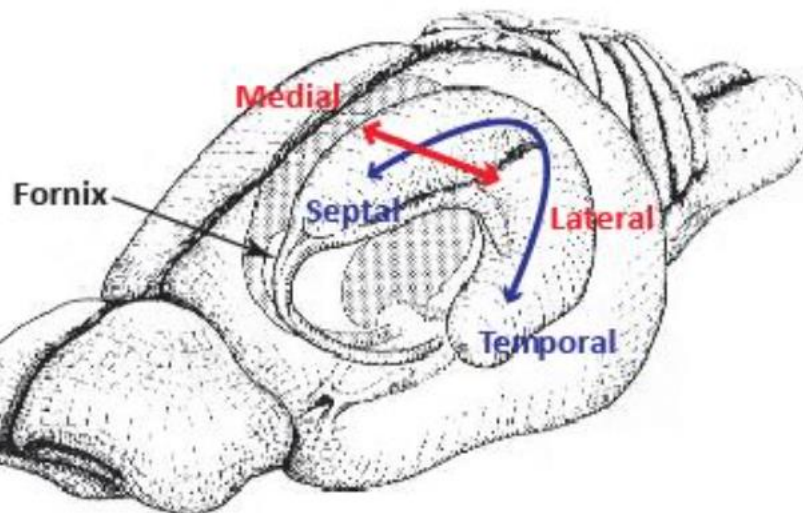


Figure 1.1 An illustration of the position of the rodent hippocampal formation from a lateral viewpoint.

The septo-temporal axis (blue line) runs from the septal pole to the temporal pole. The transverse axis (red line) runs medial to lateral. Drawing adapted from Amaral and Witter (1995).

1.3 Organization of the hippocampal formation and the parahippocampal region

Figure 1.2 shows a horizontal section of the hippocampal formation and parahippocampal region. It illustrates the trilaminar organization of the hippocampal formation and where new layers emerge at the subiculum-presubiculum border. The darkly stained areas highlight two c-shaped structures that appear to interlock. These represent the granule layer of the DG and the pyramidal layers of CA1-3. Below this is a relatively cell-free layer known as the stratum oriens. The widening at the end of CA1 becomes the subiculum. To the left of the subiculum are the pre- and parasubiculum. The border between the subiculum and presubiculum is characterized by the emergence of a more superficially positioned cortical sheet, consisting of the superficial layers of the pre- and parasubiculum. These layers are separated from the deep layers by a cell-free zone called the lamina dissecans where layer IV would be. The sudden increase in layers signals the border between the hippocampal formation and the parahippocampal region. The lamina dissecans disappears at the border between the entorhinal and perirhinal or postrhinal/parahippocampal cortices, giving way to a more homogeneously layered cortex resembling the six-layered neocortex. The 5-layered peri and postrhinal cortices, which lack the granule cell layer IV, being the exception.

subnetworks (i.e. Spatial/cognitive, Social, and Homeostasis, metabolism and sexual behaviour), which are part of the larger dorsal and ventral networks. This finding also supports the idea that the long axis is the most important anatomical axis of the hippocampal formation.

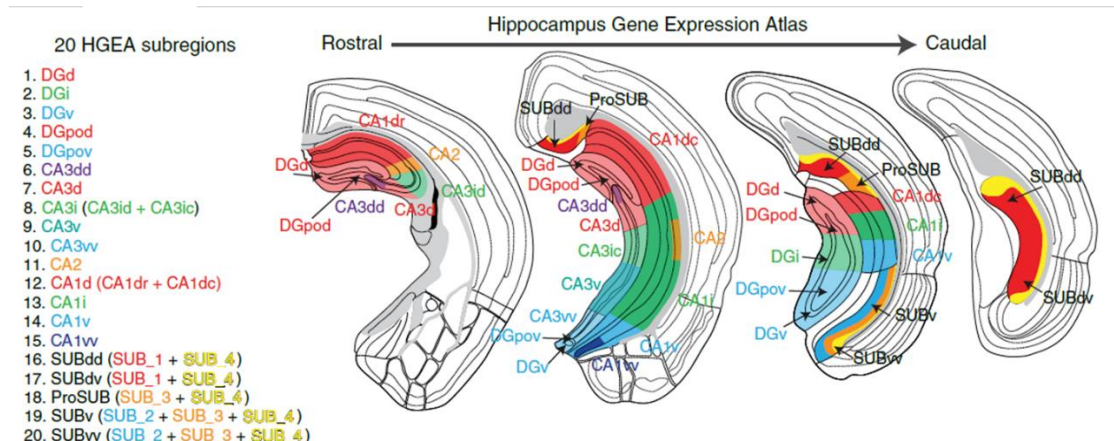


Figure 1.3 The 20 Hippocampal Gene Expression Atlas (HGEA) subregions of the hippocampal and subicular long axis.

The HGEA subregions were defined and mapped by the consensus of multiple gene expression patterns at all rostrocaudal levels of the hippocampus. To the left is a list of the 20 subregions and to the right are four representative levels of the hippocampus. Adapted from Bienkowski et al. (2018).

1.4 Cytoarchitectonic organisation

1.4.1 Laminar organization of the CA fields

The principal cellular layer of the CA fields is the pyramidal cell layer. This is densely packed in CA1-3, but more so in CA1. Beneath this is a narrow relatively cell-free layer called the *stratum oriens*, which contains the basal dendrites of the pyramidal cells along with some interneurons. It is also the region where some of the CA3 autoassociational connections and CA3 to CA1 Schaffer collateral connections are located. The narrow acellular zone located just above the pyramidal layer in the CA3 field is called the *stratum lucidum*. This is where mossy fibres originating from DG

terminate. The *stratum radiatum* is located above the *stratum lucidum* in CA3 and immediately above the pyramidal cell layer in CA1 and CA2. This is where some of the CA3 autoassociational connections and CA1 to CA3 Schaffer collateral connections are situated along with some interneurons. The last layer is called the *stratum lacunosum-moleculare* and is located deep to the *stratum radiatum*. This is where the perforant pathway fibres from neurons of the superficial layers of the entorhinal cortex terminate. More specifically, they terminate on the distal apical dendrites of CA1 pyramidal cells (the distal dendrites project into the *stratum lacunosum-moleculare*). Afferent projections from other regions including thalamic regions, such as the reuniens nucleus also terminate in the *stratum lacunosum-moleculare*. This layer also contains interneurons (Amaral & Lavenex, 2007).

1.4.2 Laminar organization of the Dentate Gyrus (DG)

The dentate gyrus (DG) comprises three layers. The principal cellular layer is the *stratum granulosum*, which is densely-packed, similar to the CA principal cellular layers. Granule cells are the principal type of dentate cells and are the only ones to project outside of the DG where they synapse with the CA3 dendrites in the *stratum lucidum*. The *stratum moleculare* is located above the *stratum granulosum* and is closest to the hippocampal fissure. This is where the granule cell dendrites are located. Granule cells are unipolar, so there are no granule cell dendrites on the other side of the granule layer. The dense projection to the DG from entorhinal cortex targets the granule cell dendrites in the molecular layer. The *hilus* (often referred to as the polymorphic cell layer of the DG) is the third layer. It contains several types of neuron including the mossy cells that project back to the granule cells. (Amaral & Lavenex, 2007).

1.4.3 Laminar organization of the Subiculum

The subiculum is comprised of 3 distinguishable layers, similar to the CA fields. The border between CA1 and the subiculum can be identified by the widening of the pyramidal cell layer. The principal cell layer of the subiculum is called the *pyramidale* and it encloses the pyramidal cells' somas. This layer is less densely packed than the CA1 pyramidal layer. The apical dendrites of these cells extend into the molecular layer located above with some reaching the hippocampus fissure (Harris et al., 2001). This is continuous with the CA1 *stratum lacunosum-moleculare* and *stratum radiatum* layers. The superficial portion of the molecular layer receives entorhinal projections while the deep portion of the molecular layer is innervated by the CA1. The third layer, known as *oriens*, is polymorphic and contains the basal dendrites (Amaral & Lavenex, 2007).

1.4.4 Laminar organization of the Entorhinal cortex (EC)

The EC contains 6 layers. These are often grouped into 2 categories: the superficial layers (I-III) and the deep layers (IV-VI). The EC superficial layers contain stellate cells (layer II) and pyramidal cells (layers II and III). The neurons from layer II project to the DG and CA3, while neurons from layer III project to CA1 and the subiculum. CA1 and the subiculum then project back to the EC, targeting its deep layers (Amaral & Lavenex, 2007).

Grid cells and border cells have been found co-mingling in all layers of the medial entorhinal cortex (MEC). However, grid cells are most abundant in layer II- making up about 50% of the layer II cell population (Boccarda et al., 2010; Fyhn et al., 2004; Sargolini et al., 2006). The grid cells in this layer are mainly pyramidal cells, while the co-mingling border cells are mainly stellate cells (Tang et al., 2014).

1.4.5 Laminar organization of the pre- and parasubiculum

The dorsal presubiculum has clearly distinguishable superficial and deep layers. Cells that are located in the more superficial layers are densely packed compared to those in the deeper layers. However, in the more ventral portion they are not as clearly distinguishable from the deep EC layers or the principle layer of the subiculum. The parasubiculum lies adjacent to the presubiculum. Layers II and III contains densely packed large pyramidal cells, which is one of the major features used to distinguish the pre- and parasubiculum. As with the presubiculum, the deeper layers are continuous with the EC (Amaral & Lavenex, 2007).

In addition to the MEC, grid cells can also be found in the presubiculum (12.8% of the cell sample) and the parasubiculum (20.3% of the cell sample) and are present in all anatomical layers (Boccaro et al., 2010). The distribution of grid cells is uniform across all layers of these two areas, which is in contrast to the grid population of the MEC where most of the grid cells are located in the superficial layers. It has been proposed that layer II of the presubiculum is the principal source of grid activity and that entorhinal grid activity may be inherited from the presubiculum, whose superficial layers have unidirectional projections to the MEC (Preston-Ferrer et al., 2016; Peng et al., 2017). This is supported by Tocker et al. (2015) who suggested that grid fields in the superficial layers of the MEC require organised feedforward projections. Border cells have also been found alongside grid cells in the presubiculum (9%) and parasubiculum (5.3%) (Boccaro et al., 2010).

1.5 General connectivity

1.5.1 Intrinsic connectivity of the hippocampal formation

Intrahippocampal circuitry is largely unidirectional. This is in contrast to the neocortex, which has strong reciprocal innervations between the neocortical regions (Felleman & Van Essen, 1991). A traditional view of hippocampal information flow emphasizes the 'trisynaptic pathway' (Anderson et al., 1971). The first part of the pathway is formed by a large bundle of axons leaving layers II and III of the EC which then contacts granular cells of the DG. This bundle of axons is termed the perforant path and is a major source of input to the hippocampus. From here the granule cells of the DG form the mossy fibres which project to CA3, terminating just above the CA3 pyramidal layer. Next, the Schaffer collateral projections from CA3 reach the pyramidal cells of CA1. Within this part of the circuit there's an inverse gradient between the proximal-distal axis of the CA3-to-CA1 connections: the distal portion of CA3 neurons target the proximal portion of CA1 neurons and vice versa (Ishizuka et al., 1990; Laurberg, 1979; Laurberg and Sørensen, 1981). The CA1 then projects to the deep layers of the EC closing the loop between EC and the hippocampal formation. Sometimes referred to as the 'fourth' connection, some CA1 axons reach the principal layers of the subiculum (Amaral & Lavenex, 2007).

This traditional view, in which the flow of information within the hippocampal formation travels unidirectionally, falls short of capturing the complexity of the whole circuit. In recent years back-projection and local collateral circuits have been found at all levels of the pathway. Several important revisions include but are not limited to: a) direct projections from Entorhinal cortex to CA3, CA1, and subiculum; b) 'reverse

pathways' e.g. subiculum to CA1; c) the importance of long-axis projections within CA1 (Jackson et al., 2014; Sun et al., 2014; Sun et al., 2018).

1.5.2 Parahippocampal afferents to the hippocampal formation

A major source of neocortical input to the hippocampus comes from layers II and III of the EC through the perforant pathway. A great deal of the entorhinal input originates in the postrhinal and perirhinal cortices, though these all project to the hippocampus (Figure 1.4). The perforant pathways from the EC to the hippocampus can be subdivided into two streams: one originating from layer II and one originating from layer III.

The projections that originate in layer II of the EC project to the DG, CA3, and CA2. The projections to the DG primarily terminate on granule cell dendrites. Projections to CA3 and CA2 terminate in the *stratum lacunosum-moleculare*. The projections from layer III project to the subiculum (terminating in the molecular layer) and CA1 (terminating in the *stratum lacunosum-moleculare*). The EC input to CA1 varies depending on the EC region. The majority of projections from the lateral EC terminates in distal CA1 (near the subiculum) with a small portion terminating in proximal CA1. Whereas, the majority of projections from the medial EC terminates in proximal CA1 (near CA2) with a small portion terminating in distal CA1 (Knierim et al, 2014; Witter, 1993).

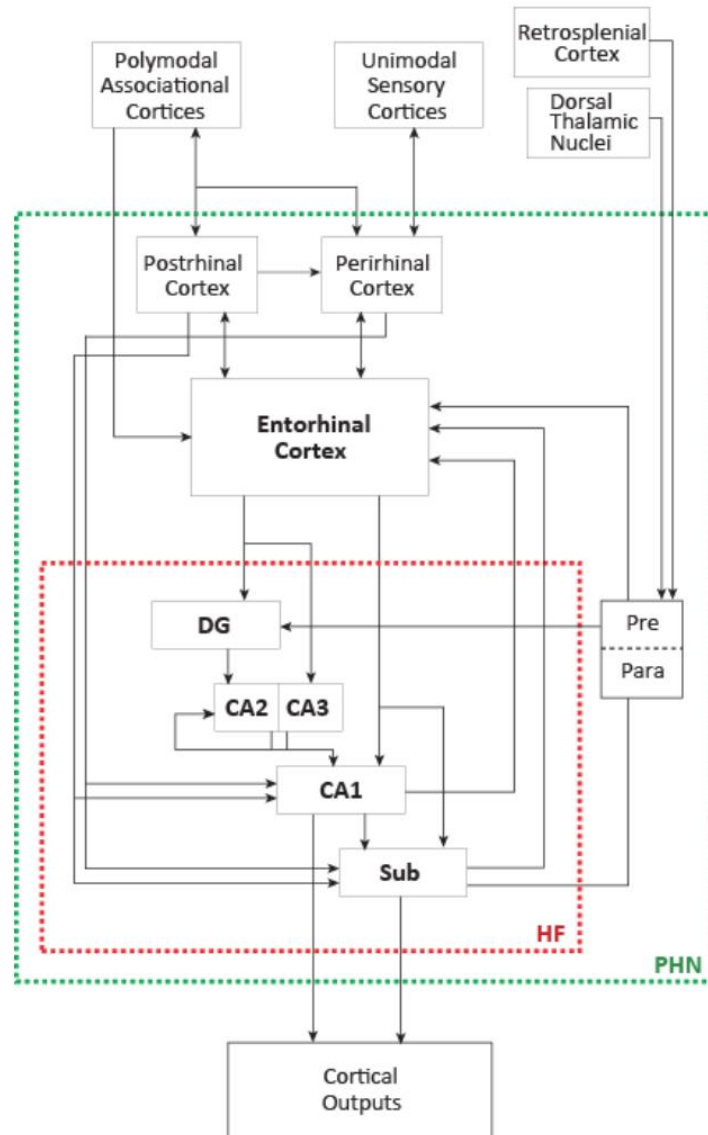


Figure 1.4 A diagram of the internal connections of the hippocampal-parahippocampal regions along with cortical input and output to and from these regions.

The red dashed box demarcates the hippocampal formation and the green box includes the parahippocampal network. Adapted from Wills (2005).

1.5.3 Subcortical afferents to the hippocampal formation

Major subcortical inputs to the hippocampal formation include the medial septum (MS), the supramammillary nucleus (SuM), the brain stem, the amygdala, and the thalamus.

The septum is part of the basal forebrain. Its projection to the hippocampus mainly originates in the medial septal nucleus and the associated region called the nucleus of the diagonal band of Broca (Amaral & Lavenex, 2007). Septal fibres terminate in all areas of the hippocampal formation. They are particularly prominent in the DG where cholinergic fibres from the MS innervate mossy cells. The MS is also a major source of subcortical input to CA3 (Amaral & Witter, 1995).

The SuM is part of the hypothalamus. It is composed of a population of large cells that partially surround the medial mammillary nuclei of the hypothalamus (Amaral & Lavenex, 2007). The projections from the SUM to the hippocampus terminate largely in the DG and CA2. The SUM projects weakly to CA1 and CA3 (Amaral & Lavenex, 2007).

The brain stem reticular formation consists of several structures: the rostral pontine region, pedunculo-pontine tegmental nucleus, and the raphe nuclei. The median raphe directly innervates GABAergic interneurons in the DG, CA1, and CA3, while the raphe nuclei are responsible for the serotonergic innervations of the brain (Freund et al., 1990). Monoaminergic input from the brain stem is primarily restricted to noradrenergic and serotonergic input. Noradrenergic input is quite dense to all regions of hippocampus and subiculum, while serotonergic input is most dense to the lateral EC, DG and layer 1 of the pre- and parasubiculum (Amaral & Witter, 1995).

Basolateral amygdalar input to the hippocampus is mostly restricted to CA1, its temporal third in particular (Amaral & Witter, 1995). In addition, CA1 directly receives a large input from the nucleus reuniens of the thalamus (Wouterlood et al., 1990),

which is largely directed at the *stratum lacunosum moleculare* and to the middle septo-temporal levels of CA1.

Several subcortical regions that project to the hippocampus have been found to control theta rhythm, which plays a prominent role in cognitive functions including spatial coding, time coding, exploratory locomotion, memory, and anxiety related behaviours (Korotkova et al, 2018). It has long been known that lesions to the MS impair hippocampal theta oscillations (Buzsaki et al., 1983; Rawlins et al., 1979). However, more recent studies have begun to reveal the roles that specific cell types within this brain region play in hippocampal theta rhythm (Boyce et al., 2016; Dannenberg et al., 2015; Mamad et al., 2015; Vandecasteele et al., 2014). For example, GABAergic cells in the MS play a key role in the generation and maintenance of hippocampal theta rhythm (Bender et al., 2015; Bland et al., 1999; Borhegyi et al., 2004; Hangya et al., 2009; Kocsis and Vertes, 1997; Wulff et al., 2009). The 'stress-reactive' nucleus incertus sends dense projections, not only to the MS and diagonal band of Broca, which project to the hippocampal formation, but also to the temporal regions of the hippocampus, which has been associated with anxiety (Bannerman et al., 2004; Goto et al., 2001; Ma and Gundlach, 2015). SuM cells exhibit theta-rhythmic activity and are phase-locked to hippocampal theta (Kirk and McNaughton, 1991; Kocsis and Vertes 1997). The median raphe nucleus, which projects strongly to the MS and hippocampus, promotes hippocampal non-theta (desynchronized) state (Graeff et al., 1980; McKenna and Vertes 2001). Lesions to this area induced hippocampal theta activity during immobility, suggesting an inhibitory influence of median raphe nucleus on hippocampal theta generation (Maru et al., 1979).

1.5.4 Efferents from the hippocampal formation

The CA1 and the subiculum both project to the deep layers of the EC (V and VI). They also give rise to a number of other efferents, to both cortical and subcortical regions (Amaral & Lavenex 2007). The CA1 and subiculum both project to the medial prefrontal cortex, retrosplenial cortex and perirhinal cortex. CA1 subcortical projections include the medial and lateral septum. Specifically, the ventral CA1 projects to areas including basal amygdala, olfactory bulb, anterior and dorsomedial hypothalamus. The subiculum is a major output region of the hippocampal formation, particularly to subcortical efferents including the lateral septum, nucleus accumbens, medial mammillary nuclei, and medial thalamic nuclei (Amaral & Lavenex 2007).

1.6 The subiculum

1.6.1 Intrinsic connections

A large number of associational connections exist within the subiculum, although they are mostly unidirectional (Harris et al., 2001). The projection extends from the cells of origin to much of the more temporal parts of the subiculum. These associational fibres terminate in all layers of the subiculum. Current evidence indicates that the intrinsic connectivity of the subiculum has a crude columnar and laminar organization: bursting cells form a set of columns and regular spiking neurons integrate the columnar activity along the transvers axis (Amaral & Lavenex, 2007).

1.6.2 Intrahippocampal connections

The subiculum sends projections to all layers of the EC, which terminate in the deep layers, particularly layer V (Amaral & Lavenex, 2007). Compared to its other intrahippocampal connections, the subiculum projects weakly to the presubiculum

(layer I and the dorsal deep layers) and parasubiculum (layer I and superficial layer II). These projections are organized topographically: dorsal parts of the subiculum project to dorsal and caudal parts of the pre- and parasubiculum, and ventral parts of the subiculum project to ventral and rostral parts of the pre- and parasubiculum (Witter et al., 2006). The EC reciprocates the subicular inputs via the perforant path, which originates in layer III (Amaral & Lavenex, 2007).

CA1 sends its primary projections to the subiculum. All CA1 regions project to and are received by all portions of the subiculum (Amaral et al., 2001; O'Mara et al., 2009): Distal CA1 projects to proximal subiculum, proximal CA1 projects to the distal subiculum, and the mid portion of the CA1 projects to the mid portion of the subiculum. Fibres beginning in proximal CA1 travel to the subiculum via the alveus and the deepest portion of the stratum oriens. Fibres originating in mid CA1 do not enter the alveus. Instead, they project to the subiculum through the deep parts of the stratum oriens. The axons of distal CA1 cells travel directly to the subiculum from all parts of the stratum oriens (Amaral et al., 2001; O'Mara et al., 2005; 2009).

It was previously thought that the subiculum did not project back to the CA1, however a recent study by Sun et al. (2018) has found evidence of a strong noncanonical back projection to the CA1. This projection has a weak-to-strong strength gradient along the proximal-distal axis of CA1. Distal CA1 receives about 4-fold more input from the subiculum compared with intermediate CA1 and proximal CA1. The connection strength of the subiculum's projections to distal CA1 is quantitatively comparable to those of the EC. Thus, the subiculum sends a major projection to CA1 in a highly topographic manner.

1.6.3 Neocortical connections

Neocortical regions targeted by the subiculum include the medial and ventral orbitofrontal cortex, the prelimbic and infralimbic cortices, the perirhinal cortex, and the retrosplenial cortex (Verwer et al., 1997; Wyss & Van Groen, 1992). There are also fewer substantial projections to the anterior cingulate cortex and the amygdaloid complex.

The perirhinal cortex and amygdaloid complex send projections back to the subiculum, terminating in the proximal 3rd near the CA1 border. Projection from the posterior cortical nucleus and the adjacent amygdalohippocampal area also terminate in the proximal 3rd of the subiculum (Pikaneen et al., 2000).

1.6.4 Connections to other regions

Subicular efferents extend to other areas of the brain including the septal complex, the nucleus accumbens, and the mammillary nuclei. The nucleus reuniens, nucleus interanteromedialis, paraventricular nucleus, and the nucleus gelatinosus of the thalamus also receive subicular input (Amaral & Lavenex, 2007).

Reciprocal projections are sent from the septal complex, mammillary nuclei, and thalamic regions. It also receives input from the locus coeruleus, the ventral tegmental area, and the medial and dorsal raphe nuclei of the brain stem (Amaral & Lavenex, 2007).

1.7 The entorhinal cortex

The EC is crucial to the functioning of the hippocampal formation. It acts as the gateway for much of the incoming sensory information processed by the hippocampal formation, and is also responsible for relaying the processed information back to the

neocortex. The EC can be subdivided into 2 sections that are cytoarchitecturally and functionally distinct: the lateral medial entorhinal cortex (LEC) and the medial entorhinal cortex (MEC). The lateral area layer II is more distinct than the medial layer II, with lateral layer II cells being smaller, more densely packed and clustered into islands (Amaral & Witter, 1995). The MEC contains a high proportion of spatial cells, whereas the LEC does not (Amaral & Witter, 1995; Witter & Moser 2006).

1.7.1 Intrinsic connections

Connections within the EC originate in both superficial layers and deep layers. Projections from layers II and III tend to terminate in the superficial layers, whereas projections from the deep layers terminate in both superficial and deep layers (Amaral & Lavenex, 2007).

1.7.2 Commissural connections

Strong commissural connections from all areas of the EC predominantly terminate in layers I and II of the homotopic area of the EC (Goldowitz et al., 1975; Hjorth-Simonsen et al., 1975; Deller, 1998). Layer III of the EC also sends commissural projections to other regions of the contralateral hippocampal formation (i.e. CA1, CA3, DG, and the subiculum), the largest of which is aimed at the DG. These commissural connections are strongest at the septal portions of the hippocampal subfields and rapidly weaken at more temporal levels (Amaral & Lavenex, 2007).

1.7.3 Intrahippocampal connections

The lateral and medial areas of the EC both project to the dentate gyrus, CA3, CA1, and the subiculum via the perforant path (Amaral & Lavenex, 2007). These projections terminate in the molecular layer of the DG, the stratum lacunosum

molecular of CA3, and along the traverse axis of CA1 (at more temporal levels) and the subiculum. At more septal levels, CA1 receives most EC projections via the alvear pathway.

Return projections to the EC from CA1 and the subiculum primarily terminate in the deep layers with few fibres reaching layer I (Amaral & Lavenex, 2007). These projections are topographically organised with septal portions of CA1 and the subiculum projecting largely to the lateral EC, and more temporal parts of CA1 and the subiculum projecting largely to the medial EC. The traverse location of the cells of origin also determines where these projections terminate. Proximal CA1 and the distal subiculum exclusively project to the medial EC, whereas distal CA1 and the proximal subiculum project mainly to the lateral EC. The DG and CA3 do not project back to the EC (Amaral & Lavenex, 2007).

The pre- and parasubiculum project heavily to the EC. The presubiculum's projections reach the MEC, while projections from the parasubiculum extend to both the MEC and LEC. These projections are topographically organised and the location of the terminal fields in the EC are determined by both the proximo-distal and dorsoventral location of the cells that they originate from.

1.7.4 Subcortical connections

Layer V of the EC sends efferent projections to the amygdala, which primarily terminate on the basal nucleus. The same layer also projects to the nucleus accumbens and the olfactory tubercle (Amaral & Lavenex, 2007).

The EC receives substantial input from the amygdaloid complex, which is presumably conveying information about the individual's emotional state (Pikkarainen

et al., 1999). The majority of the amygdaloid fibres terminate in the ventrolateral portion of the EC.

1.7.5 Neocortical connections

Only the lateral and caudal parts of the EC are heavily innervated by the neocortex (Amaral & Lavenex, 2007). This organization likely underlies the behavioural dissociations observed in dorsal versus ventral hippocampal lesion studies. Neocortical inputs to the EC can be divided into two groups: those terminating in the superficial layers and those terminating in the deep layers.

The superficial layers of the EC receive a great deal of input from olfactory structures which terminate throughout most of the rostrocaudal extent of the EC (Amaral & Lavenex, 2007). However, the majority of input to the EC comes from the peri- and postrhinal cortices, which receive most of their inputs from unimodal and polymodal neocortical association areas. This suggests that the hippocampal formation receives highly-processed information from the neocortex. Each cortical area has some associated specialisation of inputs. Prominent unimodal afferents are olfactory and visual. The perirhinal cortex receives stronger olfactory inputs and the postrhinal cortex receives stronger visual and visuo-spatial inputs. However, it is the polymodal associational cortices which provide the majority of cortical input to the rhinal cortices, in particular the ventral temporal areas. The peri- and postrhinal cortices project differently to the EC, with the postrhinal cortex projecting preferentially to the MEC, and the perirhinal cortex projecting more to the LEC. This is elucidated through a disassociation of functions between these 2 portions of the EC (Burwell & Amaral, 1998a). The deep layers of the EC receive cortical afferents from the agranular insular cortex, the medial prefrontal region, and the retrosplenial cortex (Insausti et al., 1997).

The EC sends efferent projections from layer II, III, and V back to the olfactory structures. The perirhinal and postrhinal cortices also receive afferent projections from layer V along with the infralimbic, prelimbic, orbitofrontal, and angular insular cortices. Only weak projections have been reported to the retrosplenial cortex (Amaral & Lavenex, 2007).

1.8 The presubiculum and parasubiculum

1.8.1 Intrinsic pre- and parasubicular connections

The presubiculum contains highly directional connections that interconnect all dorsoventral layers. Cells from the deep layers of the dorsal presubiculum project to the more ventral levels of the presubiculum, while layer II cells in the ventral presubiculum project to more dorsal levels of the presubiculum. Within the parasubiculum, the dorsal projections only stretch over short distances and are quite weak. However, the projections reaching more ventrally extend for long distances along the long axis of the parasubiculum. These projections are also much denser than that of the dorsal projections (Amaral & Lavenex, 2007).

1.8.2 Commissural connections

The presubiculum contains strong commissural projections to layers I and III of the homotopic part of the contralateral presubiculum, while commissural projections from the dorsal part of the presubiculum are relatively weak (Van Groen & Wyss, 1990). The parasubiculum also has commissural projections, which primarily terminate in layers I and III.

1.8.3 Intrahippocampal connections

The pre- and parasubiculum both project bilaterally to the other's layers I and III. They also project to many other regions of the hippocampal formation. The presubiculum has a modest bilateral projection to the subiculum, a weak projection to all layers of the hippocampus, and a weak projection to the molecular layer of the dentate gyrus. Unlike the transvers orientation of the entorhinal perforant pathway fibres, the presubicular fibres projecting to the dentate gyrus are arranged radially. The parasubiculum also projects to the molecular layer of the dentate gyrus, though it is relatively more substantial than that of the presubiculum (Kohler, 1985). Its fibres targeting this region are also organised radially and occupy the superficial two-thirds of the molecular layer. The parasubiculum also projects weakly to the *stratum lacunosum moleculare* of the hippocampal CA fields and bilaterally to the molecular layer of the subiculum.

The presubiculum's most prominent intrahippocampal projection is to the MEC. This projection almost exclusively terminates in layer III and to a much lesser extent layer I (Caballero-Bleda & Witter, 1993; Shipley, 1975). However, evidence from Canto et al. (2012) suggests that principal neurons in all layers of the MEC receive monosynaptic inputs from the presubiculum. This projection is topographically organised and the location of the terminal field in the EC is determined by both the proximo-distal and dorsoventral location of the presubicular cells that it originates from. The presubiculum also sends a crossed homotopic projection to the contralateral EC, which is as dense as the projection to the ipsilateral EC.

The parasubiculum projects to both the MEC (layer II) and LEC, although the LEC projection is less dense. Like the presubiculum, evidence from Canto et al. (2012)

suggests that principal neurons in all layers of the MEC receive monosynaptic inputs from the parasubiculum. The topographical organisation of these projections is similar to that of the presubiculum's projections to the EC. Also similar to the presubiculum, the parasubiculum projects to the contralateral EC, however these projections are weaker than the ipsilateral projections.

1.8.4 Subcortical inputs

The most prominent subcortical connections of the pre- and parasubiculum are with the anterior thalamic nuclear complex. Primarily, the anteroventral and laterodorsal nuclei and the anterodorsal nucleus (Kaitz & Robertson, 1981; Robertson & Kaitz 1981). There are topographical differences in the thalamic connections along the dorsoventral axis of the presubiculum. The dorsal portion mainly receives projections from the laterodorsal and anterodorsal nuclei, whereas the ventral portion mainly receives projections from the laterodorsal and anteroventral nuclei. These projections mainly terminate in layers I, III, and IV. The nucleus reuniens also projects to layer I, albeit a much weaker projection. The presubiculum sends back a strong bilateral projection to the anterior nuclear complex. This projection primarily emerges from cells located in layer IV of the presubiculum.

There is considerable evidence that the anterior thalamic nuclei are part of an interconnected circuit that is organized hierarchically and is responsible for the propagation of head directional signals. Head direction cells have been found in the anterodorsal, lateral dorsal and anteroventral nuclei, with the largest proportions located in the former two (Clark and Taube, 2012; Taube, 2007; Tsanov et al., 2011). This idea is supported by experiments showing that lesions of the lower structures of this circuitry (e.g. anterodorsal thalamus) completely abolish head direction cell

activity in higher components (e.g. postsubiculum, parasubiculum, and superficial layers of medial entorhinal cortex), whereas the destruction of the presubiculum did not disrupt head direction signals in subcortical structures (Goodridge and Taube, 1997; Clark and Taube, 2011, 2012). Border cells have also been found in the anterior thalamus and anterior claustrum (Jankowski et al., 2015a; 2015b).

1.8.5 Neocortical connections

Layers I and III/V of the presubiculum receive projections from cells in layer V of the retrosplenial cortex (Van Groen & Wyss, 1992; Wyss & Van Groen, 1992). This is the most prominent extrahippocampal cortical input that it receives. Layer V of the presubiculum projects back to the granular retrosplenial cortex, terminating preferentially on layers I and II. These projections are topographically organised, with the dorsal presubiculum mainly projecting to the dorsal part of the granular retrosplenial cortex and the ventral presubiculum projecting more ventrally. They also display a similar rostrocaudal organisation: the rostral presubiculum projects to the rostral retrosplenial cortex and the caudal presubiculum projects to the caudal retrosplenial cortex.

The parasubiculum receives weak projections from the retrosplenial cortex and the occipital lobe. The laminar distribution of these projections is similar to that of the presubiculum.

The pre- and parasubiculum both receive strong projections from visuo-spatial neocortical areas and the subiculum. The fact that they receive strong input from the subiculum, which is the major output area of CA1 and also project heavily to the EC, suggests that pre- and parasubiculum lie at the crossroad between output and input.

This functional loop may be important in re-directing hippocampally-processed information back into the hippocampus (Amaral & Lavenex, 2007).

1.8.6 Other connections

Various nuclei of the brain stem project to the presubiculum. The densest of which emerges from the dorsal and ventral nuclei. A component of this projection is serotonergic and innervates layer I. The plexiform layer is innervated by the noradrenergic locus coeruleus. Both the pre- and parasubiculum receive heavy cholinergic input from the basal forebrain. Layer II of the presubiculum receives much of the projections from the medial septal nucleus and the vertical limb of the diagonal band of Broca that are directed at this brain region. The presubiculum also receives input from the supramammillary nucleus, whose projections primarily terminate in the deeper layers (Allen & Hopkins, 1989; Thompson & Robertson, 1987). Those same layers of the presubiculum project bilaterally to the medial and lateral mammillary nuclei.

2 Chapter 2 Introduction part 2: Spatial Cells

2.1 Brief Overview: spatial information

The hippocampus, located in the medial temporal lobe, is a part of the brain that is crucial for spatial cognition. Lesion studies and neurological studies involving the hippocampus found that when parts of this brain region were damaged it affected not only memory and learning, but also the subjects' or patients' ability to navigate.

There are two types of spatial information that are sent to the hippocampus that we use to navigate through our environment. There are self-motion cues such as: optic flow, which is the flow of stimuli in the environment that occurs as an observer moves through the environment, efference copy, which is a copy of self-movement signals from the motor cortex (how many steps have I taken), vestibular input, and proprioception, which is the sense of movement in the joints or joint positioning, thus potentially indexing how many flexings have occurred. Then there are external cues such as landmarks and boundaries. Over the last four decades, five types of cells in the hippocampal formation have been found to fire in response to these cues. They work together to build an internal map of the environment, providing the scaffolding for episodic memories and enabling successful navigation. These cells include head direction (HD) cells, place cells, boundary responsive cells (i.e. border cells and boundary vector cells), grid cells, and speed cells (Figure 2.1).

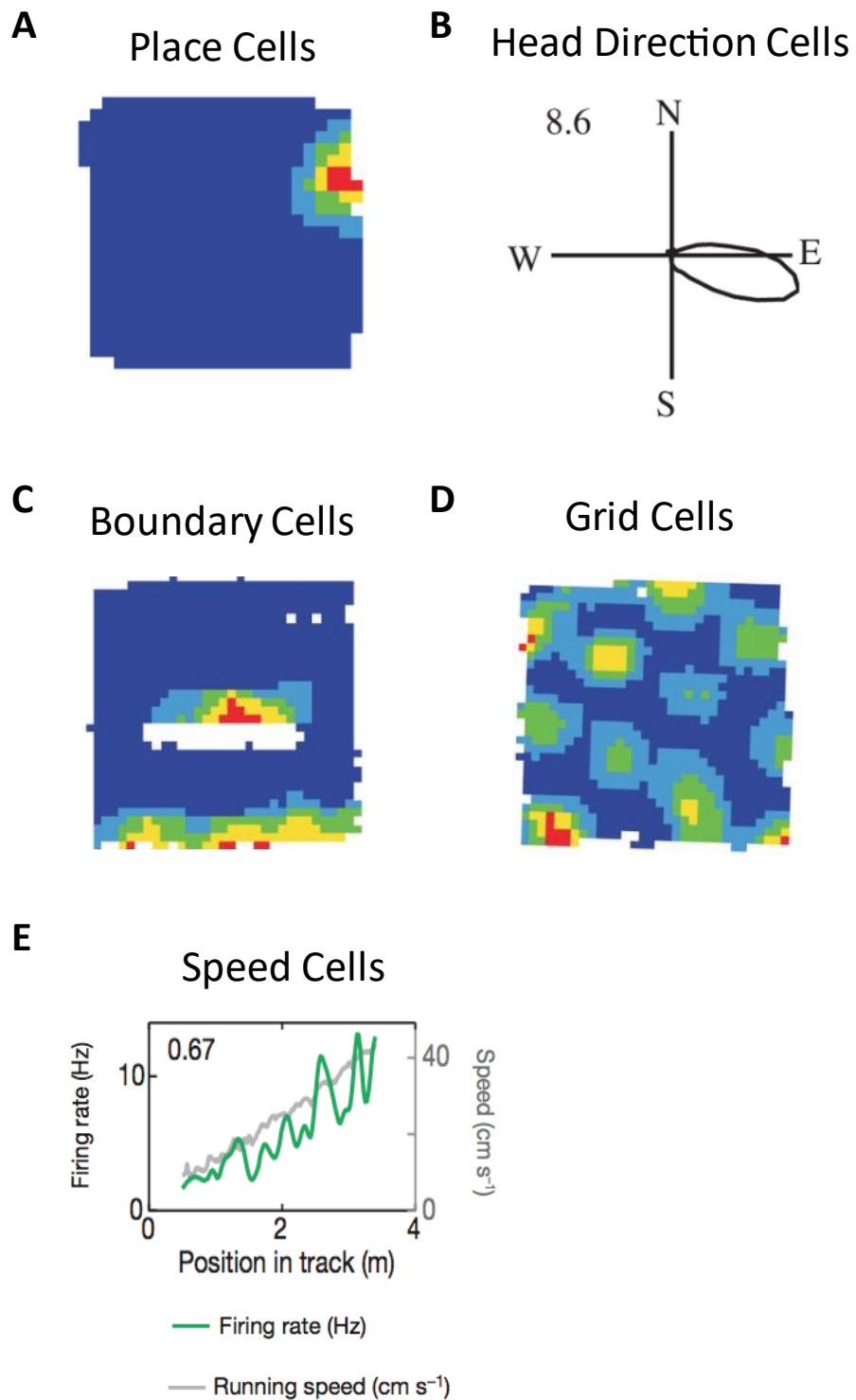


Figure 2.1 The five types of fundamental of spatial cells.

This figure shows one example of each type of fundamental spatial cell: (A) place cell; (B) HD cell; (C) grid cell; (D) boundary cell; (E) Speed cell. A-D are represented by a locational firing rate map (A, C, D) or a directional firing polar plot (B). E is represented by a graph of the mean firing rate and running speed as a function of position for an MEC speed cell. Adapted from Hartley et al. (2014) and Kropff et al., (2015).

2.2 Head-direction cells

It is widely acknowledged that head direction (HD) cells code for direction of heading. Each HD cell has a preferred firing direction that causes it to maximally fire whenever the rat's head is faced in that direction. This occurs irrespective of the rat's location in space (Taube 1990a; Muller and Kubie, 1994; Burgess et al., 2005; Jeffery, 2007). There is little firing adaptation when an animal's head is held in a cell's preferred direction (Taube and Bassett, 2003). HD cell firing is also unaffected by pitch and roll of the animal's head within a 90° horizontal plane or the animal's behavior. The tuning curves of HD cells, which are plotted on a firing rate versus head direction graph, tend to have directional firing ranges of 90°, but can range from 60° to 150°. The peak of a tuning curve is called the peak firing rate and the head direction at that peak is the cell's preferred firing direction (Taube and Bassett, 2003). The tuning curves of HD cells are quite similar across the different brain regions, with only a few differences. For example, HD cells found in the ADN tend to have higher peak firing rates and LMN HD cells tend to have broader directional firing ranges (Taube and Bassett, 2003).

The HD cell population represents the full range of cardinal directions and acts as an internal compass. Like place cells, HD are not organised topographically. In other words, neighbouring HD cells do not all fire for the same direction (Taube, 1998; Taube and Muller, 1998).

2.2.1 Anatomical locations of Head-direction cells

HD cells are found throughout much of the limbic system. They are abundant in the presubiculum (54% of the cell population) and parasubiculum (59% of the cell population) (Boccarda et al., 2010). Though the proportion of HD cells between the pre-

and parasubiculum is not significantly different to that of layers III, V, and VI of the MEC (55%), the laminar organisation does differ. Similar numbers of HD cells can be found across all layers of the Pre- and parasubiculum, whereas the number of HD cells in the deep layers of the MEC was considerably higher than that of the superficial layers (Boccarda et al., 2010). HD cells in layer III of the MEC have also been found to be topographically organised such that the most sharply tuned cells are located towards the dorsal border and the number of less directionally tuned cells increasing ventrally (Giocomo et al., 2014). A topographical organisation was not found in layers V and VI. HD cells in the presubiculum, parasubiculum, and MEC all have sharply tuned head-direction, but it is sharpest in the presubiculum (Sargolini et al., 2006; Boccarda et al., 2010). Other areas of the limbic system that contain HD cells include the anterior dorsal thalamus nucleus (60% of the cell population), lateral dorsal thalamus (30%), lateral mammillary bodies (25%), anterior cingulate gyrus, retrosplenial cortex (10%). The presence of HD cells in CA1 has also been reported (Leutgeb et al., 2000). However, the number of CA1 HD cells was small (n=6) and the authors acknowledge the possibility that the spikes, which were recorded before the electrodes reached the hippocampus, were recorded from thalamocortical fibers. Furthermore, one of their arguments for the presence of HD cells in CA1 is that the EC, which provides dense projections to CA1, does not contain HD cells. Thus, the orientation of the rat could not be conveyed to the hippocampus as a distributed code. However, since this paper was published in 2000, there have been multiple reports of HD cells within the MEC (Sargolini et al., 2006; Boccarda et al., 2010; Giocomo et al., 2014).

Head-direction cells can also be found outside of the limbic system: the dorsal striatum (6%), the medial prefrontal cortex, the medial precentral frontal cortex, and

the dorsal tegmental nucleus (DTN) (Taube and Bassett, 2003). The DTN is located in the brainstem and, along with other areas of the brainstem, is thought to generate directional signal. Though this area contains some HD cells, the majority of cells found in the DTN (~75%) fire in response to angular head velocity (Taube and Bassett, 2003). The symmetric angular head velocity cell increases its firing rate proportionately to the speed that the animal turns its head in either direction and accounts for nearly 50% of all DTN cells. The asymmetric angular head velocity cell also increases its firing rate proportionately to the speed at which an animal turns its head, but only for one direction. These cells make up ~25% of DTN cells. Asymmetric angular head velocity cells have also been found in the dorsal presubiculum (Sharp, 1996). Symmetric and asymmetric angular head velocity cells have been found in the LMN along with a third type: slow angular head velocity cells. The firing rate of these cells is negatively correlated with the speed at which an animal turns its head in either direction (Taube and Bassett, 2003).

2.2.2 Manipulating Head-direction cells with allothetic and idiothetic cues

The firing direction of HD cells can be controlled by a number of different cues. These include allothetic cues (e.g. visual, auditory, and semantic), and idiothetic cues (e.g. vestibular, proprioception, motor efference copy, and optic flow). Rotating a salient visual cue, such as a cue card, will cause a corresponding rotation of the cell's preferred firing direction (Taube and Bassett, 2003). When this rotation occurs, the HD cell population maintains their angular distance from one another, i.e. if one cell rotates by 30°, the others do as well (Muller and Kubie, 1987). Zugaro et al., (2003) showed that the rotation of a cell's firing direction in tandem with rotation a cue card can occur within 100ms of the relocated card being seen. In general, visual cues

possess a strong influence over the orientation of HD cells. However, the strength of this influence is not equal between distal cues (e.g. cue cards on the wall of the lab room) and proximal intra-environment cues (e.g. object rotation). When both cues are present HD cells tend to anchor to distal cues and remain relatively unaltered, even when the proximal cues are rotated. However, in the absence of distal cues the cells will anchor to the proximal cues (Zugaro et al., 2001). When visual cues are removed or the lights are turned off there is no change in HD cell activity. Over time, though, the preferred firing direction may begin to drift (Taube et al, 1990b; Goodridge et al., 1998).

What happens when allothetic cues and/or idiothetic cues are missing?

Stackman et al. (2003) tested whether preferred firing directions were maintained when an animal was moved from a familiar square arena to a novel circle arena while researchers manipulated visual and/or motor efference copy/proprioceptive cues. They found that preferred firing directions were profoundly disrupted when the animal was passively transported to the novel environment, whether in darkness or in light. There were only small shifts in preferred firing direction when the animal walked into the novel environment in darkness. Their findings suggest that motor efference copy/proprioceptive cues play an important role in the maintenance of preferred firing direction in HD cells. They also suggest that optic flow cues are not enough to maintain directional path integration when an animal is being passively moved between arenas.

When both allothetic cues and idiothetic cues are present the type of cue that controls HD firing activity depends on the extent of conflict between the two types of information. If there is a small conflict (45°) between visual cues and idiothetic cues,

visual cues tend to have control over the firing properties of HD cells, but when the conflict is larger (180°) idiothetic cues have control (Knierim et al., 1998).

2.2.3 Head direction input is crucial for other spatial cells

Due to the large number of brain regions that HD cells are located in, researchers have only been able to inactivate HD cells in a few regions at a time. We have yet to see what effect an inactivation of the entire HD system would have on other spatial cells. However, several of these studies have demonstrated significant effects on place and grid cell activity following the inactivation of select regions populated by HD cells. This indicates that HD cells confer orientation upon other spatial cell populations.

Following lesions to the ADN or dorsal presubiculum Calton et al. (2003) observed that the place signal of CA1 place cells becomes significantly degraded. Lesions to the LMN result in an increase in place field repetition across identical maze compartments facing different directions (Harland et al., 2017). This repetition is not present when the LMN is intact, indicating that the HD system is necessary for the angular disambiguation of visually identical environments by place cells.

Winter et al. (2015) tested the role of HD signal on grid cell activity by either inactivating or lesioning the ATN. Previous studies have shown that disruption to the theta signal disrupts grid patterns while others have suggested that HD cells convey crucial directional heading information to grid cells (Brandon et al., 2011; Koenig et al., 2011; Raudies et al., 2015). Following inactivation or lesions, both HD cell and grid cell characteristics were significantly disrupted while theta rhythm was spared. This

indicates that the HD signal from the ATN is necessary for the generation and function of grid cell activity.

These studies are supported by recordings from the presubiculum, parasubiculum, and MEC of rat pups, which show that HD cells reach adult-like firing (P16) prior to other spatial cells (Bjerknes et al., 2015; Tan et al., 2015). Place cells, border cells, and grid cells do not reach adult-like firing until P16-17, P16-18, and P20-21 respectively (Bjerknes et al., 2014; Wills et al., 2010).

2.3 Place cells

Place cells are found in CA1 and CA3 of the hippocampus (O'Keefe & Dostrovsky, 1971). These cells fire when the rat enters the cell's single preferred firing location within an environment, known as its place field (O'Keefe & Dostrovsky, 1971). The cell's firing rate increases as the rat approaches the centre of the place field, where the cell's firing peaks, and decreases as the rat exits the field, becoming almost completely silent. In environments where an animal is free to move in two-dimensions, this firing pattern is omnidirectional. That is, it occurs irrespective of which direction the animal enters and exits the place field. However, in environments where the animal can only run in one direction, such as on a linear track, place fields tend to be directional (McNaughton et al., 1983).

2.3.1 Allocentric & idiothetic input

Evidence suggests that place fields are controlled by both allocentric and idiothetic cues (O'Keefe, 2007). Allocentric information is received from the environment via visual, olfactory, and auditory signals (Wiebe et al., 1997; Wills et al., 2005). Idiothetic information, or self-motion information, is received from

proprioceptive, motor, and vestibular signals (McNaughton et al, 2006a). In the absence of allocentric cues, such as in darkness, an animal can navigate using idiothetic cues. However, this only works for a short period of time as these cues quickly accumulate error (McNaughton et al., 1996; 2006; Burak and Fiete, 2009).

2.3.2 Size and Shape

The size of place fields varies along the dorsoventral axis, with smaller place fields belonging to place cells at more dorsal locations and larger place fields belonging to those at more ventral locations (Jung et al., 1994; Kjelstrup et al., 2008; Maurer et al., 2005). Marcelin et al. (2012) reported some ventral place cells with fields that were four times the size of those belonging to more dorsal place cells. Unlike neocortical cells, hippocampal place cells are not topographically organised- their anatomical position does not correlate with their place field location (Alme et al., 2014; Dombeck et al., 2010; Wilson and McNaughton, 1993).

Changes to the environment can also affect place field size and shape. A study by O'Keefe and Burgess (1996) revealed that geometric deformation of an environment (e.g. stretching or squashing the walls) induces parametric deformation of the place field. This demonstrates direct control of environmental boundaries over place cells. This finding helped lead to the formation of the boundary-vector cell model, which was proposed to explain place cell spatial responses (Barry et al., 2006).

2.3.3 Remapping

Previous studies have shown that sufficient changes in the environment can cause place cells to change their firing response. This is referred to as remapping (Bostock et al., 1991; Muller and Kubie, 1987). It has yet to be made clear what the

purpose of remapping is, although it has been proposed that having two independent representations following changes in the environment may help distinguish between the two conditions (Leutgeb and Leutgeb, 2007). When subtle changes are made to the environment, partial remapping (i.e. changes to some but not place fields) or rate remapping (i.e. change in firing rate but not field location) are likely to occur (Anderson & Jeffery, 2003; Leutgeb et al., 2005; Shapiro et al., 1997). Larger changes to environments can cause global remapping. This includes changes in the locations of place fields as well as some cells becoming silent or starting to fire (Anderson & Jeffery, 2003; Colgin et al., 2008; Muller, 1996). It is possible that some cells are stable between different environments because they are fixed to cues that remain unchanged, while other cells remap because they are fixed to cues that have changed (Colgin et al., 2008; Paz-Villagrán et al., 2004).

2.3.4 The influence of boundaries on place cells

Evidence presented by multiple studies suggests that boundaries have a significant influence over place cell behavior. For example, place fields tend to be located near the walls of the environment (Hetherington & Shapiro, 1997; Hartley et al., 2000). As mentioned above, parametric deformation of place cells occurs when the environment is stretched or squashed (Lever et al., 1999; O'Keefe and Burgess, 1996). O'Keefe and Burgess (1996) also found that in larger rectangular environments some place fields become bimodal (separating into multiple peaks).

It is not just perimeter boundaries that have an effect on place fields. Muller and Kubie (1987) inserted a barrier into an arena so that it either bisected, touched, or made no contact with a place field. Bisecting the place field with the barrier caused it to disappear. When the barrier touched the edge of the field, the field became smaller.

When there was no contact between the barrier and the place field, the field remained unchanged. The results from Barry et al (2006) supported Muller and Kubie's findings of inhibited or unchanged fields by bisecting and non-bisecting barriers respectively. However, when testing the response of place fields adjacent to the inserted barrier they also found a third phenomenon, that the barrier could elicit a duplication of existing adjacent fields (Figure 2.2), in a manner predicted by the BVC model (Hartley et al, 2000). This field duplication provided strong support for the Boundary Vector cell model of place field formation (Hartley et al, 2000) – see next section. When an inserted barrier is rotated, some place cells rotate along with the barrier and disappear when it is removed (Rivard et al., 2004). This suggests that some place cells may signal the proximity of additional barriers. Spiers et al (2013) recorded place cells in an arena containing four separate compartments connected by a corridor. Their key result was a replication of results in Lever et al, (2002) and Barry et al (2006); that is, they often found duplication of place fields in similar regions within each compartment. Thus, a cell that would fire in the north-east corner of the westmost compartment would also fire along the north-east corner of the other compartments, albeit sometimes at somewhat different rates. These results are well predicted by the BVC model (Hartley et al, 2000).

A key manipulation that Spiers and colleagues did was to remove the walls that divided a larger area into three different compartments, while leaving a 4th compartment unchanged. When they did this, the place fields in the 4th compartment remained unchanged. However, when the first three previously-separate compartments were merged into one by the wall removal, the typical result was that there were no longer three repeated place fields, but just one place field. This further

suggested that the removed walls were directly responsible for each place field, e.g. in the example given above by creating three sets of north-east corners in that given area. This manipulation further supported the predictions of the BVC model (Hartley et al, 2000). I present this model in the next section.”

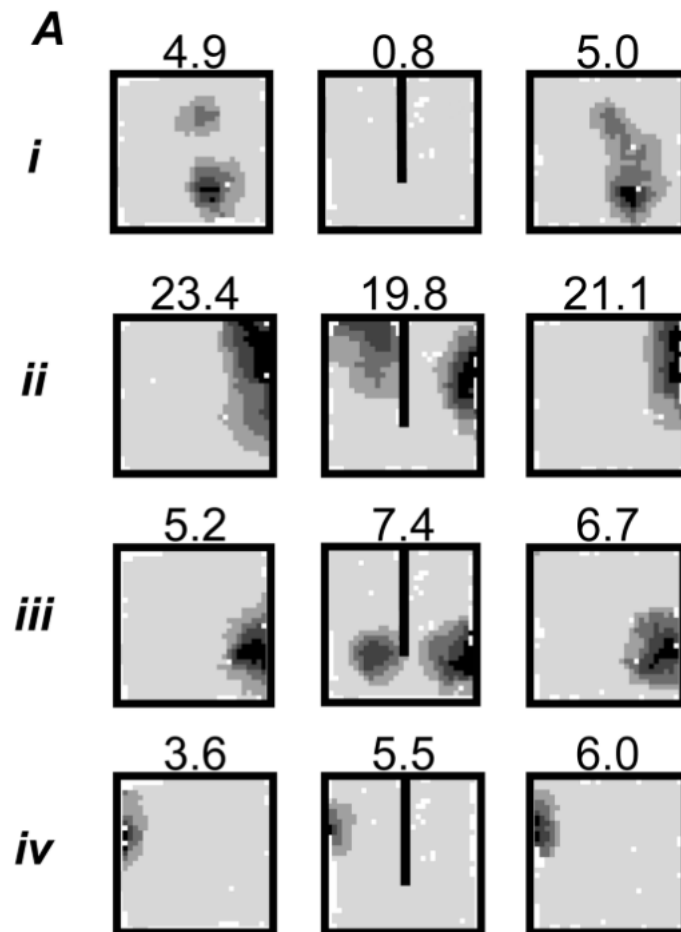


Figure 2.2 Place fields respond different to boundary insertion.

In this figure, 4 place cells are tested with the insertion of a barrier (column 2). This produced 3 different outcomes: (i) inhibition of firing; (ii-iii) doubling of the field with one on either side of the barrier; (iv) firing unaffected by barrier. Adapted from Barry et al., (2006).

2.4 Boundary cells

2.4.1 Boundary vector cells

The existence of boundary vector cells (BVC) was first predicted to explain the findings of O'Keefe and Burgess (1996)- that when a familiar rectangular environment is stretched along one axis place fields will stretch along the same axis. The role of the BVCs being that they would provide boundary information to the place cells (O'Keefe and Burgess, 1996, Burgess et al., 2000; Hartley et al., 2000).

Burgess et al. (2000) and Hartley et al. (2000) were first to put forward the BVC model. They proposed that a BVC would fire when an environmental boundary intersected the cell's receptive field, located at a particular distance and in a particular direction relative to the animal. BVCs with receptive fields that peak farther from the animal have broader fields than those peaked closer to the animal (Figure 2.3 A and B) (Lever et al., 2009). The firing fields peak at the boundary, which creates a vector from the rat.

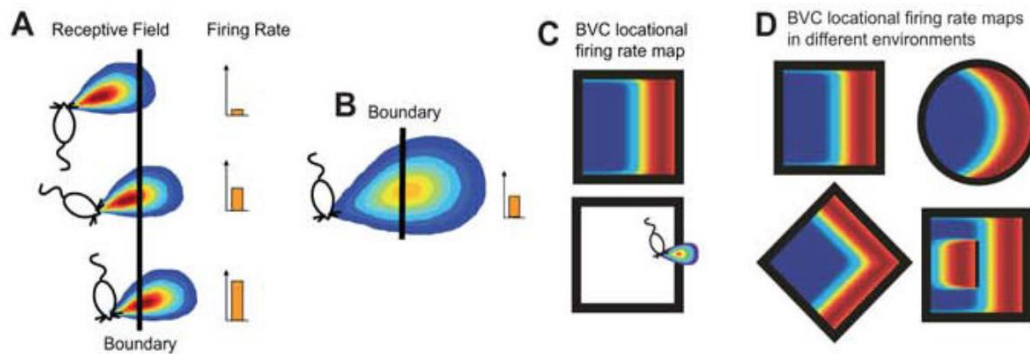


Figure 2.3 A BVC fires maximally when a boundary is located at the cell's preferred distance and allocentric direction from the rat.

A) The receptive field of a BVC tuned to respond to a barrier at a short distance east-northeast from a rat. B) BVCs tuned to respond to barriers farther from the rat will have broader receptive fields C) The firing field (shown as a rate map; top) and the receptive field tuned to respond to a boundary at a short distance to the east (bottom). D) The predicted firing fields in different environments for the BVC shown in C. The insertion of an additional environment causes a doubling of the firing field (lower right environment). Adapted from Lever et al., (2009).

2.4.2 BVC characteristics

Barry et al. (2006) simulated BVC activity to explain the shifts in place field size and location that occurred when changes were made to the environment and to put forward a candidate that would provide place cells with boundary information. This led to several predictions that have come to characterise BVC firing after they were discovered in the subiculum and behaved as predicted (Barry et al. 2006; Lever et al., 2009). Firstly, BVC firing fields follow the curvature of the boundary (Figure 2.4). Secondly, BVCs produce a second firing field in addition to the first when a barrier is inserted into the environment at the cells preferred direction. For example, a BVC that fires maximally along the western boundary of an environment will also fire along an additional boundary, inserted along the North-South axis, but only along the side that is to the west of the animal (Figure 2.5). Thirdly, when an environment is stretched, BVC firing fields also stretch, similar to the stretching of place fields mentioned above.

Fourthly, BVCs preserve their firing patterns in novel environments. This was predicted because BVCs provide a signal for any boundary that intersects the cell's receptive field. Lastly, like place cells, BVC firing occurs independent of heading direction.

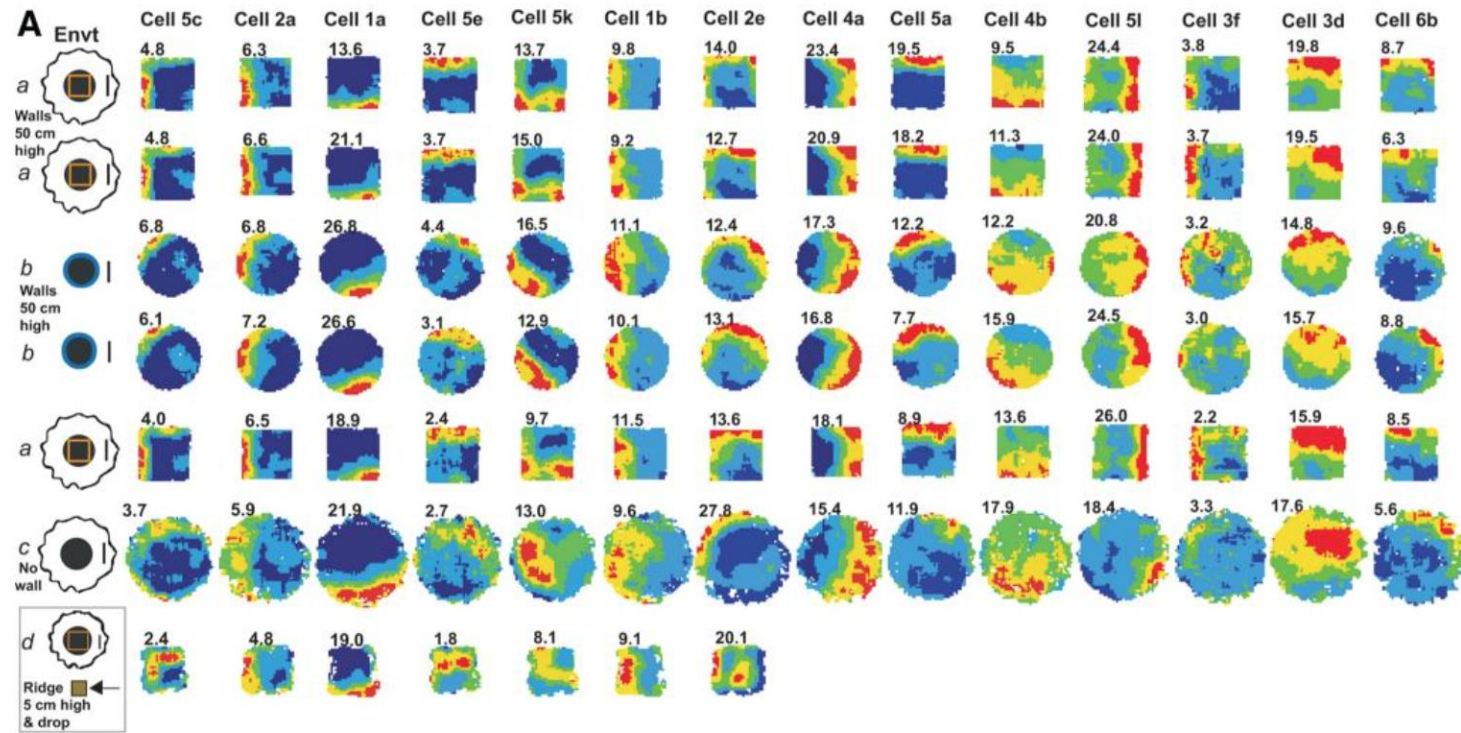


Figure 2.4 Firing fields of subicular BVCs in different environments.

Environment a, 62 x62 x 50-cm-high beige square box made of morph material; Environment b, walled, light grey, wooden, circular arena with a 79 cm diameter; Environment c, the 90-cm-diameter floor of Environments a and b; Environment d, 39x39 cm square holding platform with 5-cm-high ridges. The firing fields of each BVC followed the shape of the boundary and showed stable distal and directional preferences across all environments. Adapted from Lever et al., (2009).

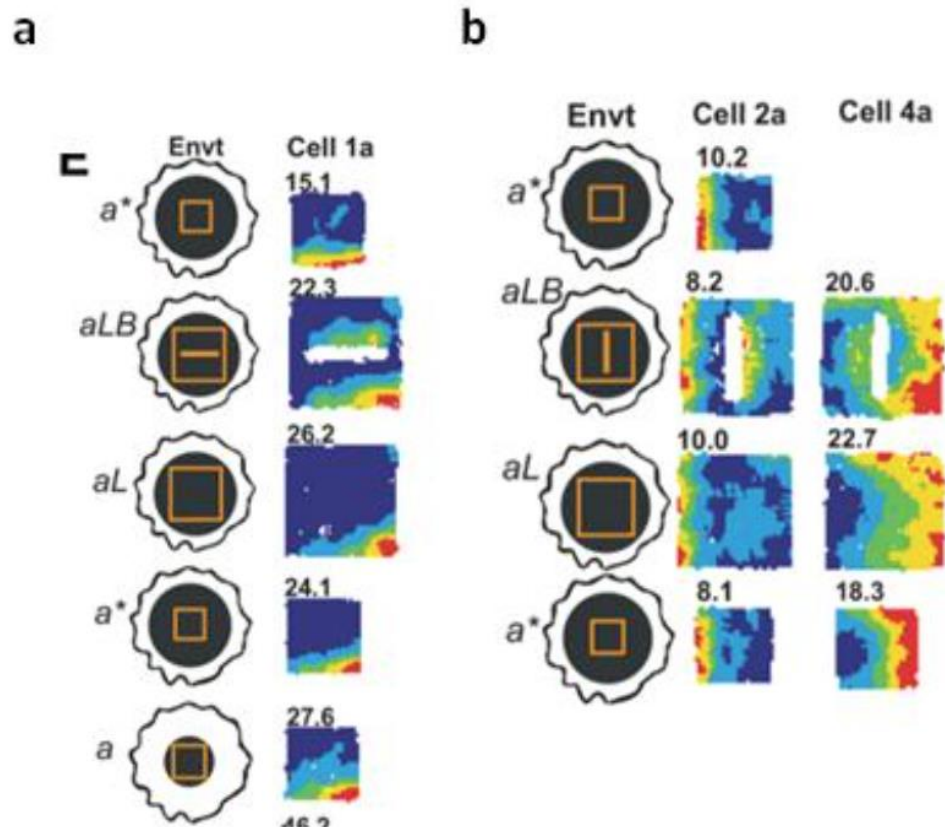


Figure 2.5 BVCs produce additional firing fields along additional boundaries.

This figure shows 3 BVCs being tested with the presence of and additional boundary placed in each cell's preferred allocentric direction. All BVCs produced a second firing field in addition to the first. Adapted from Lever et al., (2009).

2.4.3 BVCs respond to various boundary types

BVCs fire in response to both vertical walls and dropped edges (Lever et al., 2009). There have also been reports of BVCs that fire at the edge of reachable space; the furthest point that the animal can reach its head passed the dropped edge (Lever et al., 2009; Stewart et al., 2014). They have also been found to fire in response to boundaries that do not necessarily prevent movement, but can impose some limitations, such as an easily traversable gap between two platforms (Lever et al.,

2009; Stewart et al., 2014). The variation in the types of boundaries that BVCs respond to lead Lever et al., (2009) to suggest that the relative importance of each boundary type may vary across the BVC population. They also concluded that ‘a boundary is an abstract concept that may reflect sensory properties of environment features such as the sight or feel of a wall or an extended edge, as well as impediments to movement.’

2.4.4 Border cells

Border cells are found in the MEC and the pre- and parasubiculum. (Solstad et al., 2008; Savelli et al., 2008; Boccara et al., 2010). Solstad et al. (2008) found that when an environment is stretched along one axis, the firing fields of border cells with a preference for the extended wall will stretch parametrically. They also show that a border cell’s preference for a boundary in a particular allocentric direction was maintained across different rooms and environments of different shapes and sizes (square, 1x1m or 1.5x1.5m; circle, 1m or 1.5m diameter). When the researchers rotated a cue card 90°, they demonstrated that border cells rotated in concert with co-recorded grid cells and HD cells. Based on their findings, Solstad et al. (2008) suggested that border cells may play a role in planning navigational trajectories and anchoring grid cells and place cells to a geometric reference frame.

To see if border cells were primarily tuned to periphery walls or to boundaries in general, Solstad et al. (2008) recorded border cells in an environment with an additional boundary inserted at the cell’s preferred allocentric direction during one trial, and one inserted at the orthogonal direction during another. Some of the border cells showed a clear doubling of their firing fields similar to subicular BVCs, but others did not. Another difference between these cell types can be seen in wall-less environments (Solstad et al., 2008). In general, border cells will continue to fire along

the edges of the environment when the walls are removed. However, they tend to remap with their directional preferences shifting between the walled and un-walled environments, unlike BVCs, which showed stable fields across the two conditions (Lever et al. 2009; Stewart et al., 2014).

2.5 Grid cells

Grid cells fire in a hexagonal pattern that tessellates across an environment that an animal is in (Hafting et al., 2005). They were first discovered in layers II and III of the medial entorhinal cortex by researchers in the Moser lab (MEC; Fyhn et al., 2004). Since then, they have received a large amount of attention from researchers across the globe. Subsequent studies have located grid cells in all cellular layers of the MEC and in the presubiculum and parasubiculum (Sargolini et al. 2006; Boccara et al. 2010) as well as in the homologue areas of mice (Fyhn et al., 2008), bats (Yartsev et al., 2011), monkeys (Killian et al., 2012), and humans (Doeller et al., 2010). Grid cell properties (orientation, scale, phase, gridness) have been studied extensively in a variety of environments and conditions, however questions about the formation and maintenance of grid patterns remain and more research is needed. Below is brief overview of grid cell research.

2.5.1 Grid cell properties

2.5.1.1 Grid orientation

Grid orientation is determined by the angle between a horizontal reference line and the vector to the nearest firing field (counter-clockwise) of the innermost hexagon within the grid pattern (Figure 2.7A). Hafting et al. (2005) found that the full range of orientations (1-59°) was present amongst the population of grid cells that

were recorded. He also found that cells which were recorded on the same tetrode had similar orientations. As the tetrodes were moved down along the dorsal-ventral axis, the orientations of the recorded grid cells changed coherently. They were organised into discreet, overlapping modules that were independent of MEC anatomical layers (Hafting et al., 2005; Brun et al., 2008).

2.5.1.2 Grid scale

Grid scale represents the distance between a cell's firing peaks within an environment (Figure 2.7B). It is a measure of the median distance from the central peak to the 6 surrounding peaks that form the grid's classic hexagonal shape. Like that of hippocampal place cells, grid scale has been shown to increase along the dorsal-ventral axis along with an increase in field size (Figure 2.6) (Hafting et al., 2005; Brun et al., 2008; Stensola et al., 2012, Kjelstrup et al., 2008). Previous studies have shown grid scales along the dorsal-ventral axis increasing from 39cm at more dorsal locations (Hafting et al., 2005) to 3 metres at more ventral locations (Brun et al., 2008). This increase in grid scale is accompanied by a decrease in the intrinsic theta frequency and the rate of phase precession (Hafting et al., 2005; Brun et al., 2008).

Similar scales can be found among neighbouring MEC grid cells (Hafting et al., 2005). Stensola et al. (2012) recorded from large numbers of simultaneously recorded grid cells in layers II and III of the MEC (one-third of the dorsoventral length) and found that their scales were organised into overlapping, discreet, autonomous modules, unlike the continuous progression of the sensory systems found in other animals (Bonhoeffer et al., 1991; Hubel et al., 1974; Ohike et al., 2005; 2006). The boundaries of these scale modules coincided with the boundaries of the orientation modules and is consistent with the increase in spatial scale seen with hippocampal place cells

(Hafting et al., 2005; Kjelstrup et al., 2008).

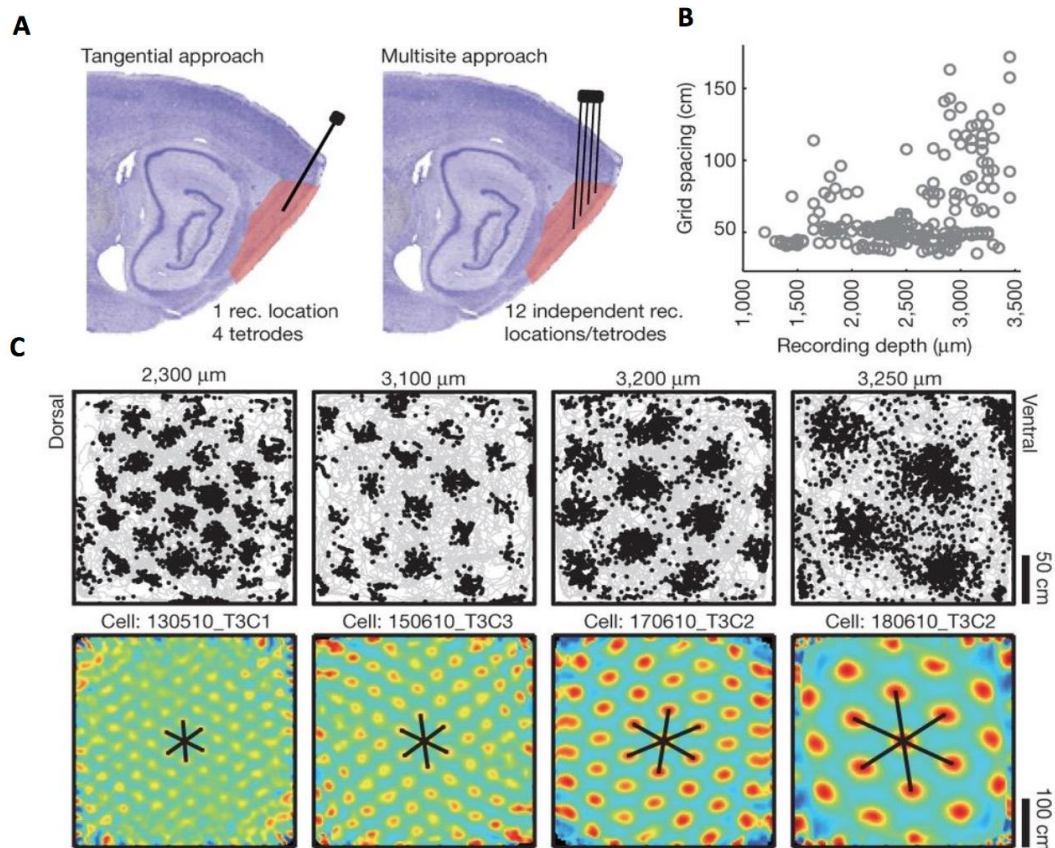


Figure 2.6 Grid scale increases along the dorsoventral axis.

(A) Schematic representation of tangential and multisite recording approaches used to sample large areas of the MEC (shaded red). (B) Scatterplot of grid scale across the dorsoventral axis. (C) Four examples of grid cells recorded at different depths along the dorsoventral axis. Note that the scale increases with depth. Adapted from Stensola et al., (2012).

2.5.1.3 Grid phase

The phase of a grid cell is the location of all of a cell's firing fields, as a whole, within an environment (Figure 2.7C). This is calculated by correlating field location in pairs of rate maps. Below, in Figure 2.7C, the black X's represent the peaks of the nodes in the autocorrelation map that surround the central peak. The spatial autocorrelation, broadly speaking, asks the question "When a spike occurs in a given

reference location, where will other spikes occur relative to that location?”. For a grid cell, the answer to this question is that those other spikes tend to occur in distinct clusters, and there are 6 distinct nearby clusters, all at a similar distance from the reference location, and separated by a similar angle (60°). The white X’s represent the nodes of another, neighbouring grid cell. Accordingly, the black X’s and the white X’s together represent the offset phases of two grid cells: in this case, the positions occupied by the white set of nodes can be obtained by translating the black set of nodes westwards by a few tens of cm. The difference between one cell’s phase and that of another is called an offset. The phase of neighbouring cells will be offset even though they share similar scale and orientation (Fyhn et al., 2004; Hafting et al., 2005). Unlike scale and orientation, the offset between cells is not affected by environmental changes and is not organised topographically; it is predetermined and persists (Fyhn et al., 2004; Hafting et al., 2005). This means that if phase was changed, it would change for all cells, but the offset between them would remain the same.

2.5.1.4 Gridness score

Gridness score (or gridness) is a measure of the six-fold symmetry present in the spatial autocorrelogram (Figure 2.7D). The region encompassing the 6 peaks closest to the origin of the spatial autocorrelogram is rotated in 30° steps and the correlation between the rotated and un-rotated data found. Gridness is then defined as the highest correlation at rotations at 30° , 90° and 150° and subtracted from the lowest correlation at 60° and 120° . Gridness scores vary between -1 and +1; the higher the score the more regular the pattern.

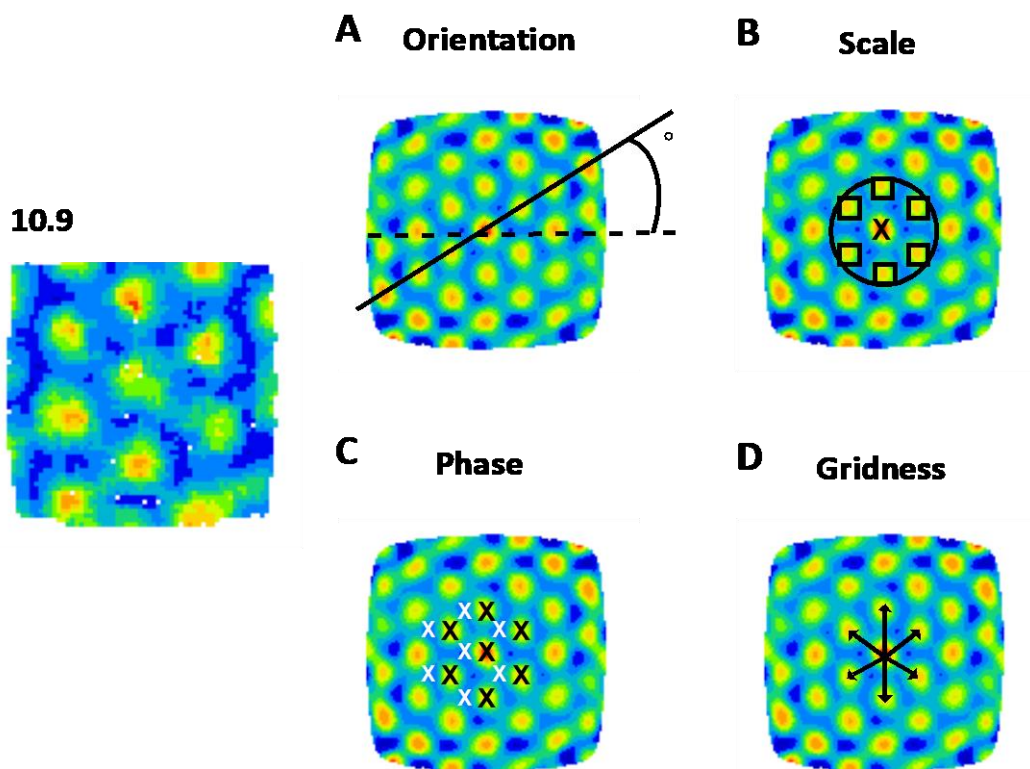


Figure 2.7 Spatial autocorrelation is used to determine the parameters of the grid pattern.

This figure shows an example of a grid cell recorded from rat 480. To the left is a rate map with peak rate (Hz). To the right are spatial autocorrelation maps adapted for illustrative purposes. (A) Grid orientation is defined by the lines that intersect the grid fields along three axes. The orientation is the angle between a horizontal reference line (dotted line) and the vector to the nearest firing field. (B) Grid scale refers to the spacing of the grid. It is calculated as the average distance between any firing field and the 6 surrounding fields. (C) The phase is the position of all the firing fields in the environment. (D) Gridness score represents the regularity of the grid pattern. This informs us of closely the 6 peaks (black squares) around the central most peak (black cross) are distributed at 60 increments.

2.5.2 Grid cells in novel environments

In novel environments, the grid scale expands and as an animal becomes more familiar with the environment it contracts back to the cell's intrinsic scale. This suggests that grid scale expansion may provide a signal for novelty (Barry et al., 2012). Barry et al., (2007) recorded grid cell activity from rats while they foraged in a rectangular environment with moveable walls. The rats were habituated to one of two

configurations (100cm x 100cm or 70cm x 100cm) prior to recording. Recording sessions consisted of 5 20-minute trials. The first and fifth trials were in the familiar configuration. For trials two through three, the environment was stretched/shortened along one or both axes. They observed that grid scale changed parametrically with changes to the size and shape of the environment. This rescaling was correlated with environmental experience; distortions reduced with continued experience. This suggests that the system reverts back to an intrinsic grid scale as an environment becomes familiar. It also suggests that grid cells become associated with the features and boundaries of the environment, explaining the parametric change in grid scale when the shape of the environment is altered.

These results are in contrast to those found by Hafting et al. (2005). The researchers recorded grid cell activity from rats in a 1m diameter circular arena, and again after it was expanded to 2m in diameter. They found that there was an increase in the number of fields, but that grid scale remained unchanged. This may be due to two reasons: 1) the environment was familiar and its shape never changed, only its size did and 2) they tested grid cells in a circular environment. Other studies have shown circular environments do not provide any points for the grids to anchor to (e.g. corners), requiring them to anchor to distal cues, which Hafting et al. (2005) did not manipulate in their experiment (Krupic et al., 2015; Stensola et al., 2015). If the anchor points and the shape of the environment remained the same between consecutive trials, and the environment is already familiar, it seems unnecessary for a grid cell to change its activity, other than to increase the number of firing fields in order to cover the additional space. Barry et al. (2007) also tested rats in a familiar environment that changed size (i.e. a big square to a small square), but these two trials were divided by a

trial in which the environment was stretched along one axis to form a rectangle. They also used a square environment, which provides anchor points for the grids, unlike circular environments. It is possible that its changes to the shape of the environment that have a significant effect of grid cell activity and not so much its size. The effect may also depend on whether changes have occurred to the anchor points.

In a study similar to Barry et al. (2007), Barry et al. (2012) recorded grid cell activity during three novel trials run between 2 familiar trials. Instead of changing the shape and size of the environment, they changed either colour, material, scent or lighting. Scale expansion persisted across days, but reduced with experience as in Barry et al. (2007). By day 5, grid scales in the novel environments were no longer significantly different to that of the familiar environments.

Barry et al., (2012) also found changes to other grid properties between familiar and novel environments. Orientation remained stable between familiar trials, but was significantly rotated between familiar and novel environments. This rotation did not revert over time to the baseline orientation, and is consistent with evidence that orientation is environment-dependent (Hafting et al., 2005). A significant reduction in gridness was also observed and, like grid scale, returned to baseline with increased familiarity over 5 days.

2.5.3 Grid scale expansion: a response to spatial uncertainty

A recent computational study by Towse et al. (2014) has suggested that the temporary expansion of grid scale seen in novel environments may be the optimal response to spatial uncertainty caused by the unfamiliarity of the new spatial cues. Their simulation also shows that the optimal overall scale for a grid system represents

a trade-off between maximizing precision (requiring small scales) and minimizing spatial uncertainty (requiring large scales).

When there is low spatial uncertainty within an environment, ambiguity errors - errors resulting from ambiguity in decoding location from periodic firing patterns- are unlikely to occur. For example, when shopping in your local supermarket, you know exactly where to find your favourite chocolate bar and can easily walk straight from the entrance to its location. In this case, uniformly increasing grid scale would only increase the potential for ambiguity errors- thus smaller grid scales, which provide more locational precision, are favoured (Towse et al., 2014). When there is greater spatial uncertainty (e.g. shopping in a foreign supermarket), ambiguity errors are more likely to occur. However, this can be mitigated by increasing grid scale. When grid scale is increased, the magnitude of spatial uncertainty is reduced relative to the grid. This then reduces the chance of making ambiguity errors. Increasing the grid scale also makes it so that a given environment occupies less of the grid's overall capacity. Since location is only decoded to locations within the environment, this means that there are fewer candidate locations (i.e. firing fields) to consider, which reduces the chance of ambiguity errors (Towse et al., 2014).

This rather interesting model suggests that we should think of environmental novelty as a special case of more general consequences of spatial uncertainty. The model invites thinking further about other experimental approaches to spatial uncertainty than that of novelty. This model was part of the inspiration for my experiments 1 and 2. What I was interested to explore was to what extent different kinds of boundary cue manipulations could affect grid scale in a systematic way,

whereby higher spatial certainty would elicit smaller grid scale, and lower spatial certainty higher grid scale.

2.5.4 Grid patterns and cue integration

As with other spatial cells, grid cell activity can be controlled by allocentric and idiothetic cues. In circular arenas, distal cues control the orientation of grid patterns; when distal cues are rotated, the grid pattern rotates by the same degree, but scale and field size remain the same (Hafting et al., 2005). This might happen because circles have infinite lines of symmetry: there is no point along the boundary of a circular environment that distinguishes one point from another. This leaves the grid cell with no geometric orientational cue to anchor to within the environment, so it must rely on distal cues. A study by Krupic et al. (2015) supports this idea. They found that when they rotated a square arena (which has 4-fold symmetry) by 45°, the grid pattern also rotated by 45°, even though the distal cues remained in their original locations. This demonstrates that in enclosures that do not have infinite symmetry, a strong influence can be exerted by the enclosure despite the presence of prominent distal cues (Krupic, 2015).

When all external cues are masked, and an internal cue card is rotated the grid pattern for each cell will rotate while maintaining their relative offset to one another (Hafting et al., 2005). This can also be seen when grid cells are recorded in similar environments located in different rooms along with a shift in grid phase and HD cell rotation (Hafting et al., 2005; Fhyn et al., 2007; Barry et al., 2012). When the walls of an arena are removed, a phase shift can be observed without a shift in grid orientation or the rotation of HD cells (Solstad et al., 2008).

When visual cues are removed via darkness grid patterns persist, suggesting that allocentric cues may not be responsible for the production of grid patterns (Hafting et al., 2005). A 2015 study by Winter et al. suggests that they might be produced by self-motion cues. In their study, they eliminated motor related self-motion cues by passively moving a rat in a clear cart. In doing so, they abolished grid cell firing patterns while HD cell characteristics were spared.

While allocentric cues may not be responsible for generating grid patterns, it has been suggested that they might help maintain them. A study by Hardcastle et al. (2015) demonstrated a dual control of self-motion cues & environmental cues over grid cell firing. The researchers recorded grid cell activity from rats as they made long trajectories across an open arena. The results showed that grid patterns were less precise and less stable when the rats were further away from the wall and that this kind of error increased by the amount of time that the animal spent away from the walls. When the rats reencountered the walls, the grid cells were able to recalibrate. The authors suggested that when the rats were in the interior of the arena, the grid-pattern was being maintained by self-motion cues, which accumulate error over time. When the rats were in contact with the walls the grid pattern was also being stabilised by environmental cues (i.e. boundaries). Not only did this study demonstrate dual cue control over grid cell firing via self-motion cues and boundaries, but it also suggested that boundaries may act as an error correction mechanism.

2.5.5 Grids and boundary geometry

Recent studies that use more complex testing arenas have begun to reveal that boundaries and environmental geometry have more control over grid cell activity than previously thought (Carpenter et al., 2015; Krupic et al., 2015; 2018; Wernle et al.,

2018). At the time of the first in depth report of grid cells, it was thought that grid scale was essentially universal, and that grids would provide a universal metric (Fyhn et al., 2007). In environments with multiple identical compartments, grid cells will fire in identical, locally bound patterns that replicate in each compartment. As the environment becomes more familiar the grid pattern becomes more global, firing across the boundary dividing the compartments, forming one coherent grid pattern (Figure 2.8) (Carpenter et al., 2015). This finding supports the theory that grid cells serve as the neural basis of path-integration-based navigation. The underlying mechanism of the shift from local to global grid maps could control which cues the grid patterns are anchored to. The initial local map might result from the grid maps anchoring to the identical visual cues found in both compartments. The global map that emerges with familiarity of the whole environment may result from self-motion cues, which would provide more disambiguating information regarding the rat's location than the identical visual cues found in both compartments, which would give no indication as to which compartment the rat was in.

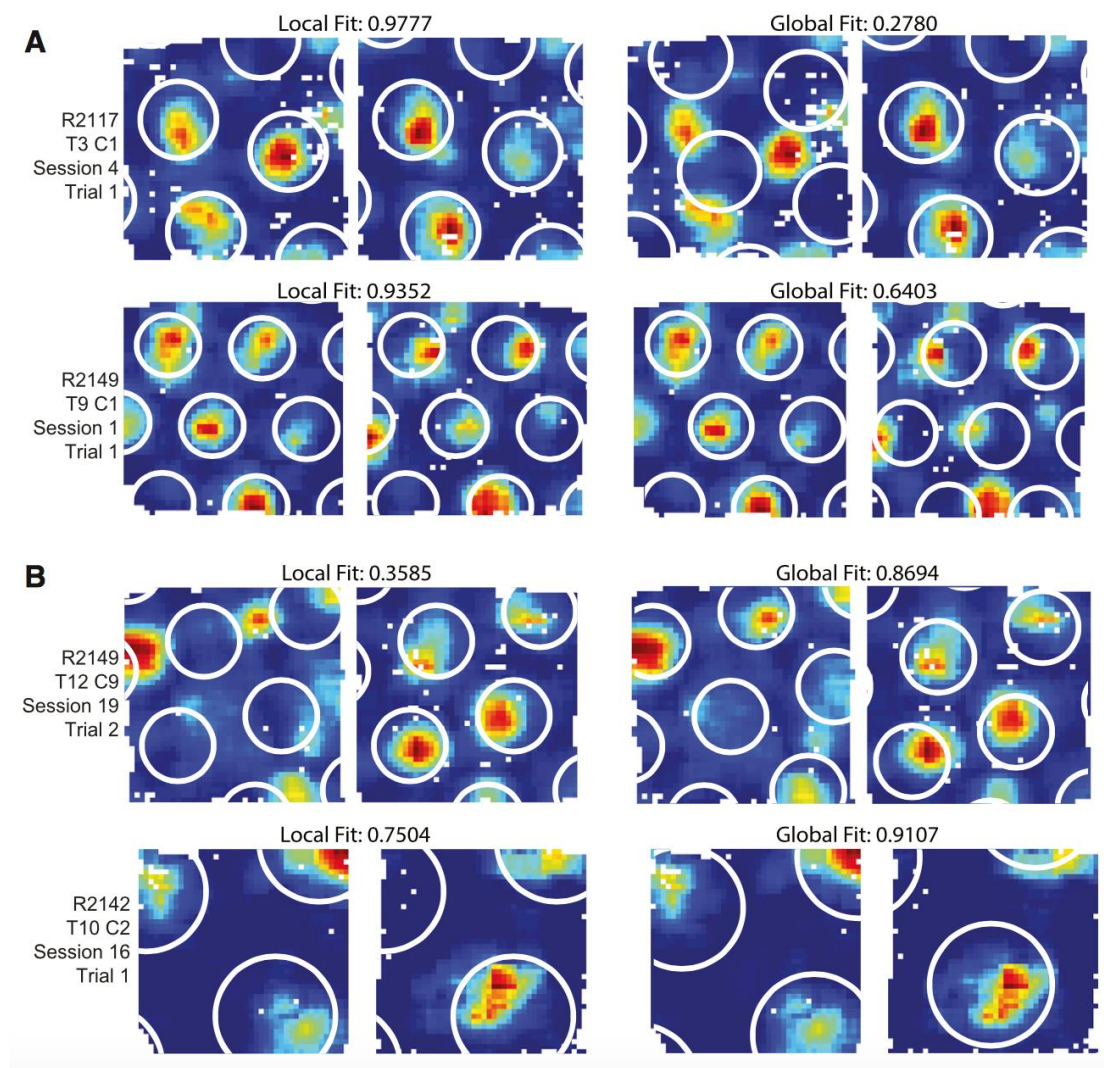


Figure 2.8 Grid cell firing patterns transition from local to global representation with increasing experience.

The fit of local and global models to grid cell firing patterns in two identical compartments. Each row is one cell in one trial. The rate maps in the left and right columns are the same. The white rings indicate the best fitting local or global model for the left and right columns, respectively. The local model best fits the data of grid cells recorded in early sessions (A), whereas the global model best fits the data of grid cells recorded during later sessions (B). Adapted from Carpenter et al., (2015).

In a study by Wernle et al. (2018), rats were tested in a large square arena bisected by a partition, forming two separate compartments. The grid patterns in each usually differed in phase, orientation, or scale. After the rats had become familiar with the environment the bisecting wall was removed. During the first trial without the

partition, the maps were found to maintain their original firing pattern along the distal walls. Along the partition axis, grid cells belonging to the same module merged coherently, whereas grid cells from different modules showed a reorganisation of firing locations. These findings differ from those found by Carpenter et al. (2015), in which the geometry of the environment never changed and exploration between the two compartments was possible. The authors here propose that these different findings indicate that there may be multiple solutions to integrating local grid maps (Wernle et al., 2018). It is possible that different changes in environmental geometry and familiarity may require different solutions, or changes to the grid pattern in order to best represent the environment. It may not be a simple case of one solution fits all.

In a study by Krupic et al. (2015), they recorded the same grid cells in a square and a trapezoid arena, a highly polarized environment. They found that even after 4 days (>2.6 h) of exposure the stable firing fields were still 20-30% larger than when they were recorded from the equally familiar square arena. They also observed a permanent decrease in the gridness score: the pattern was more elliptical and less evenly distributed. When they compared the gridness score in the narrow half of the environment to the gridness score in the wider half they found that gridness was lower in the narrow half and that individual firing fields were larger (Figure 2.9). These findings show that grid patterns are not always homogenous within or between familiar environments and that they do not always return to their intrinsic scale.

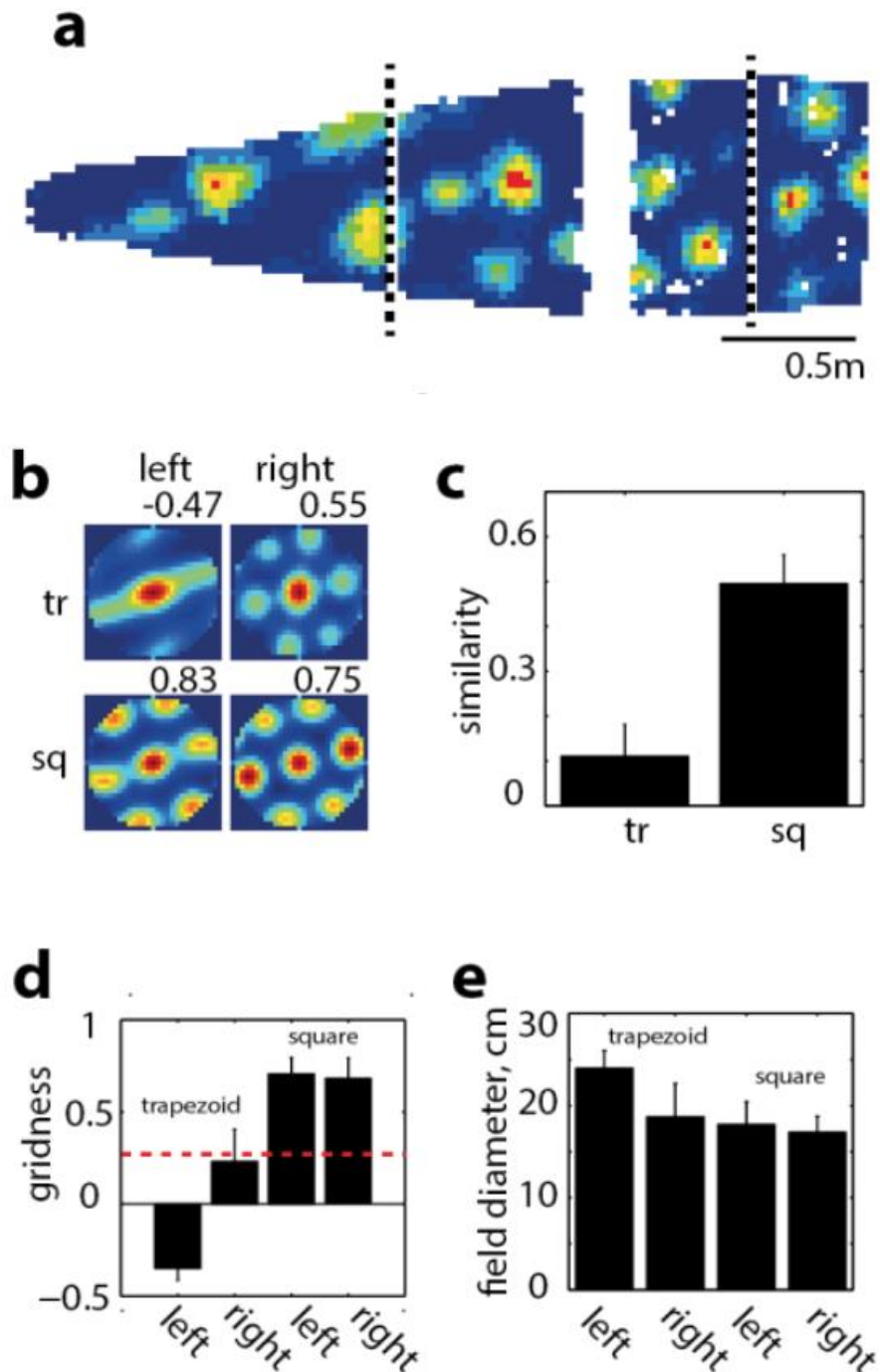


Figure 2.9 Grid patterns are not always homogenous.

a, Grid cell rate maps for the same cell in a trapezoid and square. The dashed line divides the enclosures into equal sections. **b**, **c**, Autocorrelograms for each side of the trapezoid and square are significantly more similar in the square than the trapezoid (**c**). **d**, Gridness for each side of the trapezoid and square. **e**, Field diameter is larger on the left side than the right side of the trapezoid, but not the square. Adapted from Krupic et al., (2015)

This reduced homogeneity found by Krupic et al. (2015) may be explained by a process described by Stensola et al. (2015) called shearing. In their study they found that grid patterns anchor themselves to one or more fixed points in the environment that will resist being moved by environmental boundaries. As an environment becomes familiar the grid pattern will offset itself from the walls by about 7.5° while remaining anchored to one or more points. This causes distortions in the pattern, such as elliptification, that may reduce errors in self-localization within polarized environments, such as a square.

2.5.6 Grids as a spatial metric

With research suggesting that grid patterns are stable across trials and environment, and that they may provide information on an animal's location and distance to or from a goal or starting point, it was widely thought that they served as a universal spatial metric of self-motion (Fyhn et al., 2007; McNaughton et al., 2006; Barry et al., 2012). As mentioned above, more recent studies showing distortions in the grid pattern have brought the idea of grids acting as a universal spatial metric into question (Krupic et al. 2015; Stensola et al. 2015). However, a theoretical analysis by Stemmler et al. (2015) shows that precise symmetry is not needed to successfully decode grid information and that a straightforward decoding system is able to handle large distortions in grid patterns. Additionally, perfect symmetry in the grid pattern may actually lead to errors in self-localization, such as confounding diagonal corners in a square environment (Stensola et al., 2015). By minimizing symmetry, as seen in the shearing process with the 7.5° rotational offset, the frequency of these errors can be reduced.

2.5.7 Anatomical locations of grid cells

Grid cells were first found in layers II and III of the MEC. They have since been found in all MEC layers, but are most abundant in layer II (Fyhn et al., 2004; Sargolini et al., 2006). They co-mingle with border cells and speed cells in all MEC layers and with HD cells in layers III, V, VI (Sargolini et al., 2006; Solstad et al., 2008; Kropff et al., 2015). Grid cells that also exhibit head direction, called conjunctive grid cells, have also been found in layers III, V, and VI (66%, 90%, and 28% of grid cells recorded, respectively) (Sargolini et al., 2006).

Grid cells can also be found in the presubiculum (12.8% of the cell sample) and the parasubiculum (20.3% of the cell sample) and are present in all anatomical layers (Boccarda et al., 2010). The distribution of grid cells was uniform across all layers of these two areas, which is in contrast to the grid population of the MEC where most of the grid cells are located in the superficial layers. Though cells with high grid scores were found in all three areas, the mean score of grid cells in the presubiculum was lower than that of the parasubiculum, which was lower than that of the MEC. The local organisation of grid cells in the pre- and parasubiculum was similar to the organisation seen in the MEC: among neighbouring cells, grid phase was offset relative to one another, whereas orientation and spacing were similar. It has been proposed that layer II of the presubiculum is the principal source of grid activity and that entorhinal grid activity may be inherited from the presubiculum, whose superficial layers have unidirectional projections to the MEC (Preston-Ferrer et al., 2016; Peng et al., 2017). This is supported by Tocker et al. (2015) who suggested that grid fields in the superficial layers of the MEC require organised feedforward projections. Conjunctive cells with grid and head direction were also found in the presubiculum

(8.5% of HD cells) and in greater numbers in the parasubiculum (20.7% of HD cells).

These numbers are similar to those found in the deep layers of the MEC.

2.5.8 Grid cells as place cell input

In 1976, O'Keefe proposed a path integration system that acted as one of two major inputs (self-motion and sensory information) to place cells. This path integration system is closely resembled by grid cells. Several studies have proposed that grid cells form place fields by linearly adding the overlapping fields of multiple grid patterns (10-50) with different spatial scales and similar phases (Fuhs & Touretzky, 2006; Solstad et al., 2006; Gorchetnikov & Grossberg, 2007). One prediction of this summation model is an increase in the size of place fields after inactivating grid cells with short wavelengths and a decrease in the size of place fields after the inactivation of grids with large wavelengths. Since the average wavelengths of grid cells in the MEC increases along the dorsoventral axis, researchers were able to test this prediction by inactivating these two areas and comparing the effects on place fields. However, their results did not match the models prediction. Ormond and McNaughton (2015) reported an increase in place field size after both dorsal and ventral MEC inactivation. Another study reported no change to the size of place fields of dorsal or ventral MEC inactivation (Miao et al., 2015).

If grid cells contribute to the formation of place fields, it is unlikely that they do so alone. Border cells, which also project to the hippocampus, may drive the activity of place cells with firing fields near local borders (Zhang et al., 2013). This is consistent with the finding of Muessig et al. (2015) that stable place fields are more common in rats at an age when border cells and head direction cells, but not grid cells, display adult like activity (Bjerknes et al., 2014, 2015). Muessig et al. (2015) also observed that

stable place fields appear in central locations of the environment at the same time that grid cells begin to produce adult-like grid patterns (Langston et al., 2010; Wills et al 2010). This suggests that place fields in more central locations may rely more on grid cells and path integration.

Several studies have suggested that place cells may contribute to the formation grid patterns (Bonnievie et al., 2013; Mizuseki et al., 2011). In a study by Mizuseki et al. (2011), it was found that principal neurons in the MEC fired after principal cells in the hippocampus during movement related theta. Following the inactivation of the hippocampus, Bonnievie et al. (2013) observed that grid patterns were eliminated. A study by Bush et al. (2014) considers that grid cells and place cells may not be successive stages of a processing hierarchy, but that they may actually provide complimentary spatial representations (i.e. grid cells providing self-motion information and place cells providing sensory information) that work together to support reliable coding of the environment.

2.6 Speed cells

Speed cells are the most recently discovered spatial cell. These cells are characterized by a positive linear response to running speed; as an animal increases its running speed, speed cells increase their firing rate. This information can be used to accurately decode an animal's running speed and only requires the activity from a small population of 4-6 speed cells (Kropff et al, 2015). The response to running speed is independent of visual input (e.g. different testing location and in light vs. darkness) and task (e.g. free foraging and being compelled to move by a bottomless cart). This supports the idea that the speed signal may be derived from proprioception or motor-efference information and that they dynamically update grid cell activity based on the

animal's locomotion. Research by Kropff et al. (2015) found that the firing rate of speed cells in the MEC was more strongly correlated with an animal's future speed than with past or present speed. This was observed during different tasks and only in theta modulated speed cells (37% of all speed cells). When all of this is taken into consideration it appears that speed cells play an important role in path integration and that path integration may occur on a theta-cycle basis.

Speed cells are found across all layers of the MEC (~15% of cells recorded). Cells with similar characteristics have been found in the hippocampus (~10%). There has also been a report of one in the presubiculum (O'Keefe et al., 1998; Lever et al., 2003; Kropff et al., 2015). Few speed cells from the MEC population exhibit other spatial characteristics, unlike speed cells found in the hippocampus, which also signal place (McNaughton et al., 1983; Czurko et al., 1999).

2.7 Aims of this thesis

The general aim of this thesis was to investigate the enhancing effects that environmental boundaries have on grid cells. The main thrust of much of the work on environmental boundaries and grids cells has been to show that boundaries have global or proximal effects upon grid cells. To my knowledge, previous work has not specifically addressed the question of how cues in given locations enhance the spatial firing of grid cells in distal locations. In fact, the bulk of this sort of research has focused on the global effects of boundaries upon grid cells (Carpenter et al, 2015; Krupic et al, 2015; Stensola et al, 2015). Where the analysis has not been global, but where analysis has been sensitive to the distance from particular boundary cues, the emphasis has generally been on showing boundary effects on grid cell firing patterns

are exerted in space proximal to the boundaries in question (Krupic et al, 2018; Wernle et al., 2018). In Experiment 1, my approach was more specifically guided to examine how environmental boundaries may have an enhancing effect on spatial firing in grid cells. I tested the specific hypothesis that due to lower uncertainty of spatial localization associated with the wall condition (all 4 walls attached to a square arena) versus the drop-edge condition (3 walls attached and the 4th wall removed), gridness would be higher when the 4th wall was attached compared to when it was not attached. The set-up of this environment also allowed me to see if an increase in gridness might also apply to space distal to the manipulated boundary, not just the space immediately adjacent to it.

In Experiment 2, the key hypothesis was that a barrier in the environment would reduce spatial uncertainty, and that this would reduce spatial scale. Spatial uncertainty would be reduced because of the addition of an extra space-defining cue, (both visual and somatosensory) to guide distance judgements. This hypothesis was based on two previous studies : 1) a simulation run by Towse et al. (2014), which showed that the optimal overall scale for a grid system represents a trade-off between maximizing precision (requiring small scales) and minimizing spatial uncertainty (requiring large scales) and 2) Hardcastle et al. (2015) which showed that grid cells accumulate error relative to the time and distance traveled and that this error is corrected by encountering environmental boundaries. Considering these two findings together, it seems that it might be the case that in environments where the average distance to boundaries is reduced, that there would be less error and less uncertainty about their location and thus grid scale would be smaller. To my knowledge, there is relatively little work speaking directly to the relationship between grid scale and

uncertainty, and all such work uses environmental novelty to elicit uncertainty (Barry 2007; 2012). In saying the main aim of this experiment was to test a non-novelty based manipulation, this of course does not deny that the manipulation involves novelty. Initially, the inserted barrier cue would be presumed to increase uncertainty, because it is not predicted. Thus, it is reasonable to predict that grid scale is not immediately smaller in the barrier-present condition, and is perhaps initially larger. However, with experience, grid scale is predicted to become smaller in the barrier-present condition than the barrier-absent condition.

3 Chapter 3 Methods

3.1 Ethics

All experiments and procedures were conducted in accordance with the Animals (Scientific Procedures) Act 1986. Experiments were performed under the Home Office project licenses of the supervisory team and the personal license held by myself.

3.2 Subjects

All experiments used male Lister-Hooded rats (bred in-house or purchased from Envigo, Huntingdon, UK), weighing between 387 g and 422 g at time of surgery. The rats were kept on a 12:12 hour light: dark cycle, with lights off at 10am. Water was *ad libitum* and the rats were food restricted to 85-90% of their free-feeding weight to encourage foraging during testing.

The rats were given at least 7 days habituation to the lab prior to testing. Animals lived in their home cage groups until selected for surgery. Before surgery the rats were housed in groups in cages (51 x 32 x 23 cm). After surgery they were housed individually in cages (56 x 39 x 30 cm). Cage substrate was woodchip bedding and paper towels for nesting. Food restriction began no earlier than 1 week post-surgery.

3.3 Recording apparatus

3.3.1 Electrodes

Electrodes were made from 25 μm HM-L-coated platinum iridium wire (90%/20%) (California Fine wire, Grover Beach, CA). To improve the quality of signal discrimination based on spatial position, the electrodes were configured into a tetrode formation. To create a tetrode, a length of the aforementioned wire is curved into a

loop by taping both ends together. The curved end of the electrode is then carefully hooked by a bent needle and brought to meet the taped ends of the electrode. The needle is then pierced through the tape to hold the electrode ends and curve together. This forms two loops, which are then slid over a rod and held in place by the weight of the needed. Each loop has two pieces of wire hanging down from the loop for a total of four. These four pieces of wire are then twisted together using a magnetic spinner (20 times per cm of wire). They were cut at the twisted end to produce 4 spatially-proximal tips. The two loops were stripped of their insulation and then cut to produce four loose ends.

3.3.2 Microdrives

A cannula was attached to the main screw of either a 16-channel or 32-channel moveable microdrive using dental cement (Figure 3.1). A sleeve was slid onto the cannula and held in place with blu tack (replaced with Vaseline before surgery). Four (for 16-channel microdrives) or eight (for 32-channel microdrives) tetrodes were then loaded into the cannula so that the four spatially-proximal ends of each tetrode emerged from the sleeve end of the cannula and the loose ends remain outside of the back of the cannula. Each of the loose ends were wound around one of the 16 or 32 posts located on the sides of the microdrive. They were then painted with a silver conductive paint, which was then covered with nail varnish. After all of the tetrodes had been loaded, a small amount of super-glue was used to hold them together near the cannula end to help ensure a close configuration at the tips (<500 μ m), and to ensure the stability of this configuration. The tetrodes were then trimmed to the desired length.

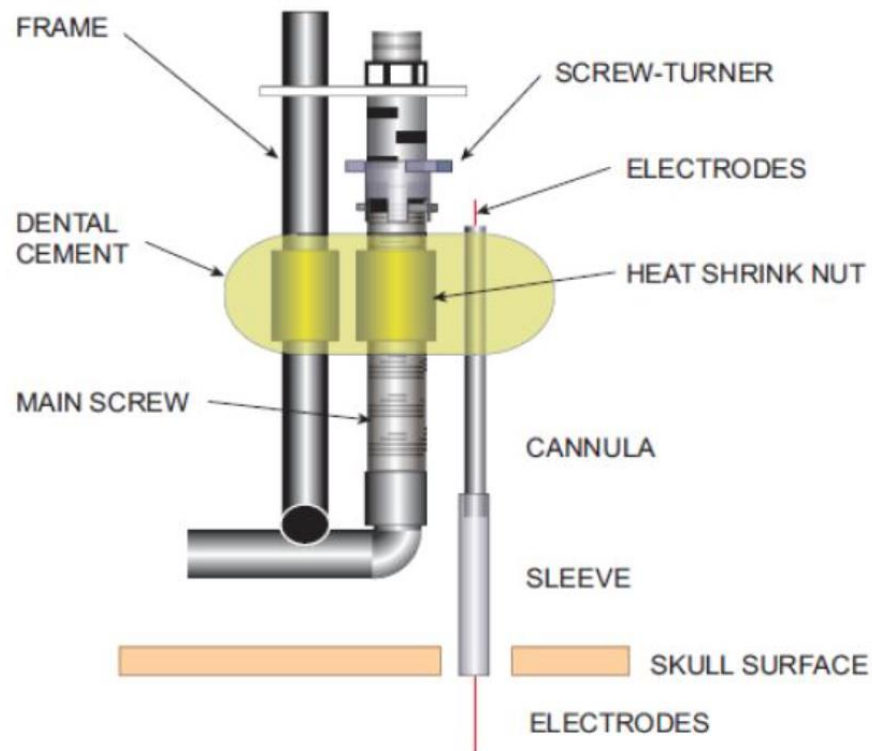


Figure 3.1 Illustration of microdrive frame.

Each Microdrive was fixed to the skull with dental cement. The cannula containing the tetraode was lowered down by turning the screw-turner anti-clockwise. Adapted from a diagram by John Huxter.

3.4 Surgery

Three rats were implanted with one 16-channel microdrive in each hemisphere, and one rat with one 32-channel microdrives in each hemisphere, while under deep anaesthesia. Thirty minutes before induction the rats were given subcutaneous injections of an analgesic [buprenorphine (Vetergesic; Reckitt Beckinser, Hull, UK), 0.4ml-0.8ml, i.m.]. General anaesthesia was induced using a combination of isoflurane (3% of the gas volume) and oxygen (flow rate: 3 l/min). Once the rats were anesthetized, the surgery site was shaved and the rats were given subcutaneous injections of antibiotic [enrofloxacin (Baytril; Bayer, Newbury, UK), 0.3ml, s.c.] and saline. After the injections were given, the rats were fixed into the stereotaxic frame.

In order to assess the stability of the anaesthesia the rats breathing was closely monitored. The isoflurane was gradually reduced to 1-2% as the surgery proceeded. A topical antiseptic (Betadine; Seton Healthcare LTD Oldham, UK) was applied to the surgery site and wiped off with surgical spirit (70% ethanol). Before making the incision, the surgeon made sure the rat was fully anaesthetised by pinching the animal's toe/tail and lightly touching its eye with a cotton swab. The rat's eyes were then covered with Vaseline to prevent them from drying out. The incision was made with a 1.5 cm scalpel and the tissue pulled back to give a clear view of the bregma and lambda brain plate joints. 7-8 screws (3-mm diameter, Precision Technology Supplies, East Grinstead, UK) were fitted into the skull to assist the attachment of the microdrive and increase drive stability. One screw with 2 pre-soldered wires attached acted as a ground. These wires were soldered to the ground wires attached to the microdrives towards the end of the surgery.

After the screws were in place, a trephine hole (1.5mm diameter) was drilled into each hemisphere. The location of each trephine hole was determined using pre-chosen stereotaxic coordinates measured from bregma (Table 3.1 Target implant coordinates for each rat). The microdrives were stereotaxically positioned into place, one at a time (right then left), so that the ends of the tetrodes were located 1.5- 2 mm above the target brain region. This was done to prevent accidentally moving the tetrodes past the target brain region before having a chance to screen for cells. The protective sleeve was then carefully lowered down onto the surface of the brain to cover the exposed part of the tetrodes to protect them from any damage. Sterile Vaseline was also placed on the exposed part of the brain and base of the sleeve as well as the top of the sleeve to prevent any dental cement from adhering to the brain

and tetrodes. The microdrives were then fixed to the skull by applying dental cement to the sleeve, screws, drive feet, and exposed skull. The surgery for one rat (480) was performed by another member of the lab (Dr. Steven Poulter).

Targeting the Presubiculum

The region targeted for this study was the dorsal presubiculum. Grid cells were first identified in the presubiculum in Boccara et al (2010). The presubiculum was chosen primarily because the grid cells in the presubiculum are much less well-studied than those in the entorhinal cortex and parasubiculum (Boccara et al, 2010; Krupic et al., 2012). To my knowledge, grid cells in the presubiculum have always been recorded in the dorsal presubiculum (Boccara et al, 2010). The intended centroids of the tetrode arrays for each of the eight hemispheres in the four rats are shown in Table 3.1.

Table 3.1 Target implant co-ordinates for each rat.

This table contains the target coordinates for the tetrode arrays implanted in each rat. The coordinates were selected based on Paxinos and Watson (2005) and are given in mm, relative to bregma. The spacing between the tetrodes of each array is also given in mm.

Rat no.	469		474		475		480	
Hemisphere	LH	RH	LH	RH	LH	RH	LH	RH
Drive type	16 channel	16 channel	16 channel	16 channel	16 channel	16 channel	32 channel	32 channel
AP	-6.6	-6.6	-6.6	-6.6	-6.6	-6.6	-6.1	-6.0
ML	2.8	3.1	2.8	2.8	2.8	2.8	3.0	3.2

3.5 Data recording

3.5.1 Head position and orientation and running speed

The rat's head position was tracked using two arrays of small, infrared light-emitting diodes (LEDs) located on opposite sides of the headstage. One array was comprised of four LEDs and the other of two. The Two LED arrays were separated by ~4 cm and were centered above the rat's head. A video camera and position-detection hardware and software (DACQUSB, Axona, St Albans, UK) tracked the two arrays based on their differential size and brightness. The rat's position was sampled at a rate of 50 Hz.

3.5.2 Single-unit recording

During recording, each rat was connected to the recording system (Axona, St Albans, UK) by headstage amplifiers, which were plugged into each microdrive before each session (see Figure 3.2). The headstage amplifiers were unity-gain buffers, which isolated the electrodes from the wires transmitting their signals to the preamplifier. The implanted electrodes were AC-coupled to these amplifiers. The wires (2-3 m) transmitting the signals were light, flexible, and slack enough to allow the rat to freely explore the entire testing arena. The signals on the channels dedicated to single-cell recording were amplified 7,000–18,000 times and bandpass filtered at 500 Hz-7 kHz. All channels on a given tetrode were recorded differentially against a channel (reference channel) on another tetrode within the same hemisphere. This helped to remove most of the common background noise. Each channel was continuously monitored at a sampling rate of 50 kHz. Whenever the signal from the recording channels exceeded the trigger threshold (set at 60% of baseline to ceiling value) the action potentials were recorded as 50 samples (1 ms: 200 μ s pre-threshold and 800 μ s

post-threshold). The gains (amplification) and reference channels were set each day before recording and kept the same for all trials on that day.

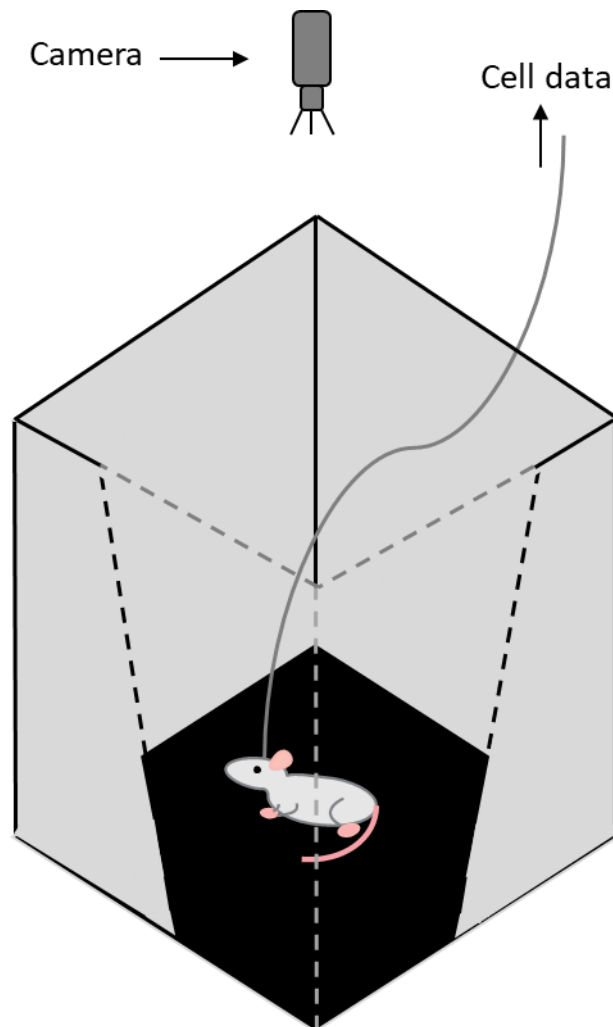


Figure 3.2 An Illustration of the testing arena; a square, walled open field.

3.6 Materials

3.6.1 Laboratory layout

During screening and testing the room was lit with a lamp located in the northwest corner of the room on top of a desk (Figure 3.3). The cue cards remained in the same positions for all trials and manipulations.

During screening and intertrial intervals the rats rested on top of a holding platform covered with woodchip bedding located in the north northeast of the room.

The top of the platform was 44cm x 44cm with 5.5cm high ridges around the perimeter and was elevated 90.5cm off of the ground.

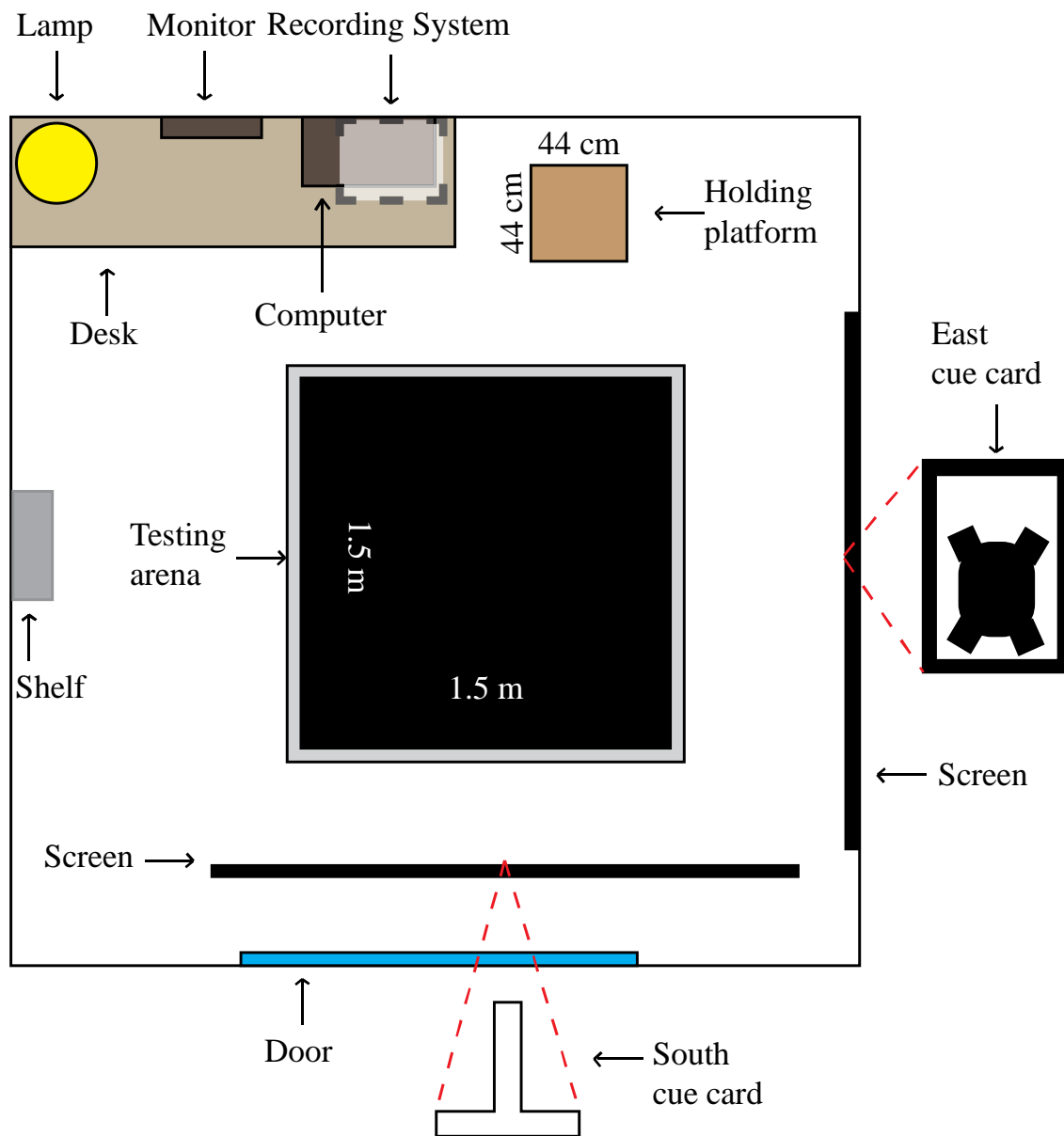


Figure 3.3 Bird's eye view of laboratory.

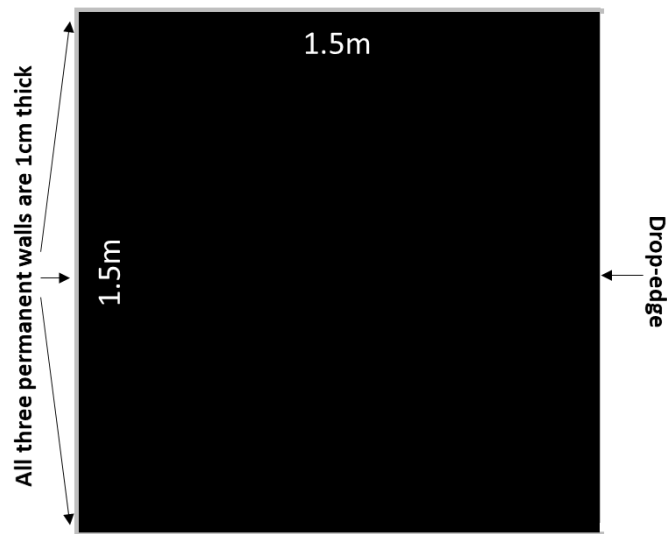
The rats experienced all experimental trials in this test environment and were placed on the holding platform during screening sessions and inter-trial intervals. For convenience, I refer to the top and right-hand side of the lab in this figure as the North side, East side, and so on.

3.6.2 Test environment and materials

A purpose built 1.5m x 1.5m square arena with a black floor and grey walls was used in both experiments. The arena floor rose 39cm above the ground. The walls rose

50 cm above the arena floor and could be removed individually. During Experiment 1 either the east wall or west wall was removed during the 1st and 6th trials (i.e. trials A and F) (Figure 3.4A) and attached during the 2nd, 3rd, 4th, and 5th trials (i.e. trials B, C, D, and E) (Figure 3.4B). During Experiment 2 all 4 walls remained attached throughout the session. A grey barrier (100 cm x 30 x 50.5 cm) was inserted into the arena (perpendicular to the South wall, apposing the South wall exactly halfway along its length) for trials B, C, D, and E (Figure 3.5B) and removed for trials A and F (Figure 3.5A).

A Environment configuration during baseline trials (trials A and F)



B Environment configuration during manipulation trials (trials BCDE)

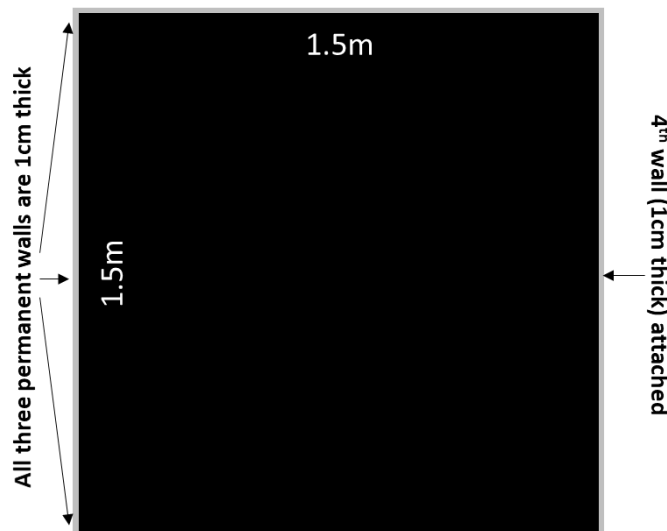
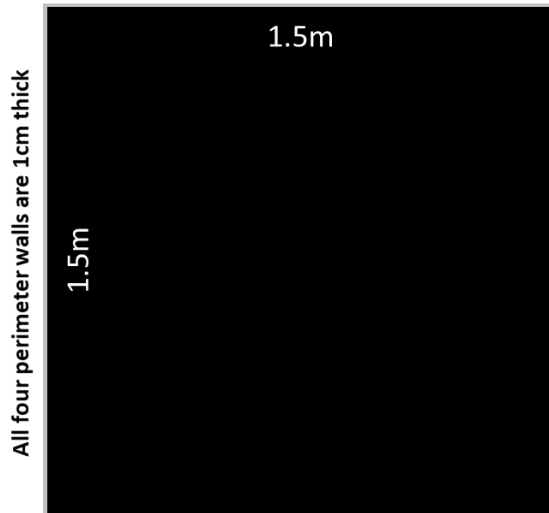


Figure 3.4 “To-scale” drawing of Environmental configurations during baseline trials (A) and manipulation trials (B) of Expt 1 to show box-to-walls ratio more accurately.

During experiment a 1.5 m x 1.5 m square arena with a black floor and grey walls was used. The walls (each 1 cm thick) rose 50 cm above the arena floor and could be removed individually. Either the east wall or west wall was removed during the 1st and 6th trials (i.e. trials A and F) and attached during the 2nd, 3rd, 4th, and 5th trials (i.e. trials B, C, D, and E). The same wall was removed for the same rat during all baseline trials.

A Environment configuration during baseline trials (trials A and F)



B Environment configuration during manipulation trials (trials BCDE)

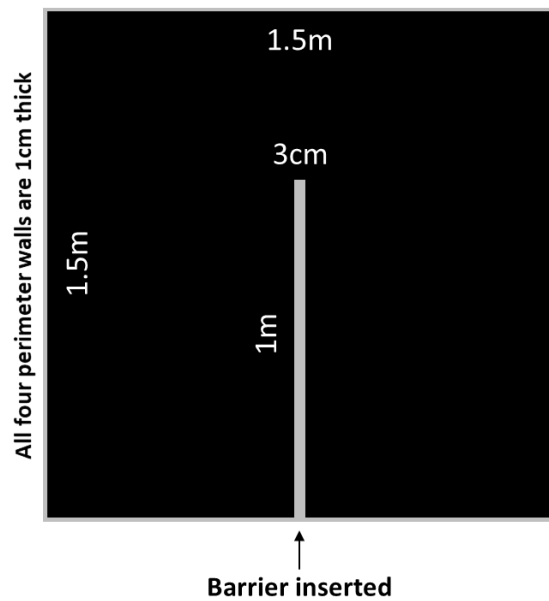


Figure 3.5 “To-scale” drawing of Environmental configurations during baseline trials (A) and manipulation trials (B) of Expt 2 to show box-to-walls ratio more accurately.

The same arena used for Experiment 1 was used for Experiment 2. All 4 walls remained attached throughout the experiment. A grey barrier (100 cm x 3 cm x 50 cm) was inserted into the arena (perpendicular to the South wall, opposing the South wall exactly halfway along its length) for trials B, C, D, and E and removed for trials A and F.

3.7 Experimental procedure

3.7.1 Screening and training

The rats were given one week of post-surgery recovery before screening. Before each screening session the recording system cables were attached to the rats headstage. During screening the rat was free to move around the holding platform. Over the weeks of screening the tetrodes were vertically lowered toward the desired brain region by in steps of 50 μ m-100 μ m. As the tetrodes neared the target region the steps were reduced to 25 μ m-50 μ m. This slow, progressive movement of the tetrodes ensured better stability of the tetrodes within the surrounding tissue.

Before Experiment 1 began, three of the rats (rats 469, 474, and 475) were habituated to foraging for sweetened rice and to the 'One wall off' configuration within the testing arena. The absent wall was the West wall for rat 474, and the east wall for rats 469 and 475. I made sure that the rats were able to easily forage for four 40-minute trials (one practice session) before beginning formal testing. Once the rats could do this, and the desired cells were found, formal testing could begin. The rats had 11-17 practice sessions. The amount of practice sessions depended on how long it took to increase their endurance to be able to run a full practice session (5-6 days) and how long it took to locate grid cells. Since the rats gained experience of a 4-walled arena during Experiment 1 (see section 3.8.1), I did not need to habituate them to it prior to the start of Experiment 2 where all 4 walls were attached throughout the whole experiment.

The fourth rat (480) had previously been used in another experiment, which used an arena of the same shape, size, and colour as mine with all four walls attached. Since this rat already had experience of a 4-walled arena, which was novel to the other

3 rats, I decided to have him complete Experiment 2 first, then Experiment 1 if grid cells were still present. As the previous experiment also required rat 480 to be able to run for six 40-minute trials, the start of Experiment 2 only depended on the rat becoming habituated to my lab room and arena, and locating grid cells- a process that took 3 days. After completing Experiment 2, I started testing the rat on Experiment 1 with a western drop-edge. I made the decision not to habituate him to the drop-edge prior to testing for two reasons: 1) I was losing cells 2) To compare changes in grid properties caused by switching from a familiar drop-edge to a novel 4th wall versus switching from a novel drop-edge to a familiar 4th wall.

3.7.2 General procedure

The rat was brought into the laboratory and placed onto the holding platform located to the north-northeast of the testing arena. The recording system cables were then attached to the rat's headstage for screening. At the start of each trial during Experiment 1, the rat was carried from the holding platform to the testing arena and placed in the centre of the arena. During experiment 2, the rat was placed in front of the north wall facing south at the start of each trial. This was done because a barrier bisected the southern 2/3rds of the arena along the north-south axis during trials 2-5. Recording began within 0-10 seconds of placing the rat in the arena, and ended about 5-15 seconds before the rat was taken out of the arena. Each trial lasted 40 minutes to give the rat adequate time to cover the entire arena. Inter-trial intervals lasted 20 minutes to allow the rat plenty of time to rest before the next trial began. Importantly, on all experimental trial days, a baseline 'warm-up' trial of 20 minutes duration (i.e. 50% of typical trials) was always run prior to the formal session of 6 trials, with the standard 20-minutes intertrial interval. This was done to avoid 'warm-up' effects in the

experimental session, whereby the first trial of the day may systematically differ from other trials for reasons unrelated to the manipulation. For instance, on the first trial of the day, rats typically rear more, theta frequency is typically lower, and place cells may fire less in at least the first few minutes of the trial (Lever et al., 2006, Jeewajee et al., 2008; Frank et al., 2004).

3.7.3 Task

A standard foraging task was used for all testing. During all trials the rats foraged for cooked rice that had been sweetened with honey. As I walked around the arena during trials, I threw the rice in at approximately $\frac{1}{2}$ a grain per minute. The majority of the rice was thrown into the arena pseudo-randomly. If the rat had not spent much time in an area of the arena, I would encourage the rat to visit it by throwing rice into that area. During each trial, I was able to monitor the rat's path through the LED tracking captured by the recording software (DACQ USB, Axona, St Albans, UK).

3.8 Experiments

3.8.1 Experiment 1

This experiment consisted of 10 sessions (1 per day) and 6 trials (A, B, C, D, E, and F) a session, after the initial 'warm up' trial. Trials A and F of sessions 2-9 were baseline (3 walls on, one off). Due to environmental restrictions, only the east or west wall was ever removed. For each rat, the same wall was removed for all baseline trials. During trials B, C, D, and E the 4th wall was put back on so that all 4 walls were attached to the arena (see Figure 3.6A). All trials on the first day and tenth day were baseline. Between each trial was a 20-minute inter-trial interval. This allowed the rat time to rest and me time to prepare for the next trial (e.g. attaching the 4th wall). Rats

474 and 475 completed all 10 sessions (Table 3.2). Rat 469 did not receive the final session. Rat 480 only completed the 1st two sessions before losing all grid cells.

Table 3.2 Each rat’s experience of the wall-off wall-on manipulation.

This table includes the order in which this manipulation was received in relation to the barrier-in barrier-out manipulation, and which sessions each rat completed. An X indicates that the rat completed the session and a – indicates that they did not.

Rat	Manipulation order	Session number							
		EARLY				LATE			
		1	2	3	4	5	6	7	8
469	1 st	X	X	X	X	X	X	X	X
474	1 st	X	X	X	X	X	X	X	X
475	1 st	X	X	X	X	X	X	X	X
480	2 nd	X	-	-	-	-	-	-	-

3.8.2 Experiment 2

This experiment also consisted of 10 sessions (1 per day) and 6 trials (A, B, C, D, E, and F) a session, after the initial ‘warm up’ trial. Trials A and F of sessions 2-9 were baseline (all 4 walls attached to the arena). During trials B, C, D, and E, a barrier (100 cm x 3 x 50.5 cm) was inserted into the arena along the north-south axis with the southern edge of the barrier touching the southern wall (see Figure 3.6B). All trials on the 1st and 10th day were baseline. Between each trial was a 20-minute inter-trial interval. This allowed the rat time to rest and me time to prepare for the next trial (e.g. inserting the barrier). Again, 469 did not receive the final session (Table 3.3). Rat 474

only completed the 1st four sessions before losing all grid cells. Rats 475 and 480 completed all 10 sessions.

Table 3.3 Each rat’s experience of the barrier-in barrier-out manipulation.

This table includes the order in which this manipulation was received in relation to the wall-off wall-on manipulation, and which sessions each rat completed. An X indicates that the rat completed the session and a – indicates that they did not.

Rat	Manipulation order	Session number							
		EARLY				LATE			
		1	2	3	4	5	6	7	8
469	2 nd	X	X	X	X	X	X	X	X
474	2 nd	X	X	X	-	-	-	-	-
475	2 nd	X	X	X	X	X	X	X	X
480	1 st	X	X	X	X	X	X	X	X

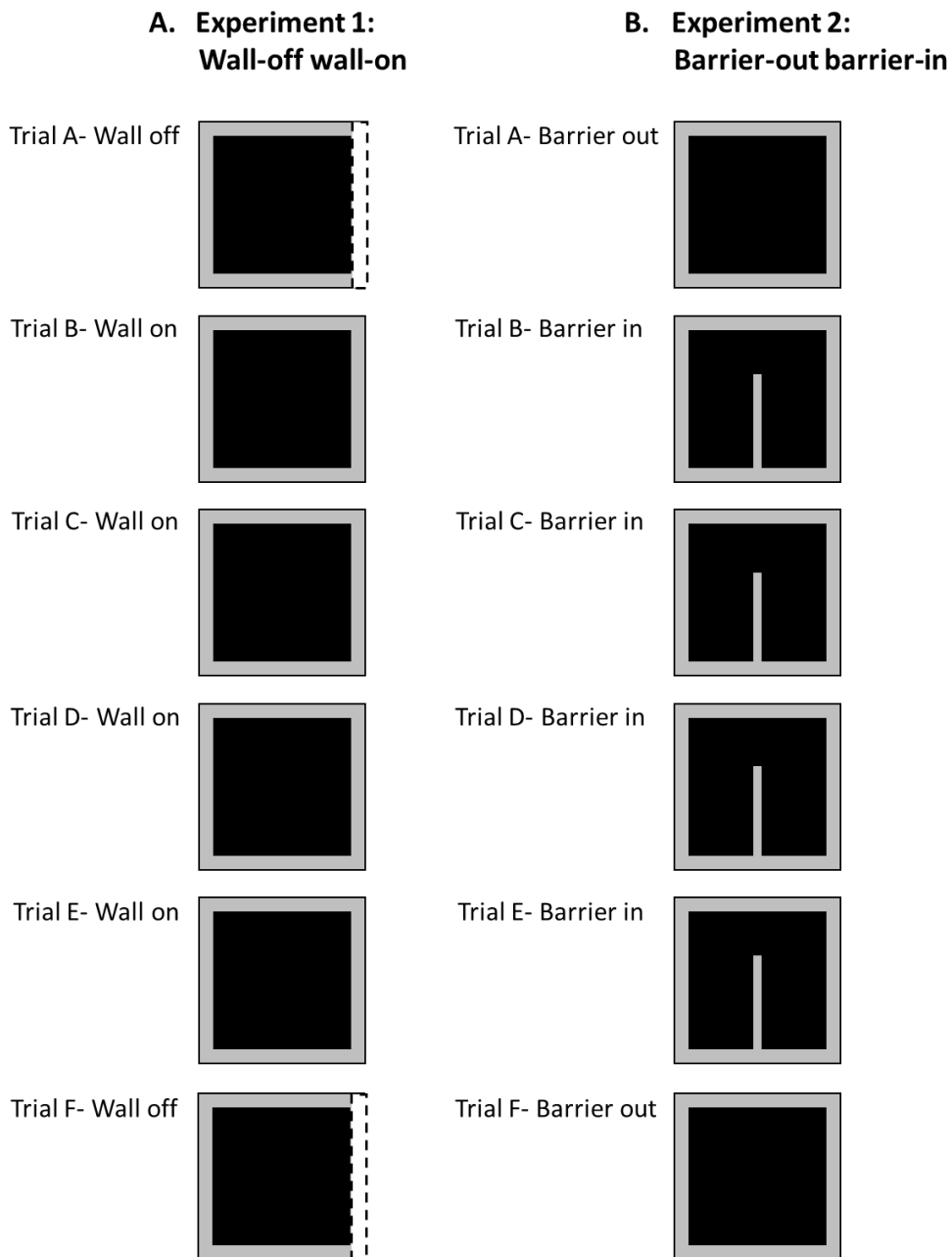


Figure 3.6 Illustration of environmental manipulations.

A) An illustration of the Wall-off wall-on manipulation for manipulation days 2-9. During this manipulation, 2 rats experienced only a western drop-edge during the baseline trials (i.e. trials A and F) and the other 2 experienced only an eastern drop-edge during the baseline trials. For ease, this figure only depicts an eastern drop-edge during the baseline trials. All four walls are attached on trials B-E. B) An illustration of the Barrier-in barrier-out manipulation for manipulation days 2-9. A barrier is placed in the arena, perpendicular to the south wall during trials B-E ('Barrier in'). It is absent during trials A and F ('Barrier out').

3.9 Data Processing

3.9.1 Cluster-cutting

Cluster-cutting is the isolation of action potentials (spikes) with similar features from all other action potentials recorded on the same tetrode during a trial. Each cluster is assumed to represent a single cell. Spike sorting was performed automatically using KlustaKwik (<http://klustakwik.sourceforge.net>). In some instances KlustaKwik overcut (i.e. one cell was split into multiple clusters) or undercut cells (i.e. multiple cells were placed into one cluster). Thus, the automatic spike sorting was followed by some manual cutting using TINT (Axona, St Albans, UK). If two clusters that had been pre-identified by KlustaKwik were overlapping in the cluster space and had similar waveforms across 4 channels they were merged manually. Pre-identified clusters were manually cut apart if they were oddly shaped (not an ovoid), as if two closely positioned clusters were merged together at the side or end, and the waveforms across the 4 channels were not very similar.

Each of the 4 channels corresponds to one of the 4 electrodes that form a tetrode. These channels record action potentials which are placed into two-dimensional scatter plots (cluster plots) where each spike is represented as a dot whose abscissa and ordinate were each a value of a spike feature on one of the channels. The plot axis represents the amplitude of 2 channels or the voltage at time t . This allows each spike to be represented across 6 cluster plots comparing each of the 4 electrode channels belonging to the same tetrode (see Figure 3.7). The discrimination between cells is based on the cluster of each cell having differing peak-to-trough amplitudes (the difference between the maximum and minimum voltages of the action potential) to each other cell across these 6 cluster plots. This is made possible by the

design of the tetrode. If a tetrode is settled among a group of cells, the position of one cell in relation to each of the 4 electrodes will be different to that of another cell, which leads to differences in recorded action potentials. This then leads to differences in position in one or more cluster plots. The time interval between the peak and trough of each waveform was also used to isolate cells. This was done with graphs generated by TINT plotting the voltage of spikes at a particular point in time (Vt) or a combination of both Vt and amplitude.

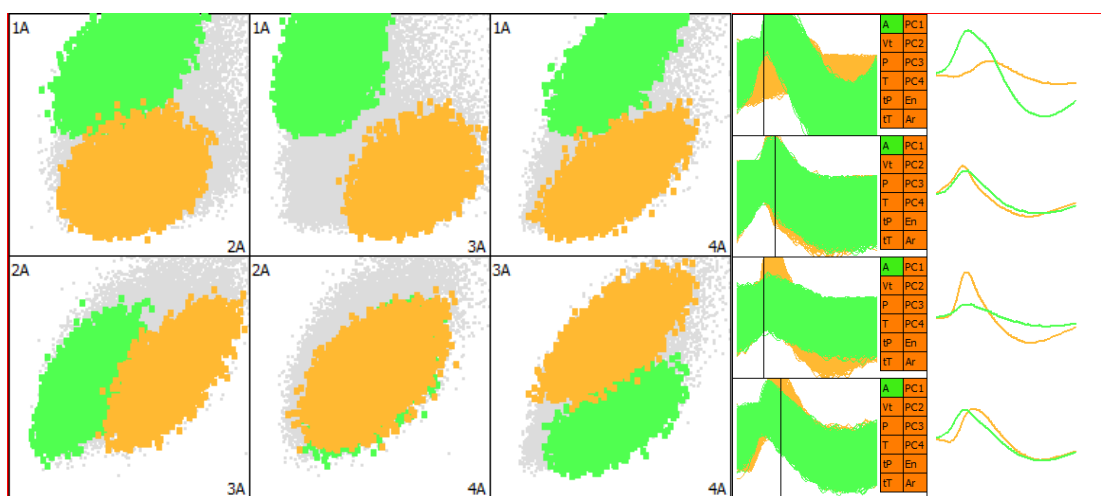


Figure 3.7 Examples of cell clusters and waveforms in Tint.

Examples of grid cell clusters (left) and waveforms (right) from rat 475, tetrode 7. Each cluster is assumed to be a different cell. Each cluster plot illustrates the amplitude (A) of the spikes on two channels simultaneously. The six plots represent all possible pairs of the four channels on the tetrode. The windows to the right show the waveforms of each selected cell's spikes and their averages.

3.9.2 Recording stability

The recording stability was monitored by checking that the position of each cell cluster occupied similar space across trials. For two or three cells in the entire dataset, there was a noticeable shift in the position of the clusters across cluster plots within the same day: in these few cases, the spatial relationship between the cells and the tetrode was considered to be unstable, and such data was not used. In cases where

tetrode instability was difficult to detect visually, a reference trial was superimposed over the other trials using transparency-enabling software (Overlay2). For one of the four rats (480), representing about 15% of the cells recorded, Trial merging software in the Tint platform was used to cut cells consistently across trials. All six trials for a given day's session were merged, cells were cut into clusters from this merged dataset, and then the spikes within each cluster were automatically parcellated into the six trials.

3.10 Data Analysis

3.10.1 Waveform analysis

To investigate differences in waveform amplitude and interval, the peak-to-trough measurements were used (Figure 3.8). These were taken from the negative peak to the positive peak (trough). In the basic properties figures in chapter 4 the peak amplitudes were given as the highest negative-to-positive amplitude (μV), and the waveform interval was given as the negative peak-to-trough interval (μS).

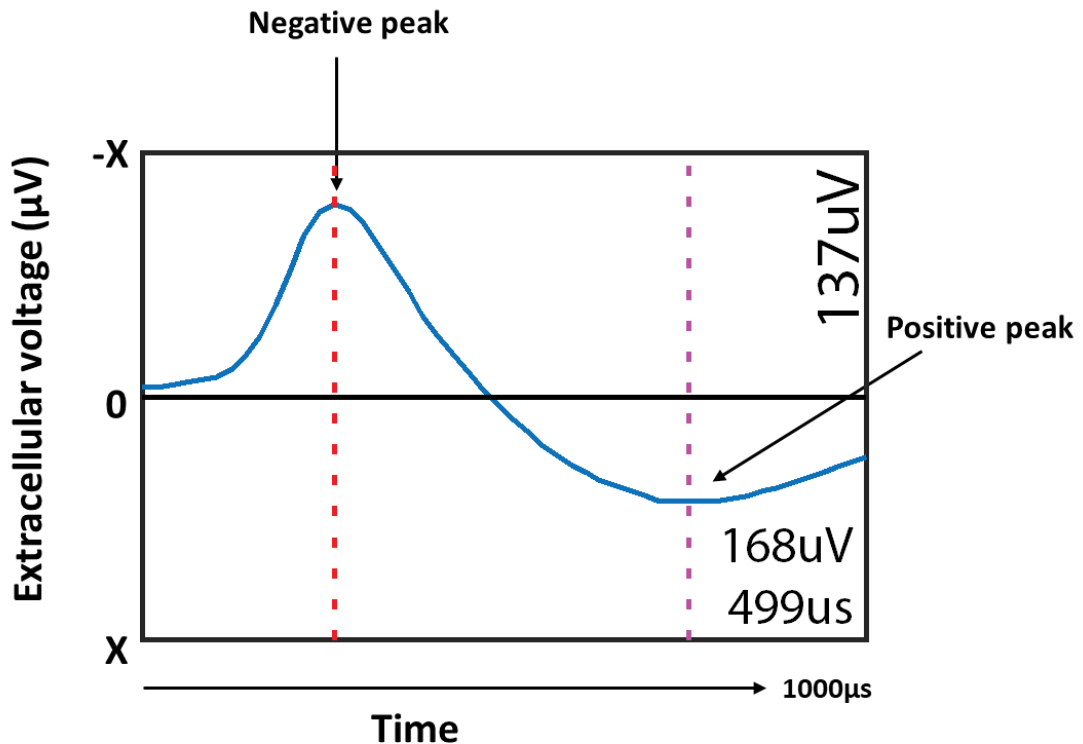


Figure 3.8 Waveform illustration.

This figure gives an illustration of the waveform graph. The Y axis shows the voltage and the X axis shows time. The waveform amplitude and interval are given in the bottom right corner of the graph. These measures are taken from the negative peak to the positive peak.

3.10.2 Figures of spatial firing

All locational firing rate maps shown in the Figures of this thesis were created from 3 x 3 cm binned data and smoothed using a 5x5 bin square around each bin (i.e. boxcar filter). The firing rates in each bin were calculated by dividing the total number of spikes during occupancy of the bin by the total duration of occupancy (i.e. dwell time). These rate maps were autoscaled false colour maps. Each colour represents a 20%-band of peak firing rate ranging from dark blue (0-20%) to red (80-100%). Bins that the rat did not visit are shown in white. The peak rate (after smoothing) for each rate map is shown top left of the map (Figure 3.9).

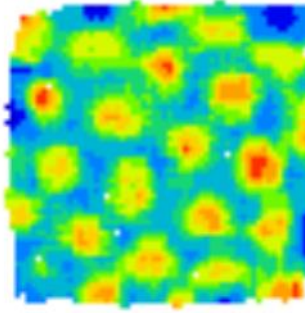
12.1

Figure 3.9 Example rate map of a grid cell.

This figure shows an example of a rate map belonging to a grid cell. Above the map is the cell identification number, which includes the rat number, testing day, tetrode number (T), and cell number (C). At the top left of the rate map is the peak firing rate given in Hz.

3.11 Grid cell analysis

3.11.1 Spatial autocorrelogram

The gridness (or grid score), scale, and orientation of each grid cell was assessed using spatial autocorrelograms of the rate maps. Each spatial autocorrelogram was generated using smoothed rate maps (smoothing was done using a 10cm-side boxcar). Spatial autocorrelograms were calculated as:

$$r(\tau_x, \tau_y) = \frac{n \sum \lambda_1(x, y) \lambda_2(x - \tau_x, y - \tau_y) - \sum \lambda_1(x, y) \sum \lambda_2(x - \tau_x, y - \tau_y)}{\sqrt{n \sum \lambda_1(x, y)^2 - \left(\sum \lambda_1(x, y) \right)^2} \sqrt{n \sum \lambda_2(x - \tau_x, y - \tau_y)^2 - \left(\sum \lambda_2(x - \tau_x, y - \tau_y) \right)^2}}$$

Where $r(\tau_x, \tau_y)$ is the autocorrelation between bins with a spatial offset of τ_x and τ_y , $\lambda_1(x, y)$ and $\lambda_2(x, y)$ are equivalent for an autocorrelation and indicate the mean firing rate in bin (x, y) , and n is the total number of overlapping bins. Correlations were estimated for all values of n . The six peaks surrounding the central-most peak on the

autocorrelogram were defined as the local maxima exceeding $r > 0$ closest to the central peak, but excluding the central peak itself. The extent of each peak was defined as the group of bins surrounding the peak with a value greater than half the value of the peak bin. The size of each bin was 3 cm.

Gridness, a measure of six-fold symmetry present in the spatial autocorrelation, was calculated by rotating the region encompassing the 6 peaks closest to the centre-most peak of the spatial autocorrelogram in 30° increments up to 150° (Figure 3.10B). For each rotation, the Pearson product moment correlation coefficient was calculated against the unrotated mask. Gridness was then defined as the lowest correlation obtained for rotations of 60° and 120° minus the highest correlation obtained at rotations of 30° , 90° , or 150° . Grid scale was defined as the median distance from the central peak of the spatial autocorrelogram to the six closest surrounding peaks (Figure 3.10C).

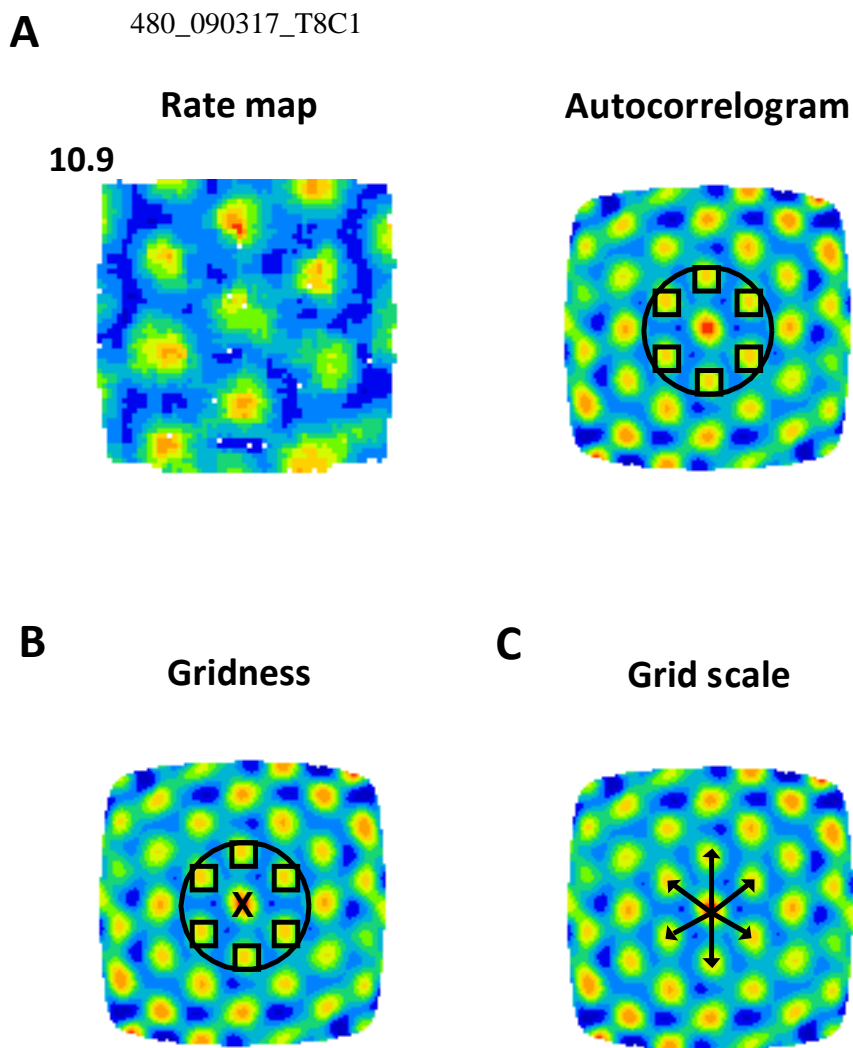


Figure 3.10 Spatial autocorrelation is used to determine the gridness score and grid scale of the grid pattern.

This figure shows a grid cell recorded from rat 480. **A)** Includes the locational rate map(left), with locational peak rate (Hz) shown top left of map, and the spatial autocorrelogram (right). **B)** Gridness calculation was based on defining a mask of the spatial autocorrelation centered on, but excluding the central peak (marked with an x) bounded by a circle passing around the outside of the outermost six central peaks. The gridness score is obtained by rotating the region encompassing the 6 peaks closest to the centre-most peak of the spatial autocorrelogram in 30° increments up to 150°. For each rotation, the Pearson product moment correlation coefficient was calculated against the unrotated mask. Gridness was then defined as the lowest correlation obtained for rotations of 60° and 120° minus the highest correlation obtained at rotations of 30°, 90°, or 150°. **C)** Grid scale was calculated as the median distance from the central peak of the spatial autocorrelogram to the six closest surrounding peaks.

3.12 The number of grid cells recorded

The dataset analysed in this thesis comprises 218 grid cells (103 in Experiment 1 and 115 in Experiment 2) (Table 3.4) and were recorded from 4 rats.

Table 3.4 Grid cell numbers in each experiment.

This table shows the number of grid cells in the manipulation trials, BaselinePre trials, and BaselinePost trials for each experiment.

Trials	Number of grid cells	
	Experiment 1	Experiment 2
Manipulation trials	74	88
BaselinePRE	16	17
BaselinePOST	13	10
Total	103	115

4 Experiment 1: Grid cell responses to a drop-edge and wall attachment

4.1 Gridness analysis

Here, I tested the specific hypothesis that due to lower uncertainty of spatial localization associated with the wall condition (vs the drop-edge condition), gridness would be higher when the 4th wall was attached compared to when it was not attached. As mentioned in the methods section, two rats experienced a western drop-edge (rats 474 and 480) and two rats experienced an eastern drop-edge (rats 469 and 475). In order to make my bar graph figures easier to interpret, I have made all images of the arena with an eastern drop-edge/4th wall.

A 2 x 2 x 2 mixed-design ANOVA was used to examine the factors of wall-state (WALL-ATTACHED vs DROP-EDGE), time-block (EARLY vs LATE), and arena-half (MANIPULATED vs STABLE) on gridness. I comment on these factors in turn.

4.1.1 Gridness increases when the 4th wall is attached

Supporting the above hypothesis, there was a significant main effect of wall-state on gridness, $F(1, 73) = 25.49$, $p = 0.000003$, partial $\eta^2 = 0.26$: gridness was significantly higher when the 4th wall was attached (WALL-ATTACHED trials BCDE: 0.69 ± 0.03) compared to when it was not attached (DROP-EDGE trials AF: 0.53 ± 0.04) (Figure 4.1; Figure 4.2). The absence of a wall-state x time-block interaction ($F(1, 73) = 2.65$, $p = 0.11$, partial $\eta^2 = 0.04$) makes this more interesting. That is, not only did the 4th wall increase gridness relative to the drop-edge during the late time-block (LATE: WALL-ATTACHED trials BCDE: 0.85 ± 0.02 ; DROP-EDGE trials AF: 0.75 ± 0.04 ; $T_{36} = -2.27$, $p = 0.03$) (Figure 4.1C), this effect also occurred during the early time block (EARLY:

WALL-ATTACHED trials BCDE: 0.52 ± 0.05 ; DROP-EDGE trials AF: 0.32 ± 0.07 ; $T_{37} = -3.30$, $p = 0.002$) (Figure 4.1B). This is interesting because the drop-edge condition was the familiar condition. That is, rats had experienced this environment as with three walls and one drop edge for an average of 44-68 trials over 5-6 days before testing began. What this shows is that, relative to a drop-edge condition, which is highly familiar, the fourth wall, which is initially novel in that location, increases gridness. This could be seen to be potentially in contrast with previous studies that suggest that novelty reduces gridness (Barry, 2007; Barry, 2012). However, unlike Barry (2012), which used different arenas of the same shape, in different locations and different rooms, or the same arena deformed into an unfamiliar shape, I used the same arena with the same shape kept in the same location within the same room. This ensured that any differences in gridness that occurred would be the result of attaching the 4th wall.

DROPPED-EDGE gridness vs. WALL-ATTACHED gridness

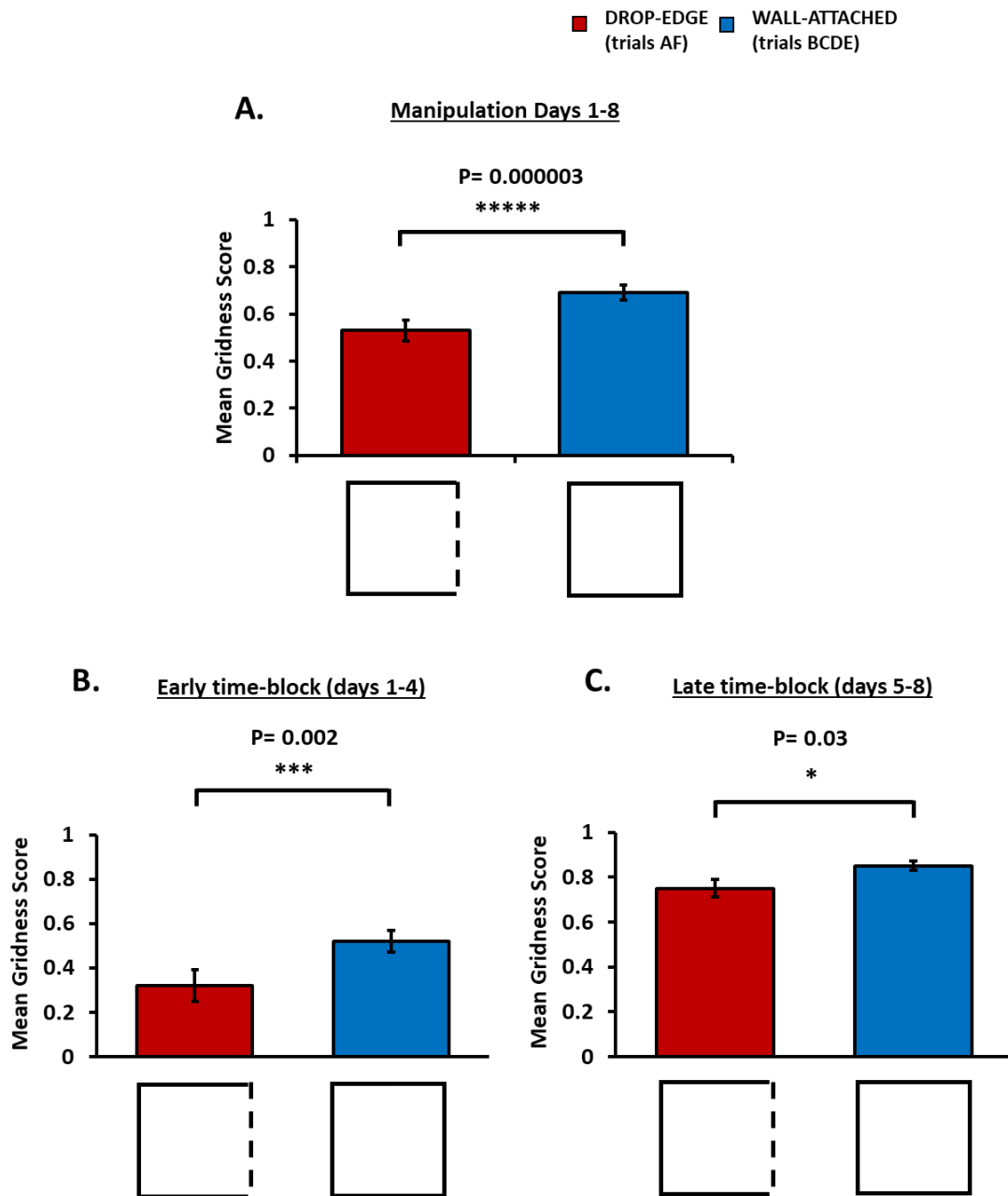


Figure 4.1 Gridness increases when the 4th wall is attached.

This bar graph shows a significant increase in gridness on manipulation days (i.e. days 1-8) when the 4th wall is attached (trials BCDE) compared to when it was not attached and the dropped-edge is present (trials AF) (A). This effect can be seen early (days 1-4) when the 4th wall is relatively novel (B), suggesting that walls provide more certainty than drop-edges.

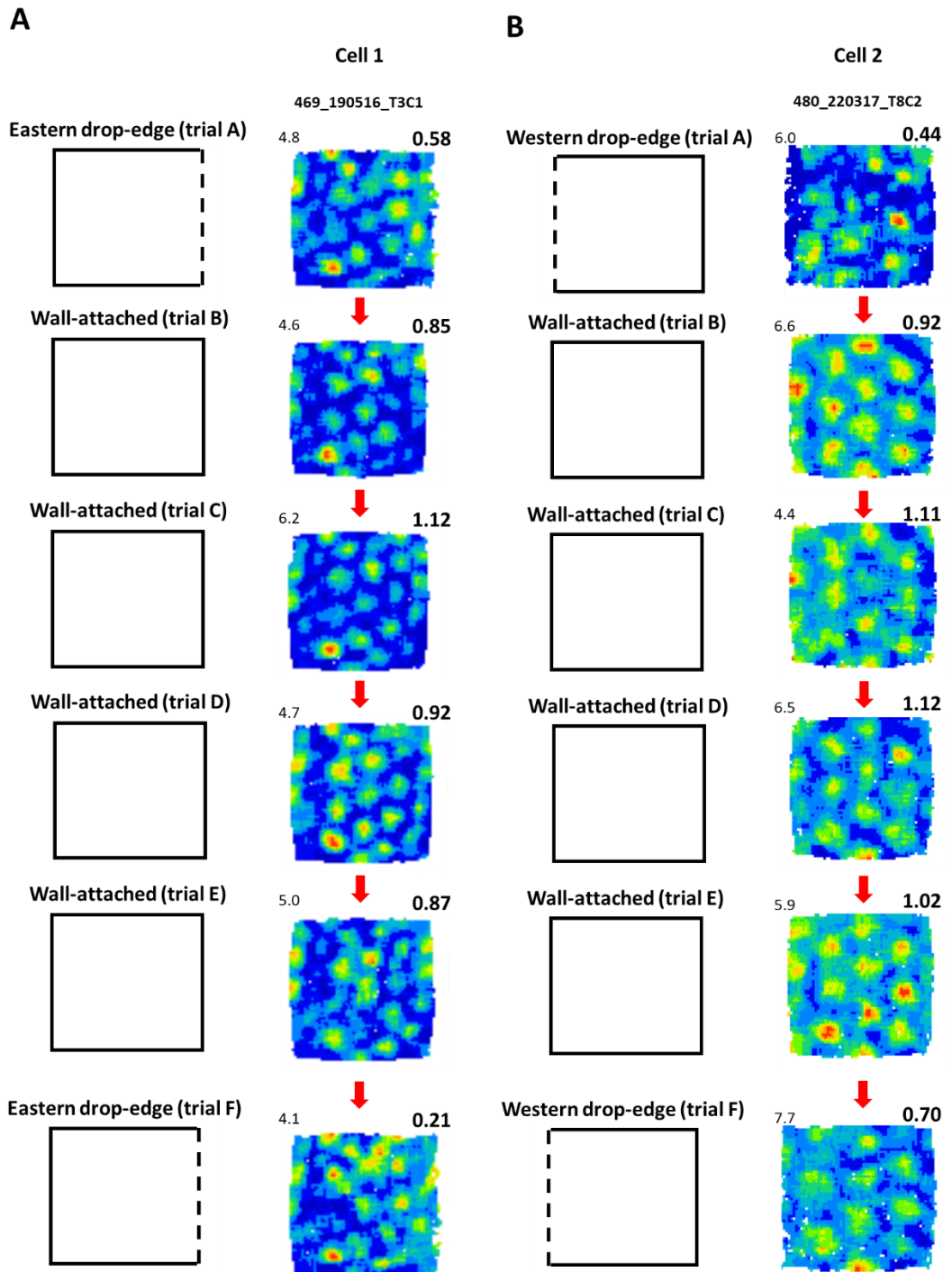


Figure 4.2 Gridness increases when the 4th wall is attached.

This figure shows the rate maps of two different grid cells across all 6 trials of a session from experiment 1. Gridness scores are located at the top right of each rate map. Part A shows a cell from one of the rats that experienced the eastern drop-edge on day 6 and part B shows a cell from one of the rats that experienced the western drop-edge on day 1.

It is unlikely that these results are due to order effects, i.e. that somehow the day's middle trials (trials BCDE) would have higher gridness than early and late trials in the day (trials A & F). Note that, as mentioned in the Methods, at the beginning of each day, each rat experiences a familiarization pretrial of 20 minutes in the environment before the day's first experimental trial, that is, before trial A. Further, although only a small number of cells were available for analysis on a baseline day after the manipulations (BaselinePOST), there was no sign that gridness on trials BCDE was higher than that on trials AF. If anything, the gridness was slightly higher on trials AF (BaselinePOST: TRIALS BCDE: 0.98 ± 0.1 ; TRIALS AF: 1.07 ± 0.05 ; $T_{12} = 1.46$, $p = 0.17$) (Figure 4.3). In summary, it seems to be a robust finding unrelated to order effects that attaching a wall instead of a drop-edge at one side of the environment increased gridness. This was exactly as we predicted. In the next section, I further explore this finding using split-arena analysis which divides the arena into two equal halves.

TRIALS AF gridness vs. TRIALS BCDE gridness

■ TRIALS AF ■ TRIALS BCDE

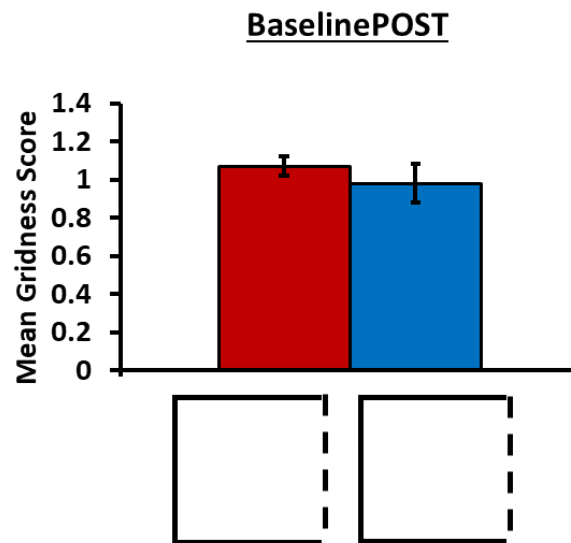


Figure 4.3 An increase in gridness does not occur on middle trials BCDE vs early/late trials AF on BaselinePOST when the drop-edge is present during all 6 trials.

4.1.2 Split arena analysis: Gridness

Previous studies have found that grid cell patterns can be inhomogeneous within the same environment, with larger distortions in the grid patterns occurring closer to local distortions in the environment (Krupic et al., 2015; Wernle et al., 2017; Krupic et al. 2018). In this thesis, I wanted to investigate whether gridness was reduced at the dropped edge/4th wall compared to the opposite stable wall.

Indeed, it was. There was a significant main effect of arena-half on gridness, $F(1, 73) = 31.45$, $p = 0.0000003$, partial $\eta^2 = 0.30$, such that gridness was higher in the stable half of the arena (STABLE: 0.71 ± 0.04) compared to manipulated half of the arena (MANIPULATED: 0.51 ± 0.03) (Figure 4.4). In other words, gridness is higher in the half of the arena that always has a wall attached compared to the half of the arena

that is repeatedly changing from one configuration to another. It may be that the stable half of the arena provides more spatial certainty than the often changing manipulated half.

MANIPULATED half gridness vs. STABLE half gridness

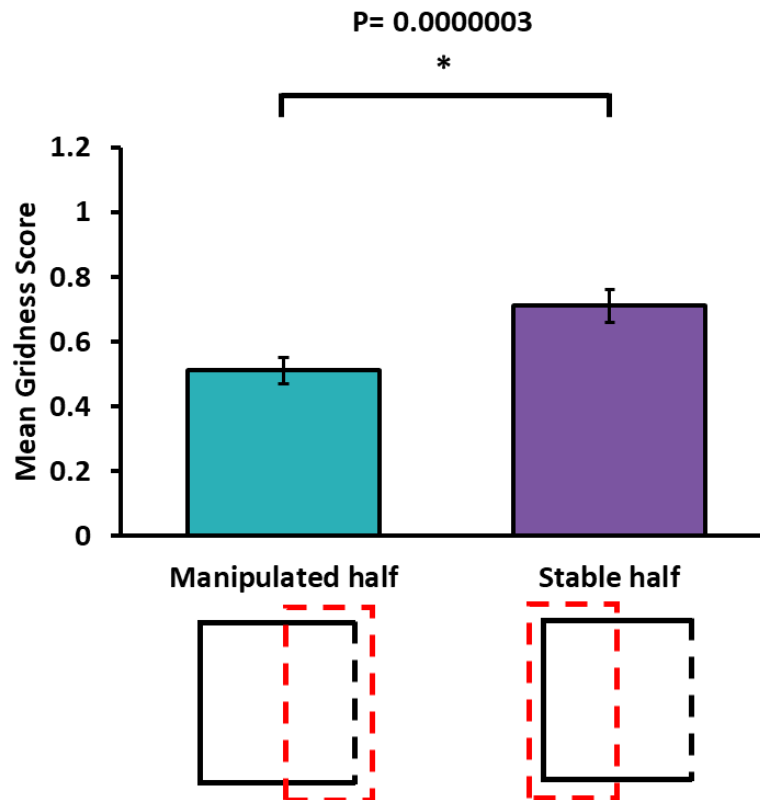


Figure 4.4 Gridness is higher in the stable half of the environment.

This figure shows that gridness was higher in the stable half of the arena, which always had a wall attached, compared to the manipulated half of the arena where the state of the 4th wall was often changing.

4.1.2.1 The 4th wall increases gridness not only in the manipulated (proximal) half, but also in the stable (distal) half

What is more interesting, is the absence of a wall-state x arena-half interaction, $F(1, 73) = 1.27$, $p = 0.26$, $\text{partial } \eta^2 = 0.02$. That is; first, gridness in the manipulated half of the arena was significantly higher when the 4th wall was attached to the

manipulated side of the arena (WALL-ATTACHED trials BCDE: 0.60 ± 0.04) compared to when it was not attached (DROP-EDGE trials AF: 0.42 ± 0.05 ; $t_{74} = -4.42$, $p = 0.00003$) (Figure 4.5A see the red dashed lines in Figure 4.5 to see precisely what is being compared); second, a similar gridness-enhancing effect was observed in the stable half of the arena, *i.e. in the half distal to the manipulated boundary*: gridness was significantly higher when the 4th wall was attached (WALL-ATTACHED trials BCDE: 0.77 ± 0.04) compared to when it was not attached (DROP-EDGE trials AF: 0.64 ± 0.06 ; $T_{74} = -3.24$, $p = 0.002$) (Figure 4.5B). I then compared the difference in gridness between the two conditions within the manipulated half of the arena to that of the stable half.

DROPPED-EDGE gridness vs. WALL-ATTACHED gridness: Arena-half interaction

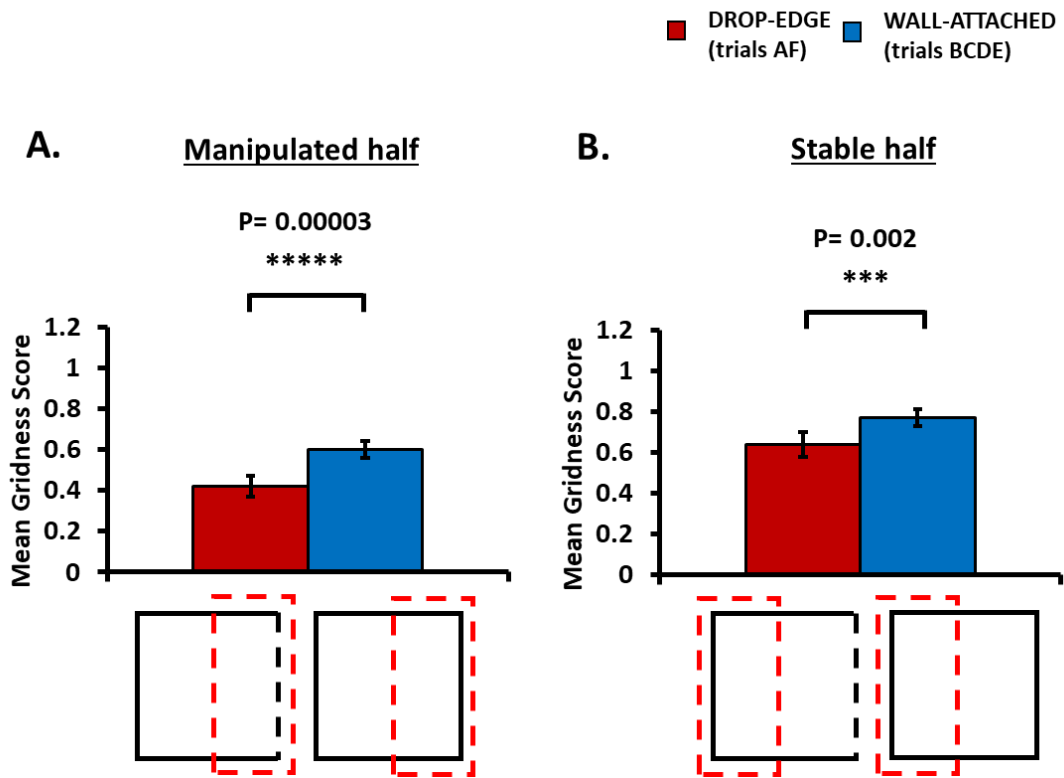


Figure 4.5 The 4th wall increased gridness across the whole arena.

The 4th wall increased gridness in both halves of the arena— up to 1.5 m away from the manipulated boundary.

Remarkably, then, a relatively subtle change, applied to only one of the four sides of the environment, was sufficient to increase gridness in both halves of the environment, i.e. increasing gridness in distal space 0.75 metres to 1.5 metres away from the manipulated boundary. To my knowledge, such an effect has not been previously shown. Arguably, then, these results give us an important insight into how changes in boundary cues in one portion of an environment can exert relatively distal as well as proximal effects. They may for instance help to explain the results of Muessig et al (2015), as further considered in the Discussion for Experiment 1.

4.1.2.2 Stable half vs manipulated half: Gridness

The above interaction is basically trial-variant invariant. It keeps one compartment of the environment constant (manipulated half or stable half), and then focuses upon whether gridness was higher in that compartment in one set of trials versus another set of trials (i.e. wall-attached vs drop-edge). This provides the clearest test of the hypothesis that the enhancement of spatial certainty conferred by a wall over a drop should increase gridness.

A second wall-state x arena-half interaction keeps the trial constant, and then focuses upon whether, within a trial, there is an observable difference in gridness between the half of the environment that is often changing ('manipulated half') and the half of the environment that stays constant ('stable half'). In the drop-edge trials (trials A & F), this is a comparison between a half with a wall and a half with a drop-edge, and the prediction is clear that the drop-edge half should show lower gridness than the wall-attached half. This is a directly complementary test of our main gridness-related hypothesis in this chapter: indeed, the results confirm this hypothesis. That is to say, in trials A & F, gridness was significantly higher in the stable half of the arena

(STABLE HALF: 0.64 ± 0.06), with an attached wall, compared to the manipulated half of the arena when the 4th wall was not attached, and this was quite a large and reliable effect (MANIPULATED HALF: 0.42 ± 0.05 ; $T_{74} = -4.83$, $p = 0.000007$) (Figure 4.7A).

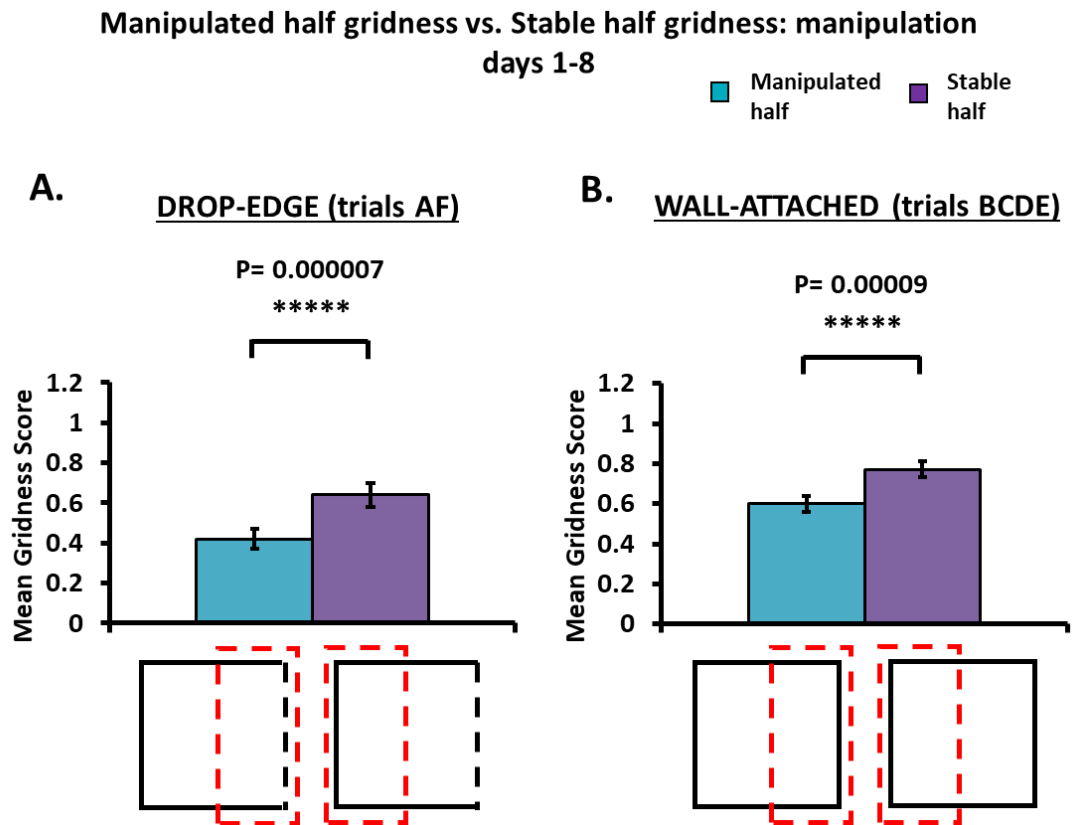


Figure 4.7 Gridness is higher in the stable half of the arena compared to the manipulated half during both DROP-EDGE trials (AF) and WALL-ATTACHED trials (BCDE) on manipulation days 1-8.

A) This graph shows that gridness is higher in the stable half of the arena compared to the manipulated half of the arena during the DROP-EDGE trials (i.e. trials AF). **B)** This graph shows the same outcome during the WALL-ATTACHED trials (i.e. trials BCDE), suggesting some interference between representations of the environment.

4.1.2.3 Non-bistable interference effects gridness

This within-trial analysis also poses the question as to whether gridness differs in the walled trials (BCDE) between the half of the environment that is often changing ('manipulated half') and the half of the environment that stays constant ('stable half'). Here, arguably, the main gridness-affecting factor is not from the boundary-material per se, but from the fact that cues are often changing in one side of the environment, and that this is a potentially disruptive influence. Two useful hypotheses regarding cue change can be distinguished. If there is good memory for the two environmental configurations, each of which can be retrieved as appropriate, gridness should be similar across the stable and changing halves. This can be called the 'bistable no-interference' hypothesis. If, however, the representation of one configuration interferes with the other configuration, we would predict that gridness is reduced in the often-changing half ('manipulated half') compared to the stable half, and this can be called the 'Non-bistable interference' hypothesis. Finally, we would have no particular explanation for a third potential result, whereby gridness was higher in the manipulated than stable half.

The results favour the second, 'non-bistable interference' hypothesis. That is to say, even when comparing two equally-walled halves of the environment in trials BCDE, gridness was significantly higher in the stable half (STABLE HALF: 0.77 ± 0.04) than in the manipulated half of the arena, and this was quite a reliable effect (MANIPULATED HALF: 0.60 ± 0.04 ; $T_{74} = -4.15$, $p = 0.00009$) (Figure 4.7B). This could suggest some interference between representations of the environment with and without the fourth wall attached.

How this occurs might be explained by the newly discovered vector trace cells. These cells are found in the subiculum (Poulter et al., 2019), which projects heavily to the presubiculum (Amaral & Lavenex, 2007), and has been implicated in navigation, spatial memory, and imagery (Knierim et al., 2014; Bicanski et al., 2018; Poulter et al., 2019). Like boundary vector cells, vector trace cells generate a firing field at a specific distance and direction from an environmental boundary (Lever et al., 2009). However, unlike boundary vector cells, they continue to generate a firing field for hours after that boundary is removed (Poulter et al., 2019). These characteristics could potentially allow them to continue to fire in response to the edge of reachable space or to the lab wall, which are no longer perceivable when the 4th wall is attached. Conflicting input from these trace fields and input from other boundary responsive cells responding to the 4th wall might result in the lower gridness seen in the manipulated half of the environment. That is, they might be blurring where the environmental edge actually lies- at the present 4th wall/drop-edge or at one of the boundaries beyond. This also suggests that persistent lower gridness indicates memory for 1. multiple representations of the environment (wall-off and wall-on) and 2. memory for space beyond what can be perceived at the time.

4.1.3 Gridness increases with familiarization

As mentioned in section 4.1, there was a significant main effect of time-block on gridness, $F(1, 73) = 30.00$, $p = 0.0000006$, partial $\eta^2 = 0.29$. Gridness was lower in the early block (EARLY: 0.42 ± 0.05) compared to the late block (LATE: 0.80 ± 0.05) (Figure 4.8), consistent with other studies that observed an increase in gridness with increased familiarization (Barry et al., 2007; 2012).

EARLY time-block (days 1-4) gridness vs. LATE time-block (days 5-8) gridness

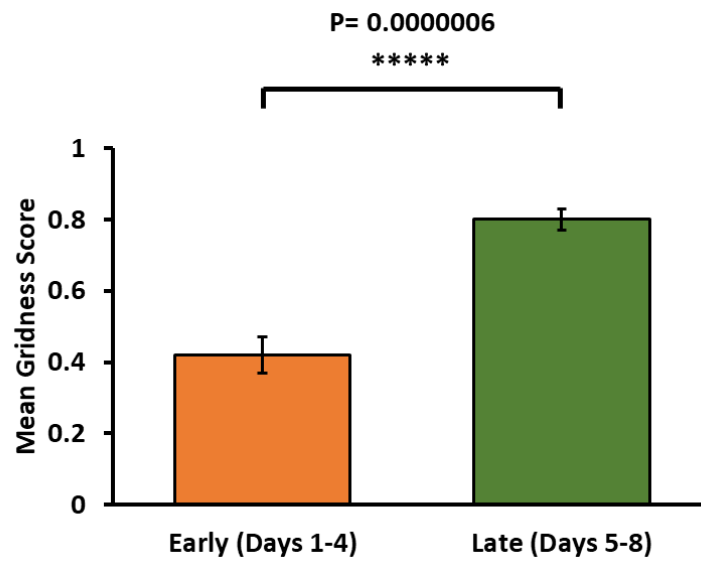


Figure 4.8 Gridness increases with increasing familiarization.

Gridness was significantly higher in the late time-block (days 5-8) compared to the early time-block (days 1-4).

4.2 Grid scale

As with gridness, a 2 x 2 x 2 mixed-design ANOVA was used here to examine the factors of wall-state (WALL-ATTACHED vs DROP-EDGE), time-block (EARLY vs LATE), and arena-half (MANIPULATED vs STABLE) on grid scale.

4.2.1 Split arena analysis: Manipulated half vs Stable half: Grid scale

I begin first of all looking at the manipulated versus stable issue. There was a main effect of arena-half, $F(1, 73) = 10.76$, $p = 0.002$, $n_2 = (.13)$: grid scale was larger in the manipulated half of the arena (MANIPULATED half: $37.74 \text{ cm} \pm 0.11$) compared to the stable half (STABLE half: $36.72 \text{ cm} \pm 0.12$) (Figure 4.9).

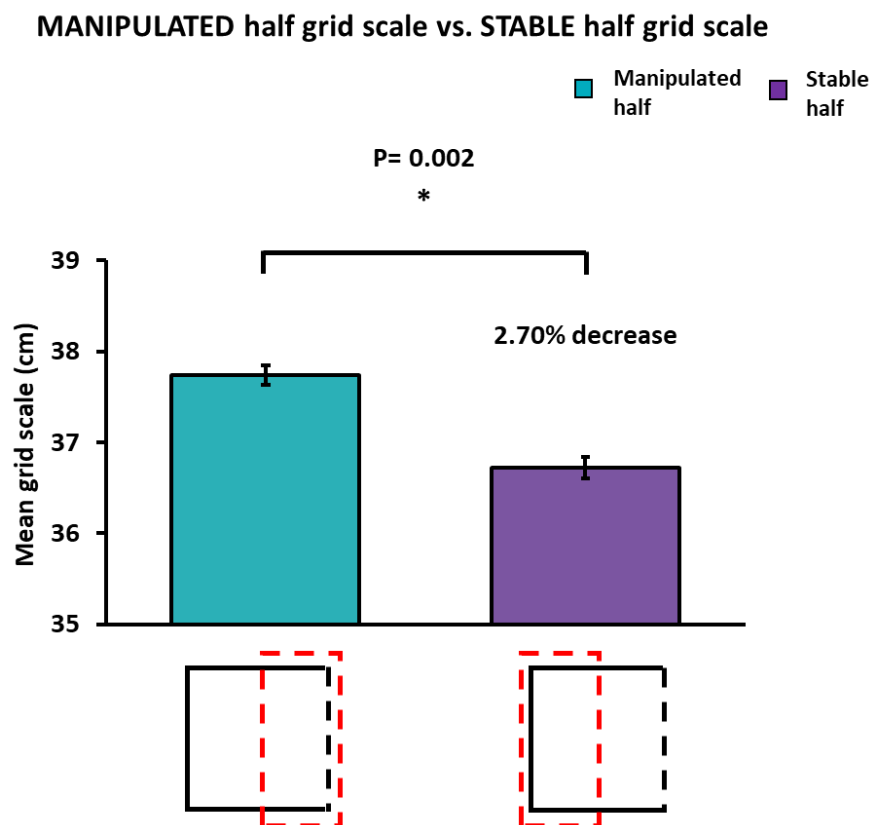


Figure 4.9 Grid scale was larger in the manipulated half of the arena.

Grid scale was larger in the half of the arena with an often changing boundary (the manipulated half) compared to the half of the arena that always had a wall at its side (the stable half).

Although the state of the 4th wall (wall-state), $F(1, 73) = 1.01$, $p = 0.30$, partial $\eta^2 = 0.02$, and familiarization (time-block), $F(1, 73) = 0.59$, $p = 0.45$, $n^2 = (.01)$, had no appreciable effect on grid scale on their own, they each interacted with arena-half to significantly effect grid scale. These are discussed in turn below.

4.2.1.1 Grid scale between arena-halves becomes similar when the 4th wall is present

According to Towse et al (2014), grid scale expands when uncertainty is high and contracts when uncertainty is low. If walls reduce uncertainty relative to drop-edges, I would predict that, in the drop-edge trials (AF), grid scale should be smaller in the half of the arena with the wall at its side (stable half) than in the half of the arena with the drop-edge at its side (manipulated half). This hypothesis was amply confirmed. A significant wall-state x arena-half interaction, $F(1, 73) = 6.16$, $p = 0.02$, $n^2 = (.08)$ revealed that, during the drop-edge trials (trials AF), grid scale was smaller in the stable half of the arena (STABLE half: $36.57 \text{ cm} \pm 0.15$) compared to the manipulated half (MANIPULATED half: $38.10 \text{ cm} \pm 0.15$; $T_{74} = 3.50$, $p = 0.001$) (Figure 4.10A).

Although the same direction of effect was seen during wall-attached trials (trials BCDE), when both the east and the west sides of the arena had walls attached, there was no significant difference in grid scale between the manipulated half and the stable half of the arena (WALL-ATTACHED trials BCDE: MANIPULATED half: $37.35 \text{ cm} \pm 0.10$; STABLE half: $36.84 \text{ cm} \pm 0.12$; $T_{74} = 1.61$, $p = 0.11$) (Figure 4.10B).

MANIPULATED half grid scale vs. STABLE half grid scale: Wall-state interaction

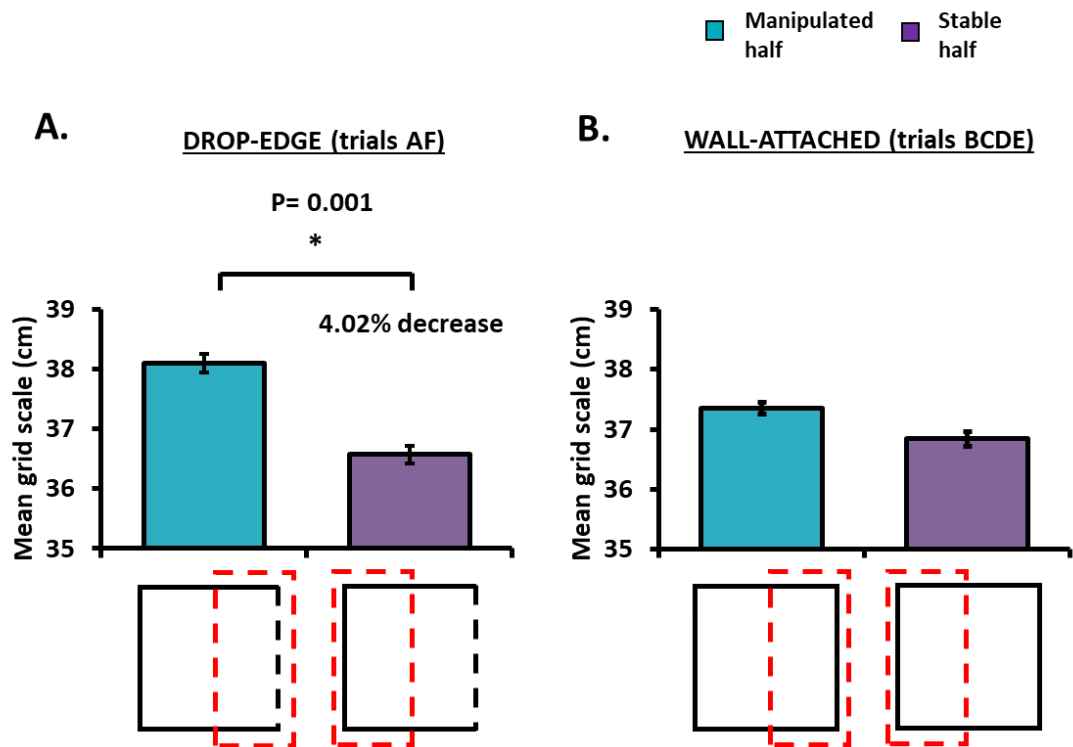


Figure 4.10 Grid scale is smaller in the stable half of the arena during the DROP-EDGE trials, but not during the WALL-ATTACHED trials.

Grid scale is smaller in the stable half of the arena compared to the manipulated half of the arena during the DROP-EDGE trials (trials AF) (A). There was not a significant difference in grid scale between the two arena halves when the 4th wall was attached (trials BCDE) (B).

4.2.1.2 Grid scale between arena-halves becomes similar with increased familiarization

There was also a significant interaction between arena-half and time-block, $F(1, 73) = 8.18$, $p = 0.006$, $n_2 = (.10)$. During the early time-block, grid scale in the manipulated half of the arena (EARLY time-block: MANIPULATED half: $38.43 \text{ cm} \pm 0.18$) was significantly larger than grid scale in the stable half of the arena (EARLY time-block: STABLE half: $36.51 \text{ cm} \pm 0.18$; $T_{37} = 4.15$, $p = 0.0002$) (Figure 4.11A). During the late time-block, grid scale between the two wall-states was similar (LATE time-block: MANIPULATED half: $37.02 \text{ cm} \pm 0.11$; STABLE half: $36.90 \text{ cm} \pm 0.17$; $T_{36} = -0.09$, $p =$

0.93) (Figure 4.11B). This shows that as familiarization increased, so did the homogeneity of the grid scale within the arena.

MANIPULATED half grid scale vs. STABLE half grid scale: Time-block interaction

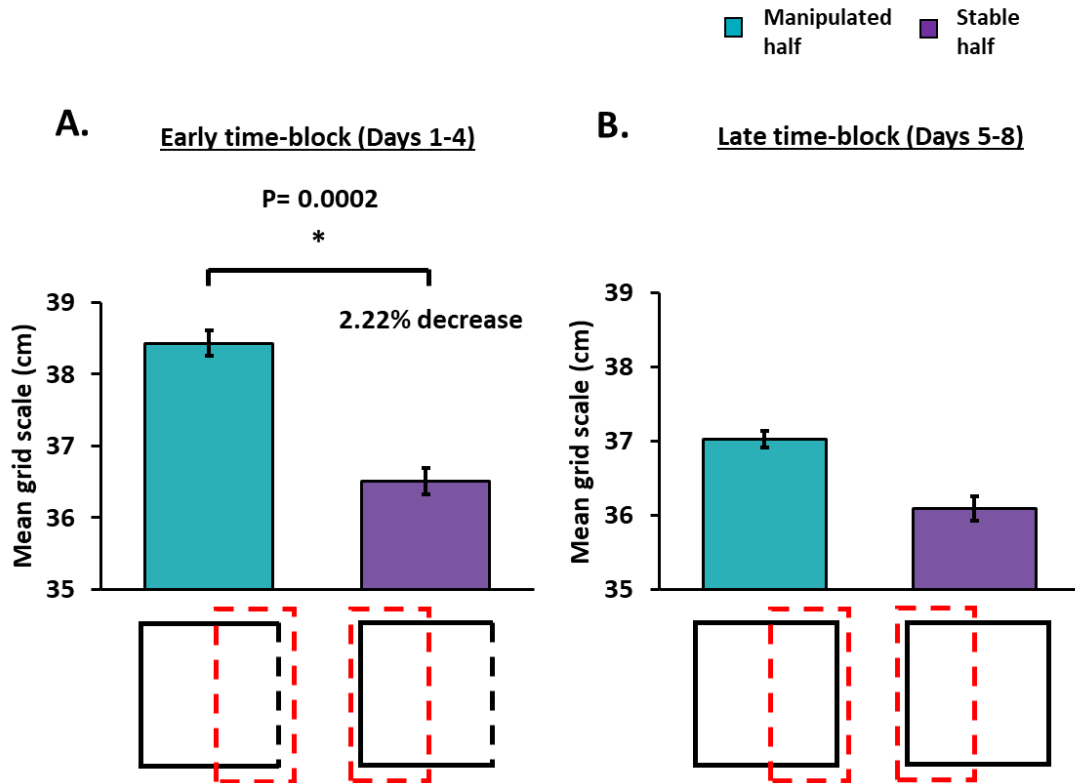


Figure 4.11 Grid scale is significantly smaller in the stable half of the arena during the EARLY time-block, but not during the LATE time-block.

Grid scale is smaller in the stable half of the arena compared to the manipulated half of the arena during the EARLY time-block (i.e. days 1-4) (A). There was not a significant difference in grid scale between the two halves of the arena during the LATE time-block (i.e. days 5-8) (B).

4.2.2 Initial exposure to the 4th wall, despite its relative novelty, did not cause grid scale to expand

Here, the ratio of grid scale from trials BCDE to grid scale from trials AF was used to avoid interpreting a change in grid scale resulting from the trial sequencing instead of the barrier itself e.g. is there something about the first trial of the day (trial A) that causes grid scale to expand? (I do of course remind the reader that I always ran

a trial before the A sequence precisely to diminish any such novelty.) Is there something about the four middle trials that causes grid scale to contract (they are flanked by the first and last trials of the day)?

To see if grid scale expansion occurred when the rats first experienced the 4th wall, I compared grid scale from a pre-experiment baseline day (BaselinePRE) to grid scale from day 1 (the first manipulation day) within each half of the arena. A 2x2 mixed-design ANOVA (i.e. DAY and ARENA-HALF) revealed that grid scale between the two days was similar, $F(1, 28) = 0.13$, $p = 0.72$, $n_2 = (.005)$ as was grid scale between arena halves, $F(1, 28) = 0.27$, $p = 0.61$, $n_2 = (.01)$. The lack of an interaction effect also showed that expansion due to novelty was not being restricted to one half of the arena, DAY x ARENA-HALF: $F(1, 28) = 0.05$, $p = 0.81$, $n_2 = (.002)$.

I also compared the first baseline trial (trial A) of day 1 to the first manipulation trial (trial B) of day 1. Again, no expansion was seen in the manipulated half of the arena (Day 1A: 13.81 ± 0.79 ; DAY 1B: 13.73 ± 0.41 ; $T_{29} = 0.17$, $p = 0.87$) or the stable half of the arena (Day 1A: 12.69 ± 0.42 ; DAY 1B: 12.57 ± 0.37 ; $T_{29} = 0.47$, $p = 0.64$). One explanation might be that walls provide much more certainty about the environment compared to drop-edges, and this immediately counteracted the relatively subtle environmental novelty.

4.3 Firing rates

I first consider mean firing rates, then consider peak rates further below

4.3.1 Mean rate

A 2x2 mixed-design ANOVA was used to examine the factors of wall-state (DROP-EDGE vs WALL-ATTACHED) and time-block (EARLY vs LATE) on mean rate.

There was not a significant main effect of wall-state, $F(1, 73) = 0.113$, $p = 0.738$, $n_2 = (.00)$, (Table 4.1A) or time-block, $F(1, 73) = 1.915$, $p = 0.171$, $n_2 = (.03)$ (Table 4.1B), on mean rate. Nor was there was a significant interaction between wall-state and time-block on mean rate, $F(1, 73) = 0.131$, $p = 0.719$, $n_2 = (.01)$. In other words, neither the presence of the wall, nor increasing familiarization had an effect on mean firing rates.

Table 4.1 There were no significant main effects of wall-state or time-block on mean rate.

			Mean Rate
A) WALL-STATE (n= 75)	Mean ± SEM	AF:	3.34 ± 0.39
		BCDE:	3.31 ± 0.37
	P value		0.73
B) TIME-BLOCK (n= 75)	Mean ± SEM	EARLY:	2.81 ± 0.39
		LATE:	3.85 ± 0.63
	P value		0.16

* $p < 0.05$ ** $p < 0.01$ *** $p < 0.005$ **** $p < 0.001$ ***** $p < 0.0005$

4.3.2 Peak rate

A 2x2 mixed-design ANOVA was used to examine the factors of wall-state (DROP-EDGE vs WALL-ATTACHED) and time-block (EARLY vs LATE) on peak rate.

There was not a significant main effect of wall-state, $F(1, 73) = 0.193$, $p = 0.661$, $n_2 = (.00)$, (Table 4.2A) or time-block, $F(1, 73) = 2.241$, $p = 0.139$, $n_2 = (.03)$ (Table 4.2B), on mean rate. However, there was a significant interaction between wall-state and time-block on peak rate, $F(1, 73) = 5.861$, $p = 0.018$, $n_2 = (.07)$, (Table 4.3). During the

late manipulation days (days 5-8), peak rate was significantly higher when the 4th wall was attached (WALL-ATTACHED trials BCDE: M= 8.76, SEM= 1.17) compared to when it was not attached (DROP-EDGE trials AF: M= 8.22, SEM= 1.19; T36 = -2.74, p = 0.01) (Table 4.3B). During the early manipulation days (days 1-4), the wall did not have a significant effect on peak rate (WALL-ATTACHED trials BCDE: M= 6.25, SEM= 0.71; DROP-EDGE trials AF: M= 6.62, SEM= 0.77; T37 = 1.172, p = 0.249) (Table 4.3A).

Table 4.2 There were no significant main effects of wall-state or time-block on peak rate.

			Peak Rate
A) WALL-STATE (n= 75)	Mean ± SEM	AF:	7.42 ± 0.71
		BCDE:	7.51 ± 0.69
	P value		0.69
B) TIME-BLOCK (n= 75)	Mean ± SEM	EARLY:	6.44± 0.71
		LATE:	8.49± 1.18
	P value		0.11

*p< 0.05 **p< 0.01 ***p< 0.005 ****p<0.001 ***** p<0.0005

Table 4.3 There was a significant interaction between wall-state and time-block

			Peak Rate
A) EARLY:	Mean ± SEM	AF:	6.62 ± 0.77
		BCDE:	6.25 ± 7.1
	P value		0.25
B) LATE:	Mean ± SEM	AF:	8.22 ± 1.19
		BCDE:	8.76 ± 1.17
	P value		0.01*

*p< 0.05 **p< 0.01 ***p< 0.005 ****p<0.001 ***** p<0.0005

4.4 Experiment 1 specific Discussion

4.4.1 Boundaries confer enhancements in spatial firing of grid cells both distally and proximally

The main thrust of much of the work on environmental boundaries and grids has been to show that boundaries have global or proximal effects upon grid cells. To my knowledge, previous work has not specifically addressed the question of how cues in given locations enhance the spatial firing of grid cells in distal locations. In fact, the bulk of this sort of research has focused on the global effects of boundaries upon grid cells. For instance, findings from the Moser lab showed that boundaries exert an experience-dependent effect upon grid orientation (Stensola et al, 2015). As an animal becomes familiar with an environment, the orientation of grid patterns relative to the boundaries of a square shift from a parallel alignment to an offset by $\sim 7-9^\circ$. The grid pattern also anchors itself to one or more points along the local boundaries. Where the grid pattern is anchored, it resists movement. This anchoring combined with a shift in orientation causes a distortion in the grid pattern, making it appear less hexagonal and more elliptical. Relatedly, findings from the O'Keefe lab showed powerful effects of the geometry of environmental boundaries upon grid cells recorded in a familiar environment (Krupic et al, 2015). When they recorded grid cells in a highly familiar trapezoid shaped arena, they found that the grid pattern was elliptical and that the distortion was greater at the narrower end of the arena. The distortions that they observed may result from the same shearing forces described by Stensola et al. (2015) occurring and being exaggerated by the asymmetrical shape of the recording environment. Additionally, a study that used a compartmentalized environment focused on grid patterns switching from two identical local maps to one global map

spanning across the dividing wall as the animals became more familiar with the environment (Carpenter et al, 2015).

Where the analysis has not been global, but where analysis has been sensitive to the distance from particular boundary cues, the emphasis has generally been on showing boundary effects on grid cell firing patterns are exerted in space proximal to the boundaries in question. For example, another study from the O'Keefe lab showed that when local changes to environmental geometry occur, individual grid fields shift by an amount that is inversely related to their distance from the manipulated boundary-i.e. distortions were greater nearer the manipulated boundary (Krupic et al, 2018). In a study that utilized merged environments, Wernle et al. (2018) discovered that when a dividing wall is removed grid fields rapidly reorganize to establish spatial periodicity along the former partition line where the two original grid maps meet, resulting in one coherent map.

The approach taken in Experiment 1 was more specifically guided to examine how environmental boundaries may have an enhancing effect on spatial firing in grid cells. A long-standing idea in spatial research was that path integration accumulates error and therefore fixed external landmarks are needed to correct this. This was further instantiated in the hippocampal formation system following the discovery of head-direction cells and place cells by saying that the hippocampus proper was a path integration device (McNaughton et al, 1996). The primary evidence for this claim came from the observation that place fields are largely preserved in darkness or when a landmark is removed (O'Keefe and Speakman, 1987; Muller and Kubie, 1987; Muller et al., 1987; McNaughton et al., 1989; Markus et al., 1994). The subsequent discovery of boundary cells, presumably representing the fixed landmarks, and grid cells,

presumably performing path integration, lent more precision to this idea. Thus, for instance, the Mosers suggested that entorhinal border cells would enable the grid cells to correct for path integration error (Solstad et al, 2008). Several computational models have used place cells to reduce error and drift in entorhinal grid cells (Guanella et al., 2007; Pastoll et al., 2013). However, border cells provide a versatile neural representation of boundaries, firing near impassable walls, short but passable walls, and drop-edges (Solstad et al., 2008). Unlike place cells, border cell firing patterns generalize across different environmental geometries- something that would cause place cells to remap (Leutgeb et al, 2005; Savelli et al., 2008; Solstad et al., 2008).

Poulter and colleagues reviewed various ethoexperimental studies to note that rats and other rodents form 'home bases' in initial explorations of novel environments (Poulter et al, 2018). A 'home base' is a highly over-visited location to which the rodent repeatedly returns, throughout the exploration period, and in which the rodent executes various investigatory activities such as head scans and rearing on hind legs, presumably to provide allothetic spatial information. Home bases are typically a corner of an environment (where two boundaries converge) or along one wall. The rodents leave the home base in a somewhat meandering pattern but return to the home base fairly directly, likely using path integration on the return journey. Poulter and colleagues argue that this highly over-visited home base has arisen from the need to solve two important and interacting problems. Very briefly, these are: 1) re-identifying what is allocentrically 'the same place' (i.e. analogous to loop closure in robotics), given challenges such as that viewing space is always done egocentrically, time passes between views, and the world changes over time; 2) path integration error, where the home base helps to reset head direction, and to recalibrate gains in both the angular

(HD cells) and linear (grid cells) contributions to path integration. These theoretical considerations and empirical observations all speak to the strong expectation that increasing spatial certainty at environmental boundaries should enhance the spatial firing of grid cells. One very interesting study, and part of the motivation for the current experiment, showed that error in mouse grid cells was positively correlated with the distance an animal had travelled since its last encounter with a wall-boundary (Hardcastle et al, 2015). It should be noted that this study did not examine the effect of the animal's instantaneous Euclidean distance to boundaries, but was a study of the effects of path distance since wall contact. Moreover, (Hardcastle et al, 2015) was a purely observational study. There was no manipulation of boundary cues as such. Clearly, however, the study strongly suggested the spatial coding enhancing effects of boundaries upon grid cells.

The idea of the present study was to build on such demonstrations, to directly test the hypothesis that there would be enhancing effects of a boundary material manipulation on distal as well as proximal space. The manipulation of a cue on only *one side* of a relatively large square (1.5m x 1.5m), enabled me to make observations directly testing this prediction. The reasoning was that a wall provides better spatial information both somatosensorily and visually than a drop-edge, and thus the hypothesis was that the 'fourth-wall' configuration would improve grid cell characteristics, relative to the 3-walls-and-1-drop-edge configuration. While it was entirely reasonable to suppose that space proximal to the boundary cue might be most affected, an important prediction to test was that grid cell spatial firing in the space distal to the boundary would also be enhanced. Importantly, each boundary cue (wall vs drop-edge) was placed at the same orientation as the other, so any resulting effects

would be related to the materiality of the boundary cue only, rather than its orientation. It might be considered a relatively subtle manipulation.

Interestingly, this relatively subtle boundary change was sufficient to alter gridness, and in the expected direction. That is to say, as predicted, *the wall-replacement cue increased gridness relative to the drop-edge cue*. Even more interestingly, I would argue, the wall-replacement cue was sufficient to increase gridness in both halves of the environment, i.e. not only in the proximal half with the cue at its lateral edge, but also *in the other, distal half of the environment*. To be precise, the wall-replacement cue increased gridness in distal space up to 1.5 metres away from the manipulated side. To my knowledge, such an enhancement effect has not been previously shown in studies of grid cells. Arguably, then, these results of Experiment 1 give us an important insight into how changes in boundary cues in one portion of an environment can exert relatively distal as well as proximal effects. Simply put, boundaries appear to define spatial frameworks and enhance spatial coding in regions further from, as well as close to, those boundaries. If we accept this point, then arguably my findings potentially offer some important insights in the function of grid cells.

4.4.2 Grid cell function: extending boundary-based spatial certainty into open space

The function of grid cells is less discussed than the mechanisms of the grid code, but it is interesting that their global primacy in spatial coding is increasingly challenged. Whereas initial assumptions tended to be that grid cells were necessary for place cell function, these assumptions have been largely overturned. Indeed, there is good support for the opposite view, i.e. that place cells are necessary for grids

(Bonnevie et al., 2013). Thus, developmental studies demonstrated that grid cells developed after place cells were already established (Langston et al., 2010; Wills et al., 2010). Similarly, pharmacological studies disrupting the medial septum disrupted grid cells while leaving place cells remarkably intact (Brandon et al., 2011; Brandon et al., 2014; Koenig et al., 2011). However, in a study using a larger novel environment place cells did not form spatial firing fields when the medial septum was inactivated (Wang et al., 2015). It is possible that path integration is less critical for self-localization or map building in a small environment where the animal does not have to go far to come into contact with environmental boundaries, which have been shown to help stabilize place fields (Zhang et al., 2014). In addition, boundary cells can look indistinguishable from grid cells in small environments (Savelli et al., 2008). Thus, place cells may be less effected by grid inputs if boundary inputs are spared. In familiar environments, both small and large, place cells also function normally (Koenig et al, 2011; Wang et al., 2015). It is possible that within familiar environments, place cells maintain their firing fields during medial septum inactivation (and the disruption of grid input) by relying on previously learned associations with landmarks as suggested by Savelli and Knierim (2019).

This is not the place for a full discussion of the set of functions of grid cells. Rather, I focus on one potential view, taking as a point of departure the findings of Muessig et al (2015) in place cells. This intriguing study showed that place cells were less accurate, less stable, and less dense away from the boundaries (i.e. in the central portions of the environment) in pre-weanling rats compared older post-weanling and adult rats. Interestingly, the study found that these characteristics in place cells became adult-like in a step-like function, and this took place at the time of grid cell

emergence. Thus, a plausible view to take from this work is that later-developing grid cells confer a 'gain of function' upon place cells. That is, a key function of grid cells is to leverage the enhancement of spatial certainty that environmental boundaries provide, and extend this certainty into open space (Poulter et al, 2018).

If this model of grid cell function is correct, it is crucial to ask if an environmental boundary can enhance grid cell firing relatively far from the boundary in question. To my knowledge, Experiment 1 is the first study designed to address this question. Experiment 1 answers the question affirmatively: yes, gridness was increased in space up to 1.5 metres away by replacing a less spatially informative cue with a more spatially informative boundary cue. Accordingly, these findings provide a useful first general proof-of-concept demonstration that boundary cues can enhance grid cell firing distally. More specifically, they suggest a possible mechanism by which grid cells could define space distal to boundaries in a more regular and stable way for the benefit of place cells, as in the findings of Muessig et al (2015).

A potential cause for the lower gridness observed during the drop-edge trials might arise from a conflict in where the key 'anchoring' environmental boundary lies. During trials when the 4th wall is absent there are three broadly parallel boundaries present: 1) the drop-edge; 2) the edge of reachable space for the head- i.e. the furthest point that the subject can reach its head past the drop-edge while it clings to the drop-edge; 3) the closest lab wall. To some extent, the lab wall is also available in the wall-attached condition, but at a further distance. The first two boundaries represent limits in space through which the rat can locomote, while the third is a boundary only available visually (and conceivably auditorily).

The drop-edge is the only one of these three boundaries that represents the simple somatosensory edge of the local environment. Most BVCs in the subiculum that have been tested have been shown to fire along the edge of reachable space indicating that drop edges are treated as boundary cues (Lever et al, 2009, Stewart et al, 2014) and may represent the edge of space that can be physically explored.

The lab wall stands outside of the rat's reach and can only be visually explored. To what extent rats' grid code space that is not locomoted through is unclear, but it is likely to be limited. We cannot however entirely exclude this possibility. There is a growing body of evidence showing that grid activity does not critically depend on physical movement in more visually-driven animals like monkeys. For example, in-vivo electrophysiological studies using non-human primates have discovered cells in the entorhinal cortex that encode a map of visual space (spatial view cells, visual grid cells, visual border cells, and saccade direction cells) (Georges-Francois et al., 1999; Killian et al., 2012; Killian et al., 2015; Wilming et al., 2018). These spatial cells are driven by attention (overt and covert) to a visual location in a scene. For example, a visual border cell with an eastern tuning will fire when the animal's attention is focused near any eastern boundary of a distal screen.

Grid patterns in familiar environments are typically stabilised by and anchored to local geometric boundaries (Hardcastle et al., 2015; Krupic et al., 2015; Stensola et al., 2015). However, when the local environment is viewed as being unstable, grid patterns might dissociate from both the physical local boundaries and their neural representation (i.e. boundary cells) and anchor to remote cues that are stable, such as remote boundary walls or remote landmarks via distal BVCs or landmark vector cells respectively, as suggested by Savelli et al (2017). In their study they rotated or shifted

a square testing arena while all remote cues in the room remained stable. They found that even though the local geometric boundaries often exerted the strongest control over the grids, the distal cues (i.e. lab walls and cue cards) demonstrated a consistent, sometimes dominant countervailing influence causing the grid pattern to under-rotate or under-translate relative to the arena boundaries. This indicates that grid cells are controlled by both local geometric boundaries and remote spatial cues simultaneously and supports previous work demonstrating that grid cells can anchor to distal cues and that spatial cells can anchor to a different cue if the one they were originally anchored to becomes untrustworthy (Hafting et al., 2005; Knierim et al., 1998).

This is all to say that the distal walls, in particular the closest wall, could act as a greater influence upon the grids in the drop-edge condition than in the wall-attached condition, contributing to ambiguity about which boundary best serves to anchor grids.

4.4.3 Grid scale – lack of expansion

In this experiment, I did not see grid scale expansion - something that a number of studies have reported to occur when an animal is exposed to environmental novelty (Barry et al., 2012). Additionally, a computational study by Towse et al. (2014) has suggested that the temporary expansion of grid scale may be the optimal response to spatial uncertainty. So, the fact that I did not observe grid scale expansion was surprising considering that the drop-edge was highly familiar and the 4th wall was novel. One explanation might be that walls provide much more certainty about the environment compared to drop-edges, and this immediately counteracted the relatively subtle environmental novelty. In this experiment, the 4th wall might increase certainty by providing a more definitive environmental boundary. That is, the 4th wall

acts as a boundary to more sensory and idiothetic means of exploration than the drop-edge, the edge of reachable space, and the lab wall. Relatedly, it curtails visual exploration beyond the edge of the arena.

In experiment 2, we will see that both an initial expansion and a contraction in grid scale occurred following a much less subtle manipulation of the boundaries. I turn to this experiment now.

5 Experiment 2: Grid cell responses to an inserted barrier, which partially divided the environment

For the following manipulation, I inserted a barrier (100 l x 50.5 h) into the arena perpendicular to the south wall so that it bisected the southern two-thirds of the arena. In doing so, I have manipulated the inner space of the arena, which has retained its overall shape and size (1.5 m x 1.5 m square) without creating multiple smaller compartments. The barrier was present during trials B, C, D, and E on manipulation days 1-8. It was not present on trials A or F on days 1-8 and remained absent during all 6 trials on the pre-experiment baseline day (BaselinePRE) and post-experiment baseline day (BaselinePOST).

As discussed in the Introduction (Chapter 2), theoretical modeling has suggested that grid scale is systematically linked to spatial uncertainty (Towse et al., 2014). To my knowledge, the only data motivating and testing this model is that of environmental novelty, when grid scale expands. A key idea of this model is that grid scale is adaptive. E.g., in an unfamiliar environment, errors in distance and direction judgements, including those related to the 'same place' problem combine to increase spatial uncertainty (Poulter et al., 2018). Expanding grid scale reduces the misalignments arising from unattainable precision. The main purpose of this experiment was to test the model using a spatial uncertainty manipulation that was not novelty. The key hypothesis was that a barrier in the environment would reduce spatial uncertainty, and that this would reduce spatial scale. Spatial uncertainty would be reduced because of the addition of an extra space-defining cue, (both visual and somatosensory) to guide distance judgements. In saying the main aim was to test a non-novelty based manipulation, this is of course not to deny the manipulation

involves novelty; at least initially, the inserted barrier cue would be presumed to increase uncertainty, because it is not predicted. Thus, it would be reasonable to predict that grid scale is not necessarily immediately smaller in the barrier-present condition, and is perhaps even initially larger; with experience, grid scale is predicted to become smaller in the barrier-present than barrier-absent condition.

5.1 Gridness

The above prediction regarding grid scale, relating scale to uncertainty, was the key prediction to test in Experiment 2. Nevertheless, I also looked at gridness. In Experiment 1, the manipulation replaced one boundary cue type with another type, both identically positioned, such that environmental geometry was unaffected. To my knowledge, that kind of experiment has not been done before with grid cells. Here in Experiment 2, the boundary cue manipulation did affect environmental geometry. Importantly for the consideration of gridness, the boundary cue manipulation, the insertion of a 1-metre long barrier (here called BARRIER-IN configuration), i.e. 2/3rds of the length of the walls, also had the effect of partially dividing the environment in two. That is to say, compared to the completely open square configuration without the barrier (here called BARRIER-OUT), the square was bisected in the Southern 2/3rds of the environment in the BARRIER-IN configuration (see figures 3.4B and 5.3). Accordingly, the set-up had some similarities to that tested in Carpenter et al (2015). In their experiment, rats were tested in an arena comprised of two identical compartments connected by a corridor, which allowed the rats to freely travel between compartments. The rats were tested for one session (two 40-minute trials) per day for a maximum of 20 session. grid cells fired in identical, locally bound patterns that replicated in each compartment. As the environment became more familiar the

grid pattern became more global, firing across the boundary dividing the compartments, forming one coherent grid pattern. One difference was that in Experiment 2 here, there were also trials, at the beginning and end of every day, where the environment was configured as an open walled square (see figures 3.4B and 5.3). To the extent that Experiment 2 was like the Carpenter study set-up, the prediction would be that gridness would initially be reduced in the BARRIER-IN configuration, then increase in this BARRIER-IN configuration, as the grid representation becomes globally coherent across the West and East portions of the environment bisected by the inserted barrier. As we shall see, this prediction was confirmed.

5.1.1 The presence of the inserted barrier initially reduced gridness in the Early days, but in the Late days, gridness was similar across both environmental configurations

A 2x2 mixed-design ANOVA was used to examine the factors of barrier-state (BARRIER-OUT vs BARRIER-IN) and Time block (EARLY vs LATE). This revealed a significant main effect of barrier-state on gridness, $F(1, 88) = 8.54$, $p = .004$, partial $\eta^2 = 0.088$, such that gridness was reduced when the barrier was present (BARRIER-IN trials BCDE: 0.86 ± 0.03) compared to when it was not present (BARRIER-OUT trials AF: 0.94 ± 0.03) (Figure 5.1).

BARRIER-OUT gridness vs. BARRIER-IN gridness: manipulation days (1-8)

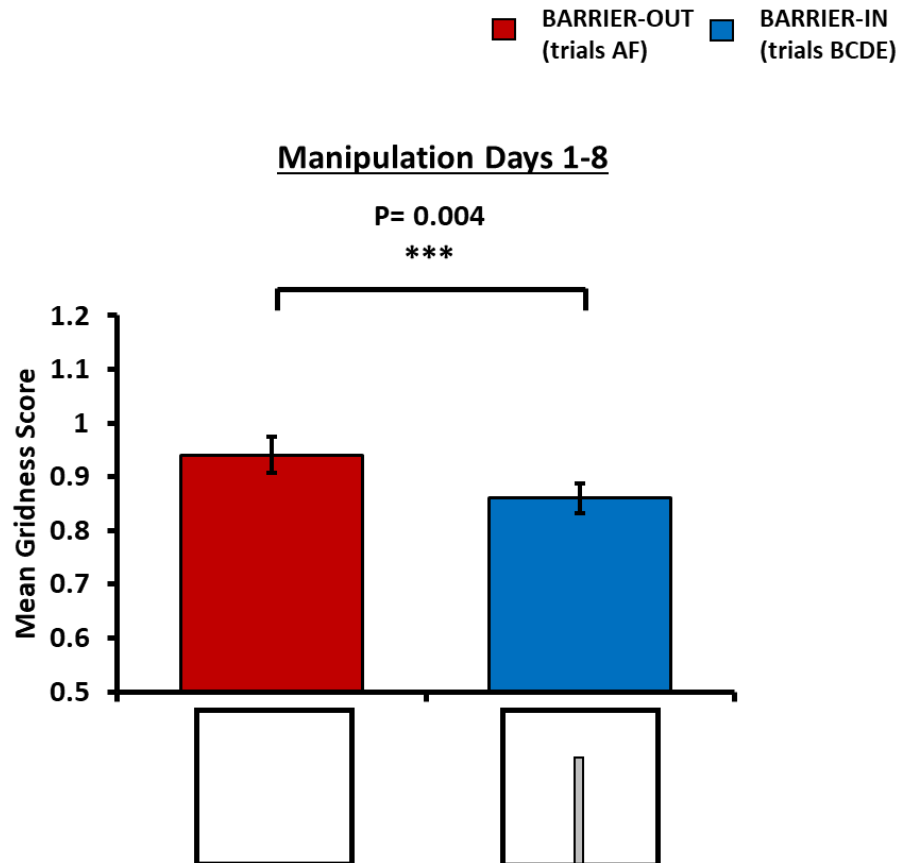


Figure 5.1 Gridness decreases when the barrier is present.

This figure shows that gridness is significantly reduced when the barrier is present compared to when it is absent on manipulation days 1-8.

The ANOVA also revealed a significant interaction effect between barrier-state and time-block $F(1, 88) = 6.24, p = 0.014, \text{partial } \eta^2 = 0.066$ (Figure 5.2). Within the early time-block, gridness was lower when the barrier was present compared to when it was not present (BARRIER-IN trials BCDE: $M = 0.74, \text{SEM} = 0.04$; BARRIER-OUT trials AF: $M = 0.88, \text{SEM} = 0.05; T_{49} = 3.54, p = 0.0009$) (Figure 5.2A). This difference did not occur during the late time-block (BARRIER-IN trials BCDE: $M = 0.99, \text{SEM} = 0.02$; BARRIER-OUT trials AF: $M = 1.00, \text{SEM} = 0.04; T_{39} = 0.37, p = 0.72$) (Figure 5.2B). These results suggest that the gridness reducing effect of the barrier was time-limited.

BARRIER-OUT gridness vs. BARRIER-IN gridness: early and late manipulation days

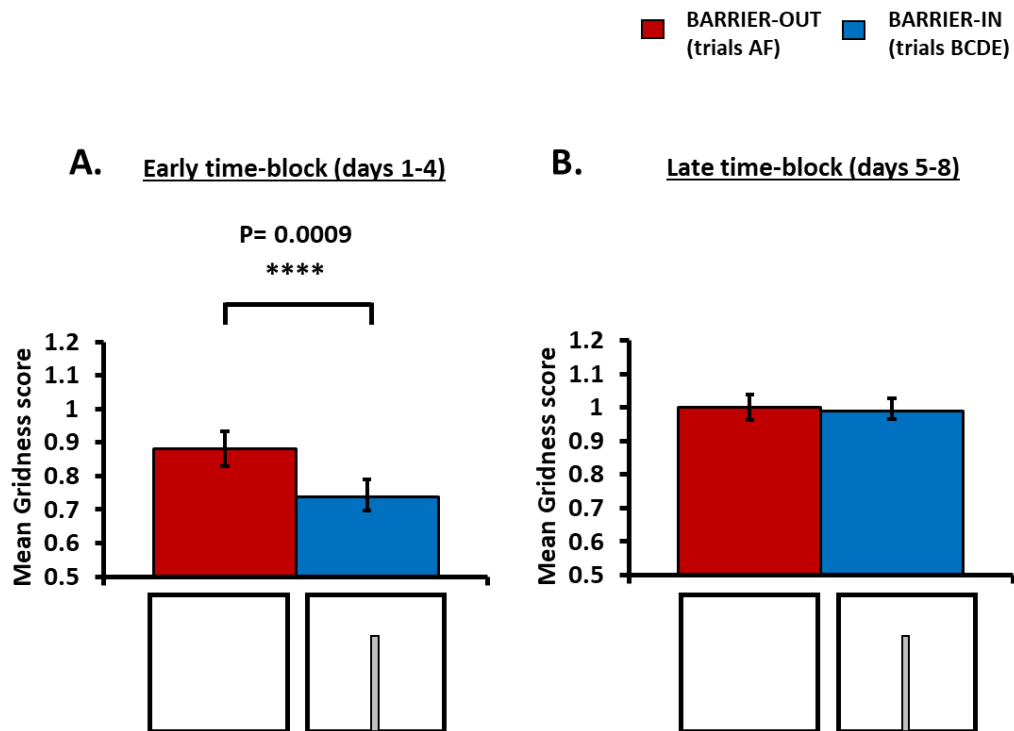


Figure 5.2 The gridness reducing effect of the barrier is time-limited.

Within the early manipulation days (A), gridness was lower when the barrier was present compared to when it was not present. Gridness was not significantly different during the late manipulation days (B). These results suggest that the effect that the barrier had on gridness was time-limited.

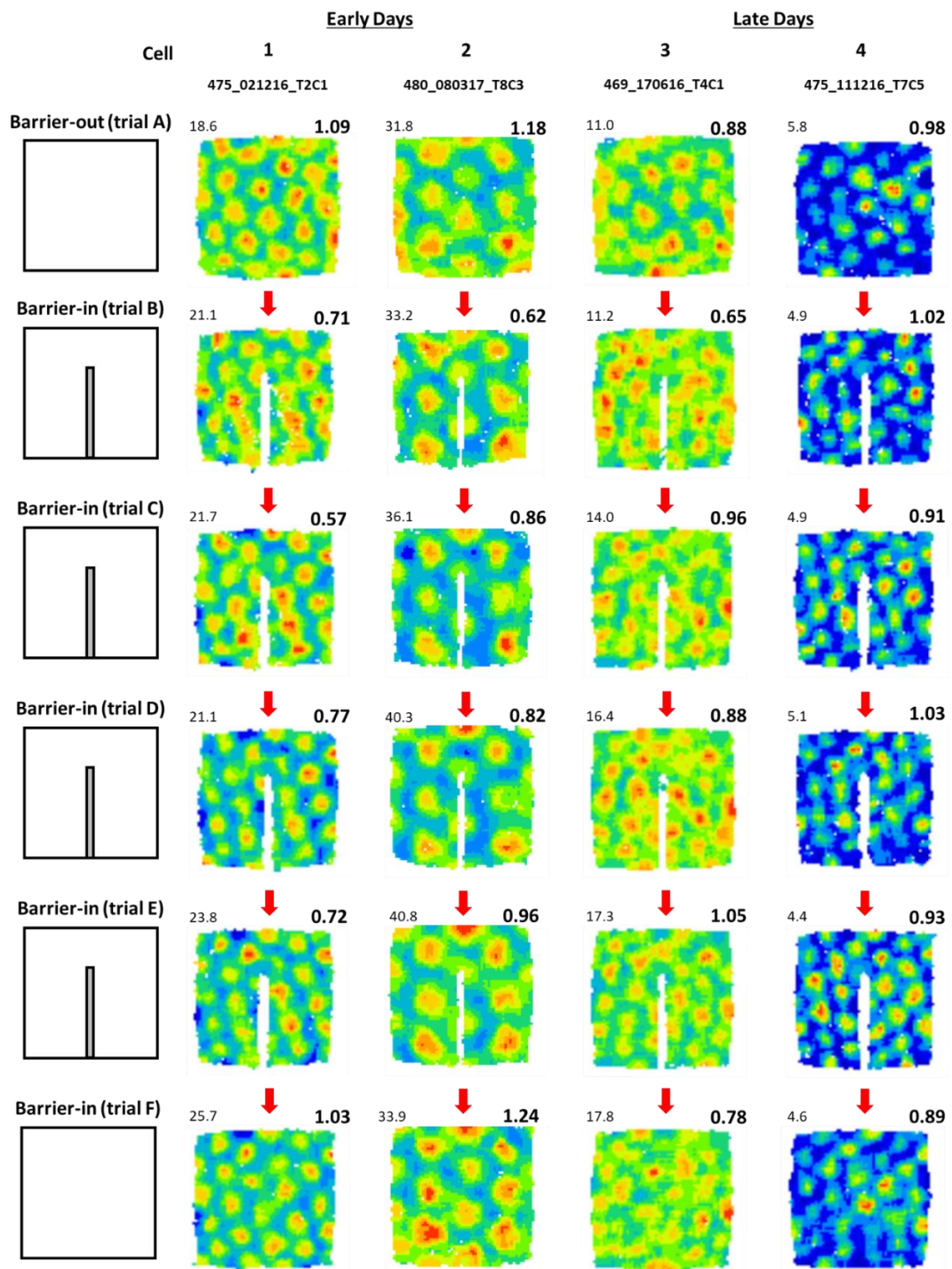


Figure 5.3 Gridness was significantly reduced in the barrier-in condition during early manipulation days (i.e. days 1-4) when the barrier was present, but not during late manipulation days (i.e. days 5-8).

This figure shows the rate maps of four different grid cells recorded across all 6 trials of a session from experiment 2. Cells 1 and 2 were recorded during early manipulation days and cells 3 and 4 were recorded during late manipulation days. Gridness scores are noted at the top right, and Peak rates at the top left, of each rate map.

I also recorded grid cells on a baseline day before the early block (n = 17 cells), and a smaller sample of grid cells on a baseline day after the late block (n = 8 cells). Although some caution is merited given these smaller samples, particularly for the baseline day after day 8, these days, when there was no barrier in the environments (i.e. BARRIER-OUT across all 6 trials) can serve as controls. Above, it was clear that gridness was greatly reduced in the BARRIER-IN condition in the early block (days 1-4), i.e. reduced in trials BCDE compared to AF. On the Pre-Early baseline day (BaselinePRE) immediately before the early block, gridness did not differ in trials BCDE compared to AF, and if anything was higher in trials BCDE (TRIALS AF: 0.99 ± 0.05 ; TRIALS BCDE: 1.01 ± 0.06 ; $T_{16} = -0.94$, $p = 0.36$) (Figure 5.4A). Accordingly, the finding that the barrier reduced gridness in the early block cannot be attributed to a potential order effect, whereby somehow middle trials reduced gridness. Gridness was also not different across trials AF and BCDE on the post-late block baseline day (BaselinePOST) (TRIALS AF: 1.06 ± 0.08 ; TRIALS BCDE: 1.09 ± 0.06 ; $T_7 = -0.95$, $p = 0.37$) (Figure 5.4B).

Trials AF gridness vs. Trials BCDE gridness: baseline days

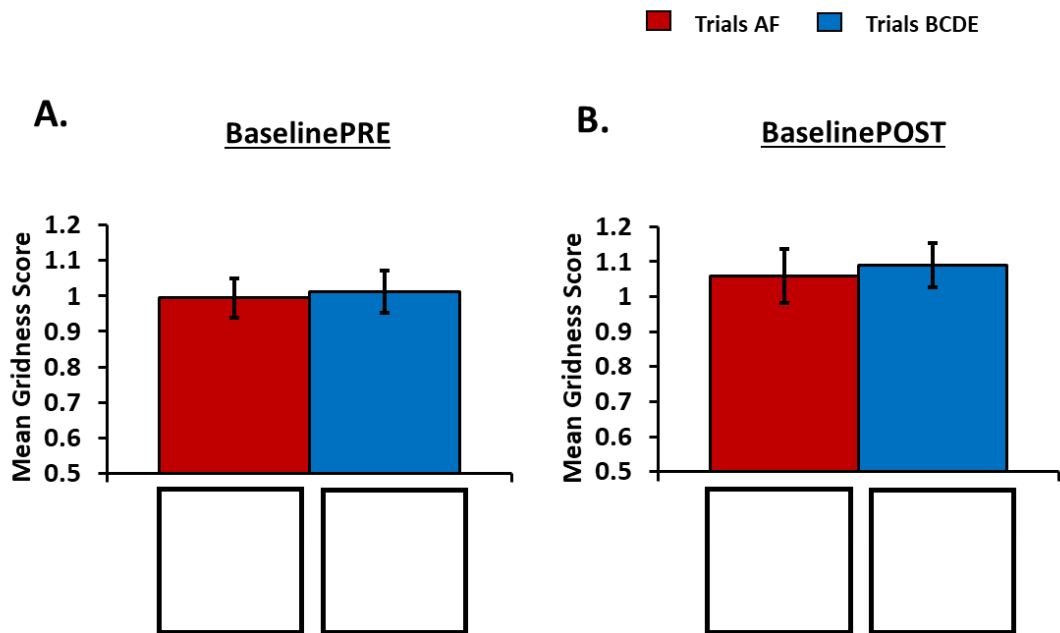


Figure 5.4 Gridness on trials AF and trials BCDE are not significantly different when the barrier is absent across all six trials.

This figure shows that there is no difference in gridness between trials AF and trials BCDE on BaselinePRE (A) and BaselinePOST (B) when the barrier is not present in any of the 6 trials. Considering that gridness was greatly reduced when the barrier was present on trials BCDE in the Early block (days 1-4), but was not reduced when it was absent on trials BCDE on BaselinePRE and BaselinePOST means that the reduced gridness in the early block cannot be attributed to a potential order effect.

5.1.2 Gridness increased with increasing familiarization

There was also a significant main effect of time-block on gridness, $F(1, 88) = 12.32$, $p = 0.001$, partial $\eta^2 = 0.123$, where gridness was lower in the early time-block (days 1-4) (EARLY: 0.81 ± 0.04) compared to the late time-block (days 5-8) (LATE: 1.00 ± 0.03) (Figure 5.5). This suggests an effect of familiarization, i.e. an experience-dependent increase in grid coherence.

EARLY block gridness vs. LATE block gridness

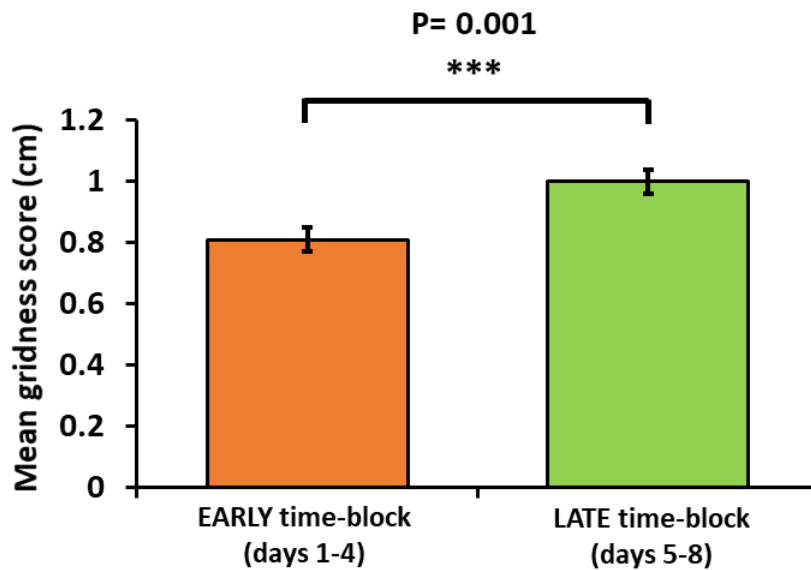


Figure 5.5 Gridness is higher in the late manipulation days (days 5-8) compared to the early manipulation days (days 1-4).

Gridness significantly increases from the early manipulation days (i.e. days 1-4) to the late manipulation days (i.e. days 5-8), suggesting an effect of familiarization.

5.1.3 Gridness increased in the BARRIER-IN condition with increasing familiarization

A second barrier-state x time-block interaction showed that gridness was lower during the early time-block (EARLY days trials BCDE: $M = 0.74$, $SEM = 0.04$) compared to the late time-block (LATE days trials BCDE: $M = 0.99$, $SEM = 0.02$; $T_{76,28} = -5.35$, $p = 0.0000009$) when the barrier was present (trials BCDE) (Figure 5.6A). When the barrier was not present (trials AF), there was not a significant difference between the time blocks (EARLY days: $M = 0.88$, $SEM = 0.05$; LATE days: $M = 1.00$, $SEM = 0.04$; $T_{88} = -1.79$, $p = 0.08$) (Figure 5.6B), albeit the effect approached significance, consistent with a weaker general effect of increasing experience improving spatial coding.

Early time-block (days 1-4) gridness vs. Late time-block (days 5-8) gridness

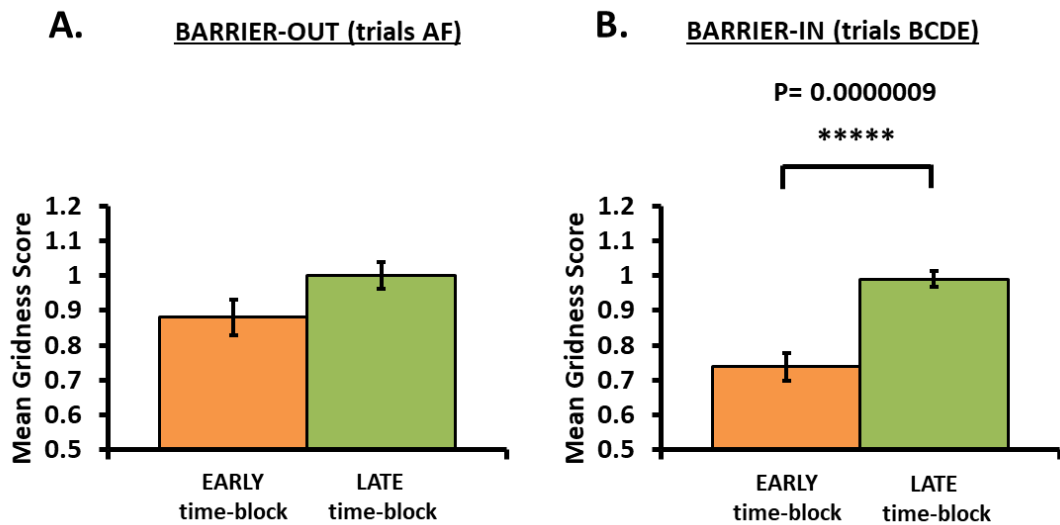


Figure 5.6 Gridness in the BARRIER-IN condition increases with familiarization.

In the BARRIER-IN condition (trials BCDE), gridness was lower during the early manipulation days compared to the late manipulation (B). In the BARRIER-OUT condition (trials AF), there was not a significant difference between the time blocks (A).

5.1.4 Gridness increases to baseline levels following barrier induced reduction

A comparison of gridness from trials BCDE on day 8 (the last manipulation day) to gridness from trials BCDE on the pre-experiment baseline day (BaselinePRE) showed that, after the reduction of gridness elicited by the initial insertion of the barrier, gridness increased, such that there was not a significant difference between gridness on BaselinePRE and gridness on the last manipulation day (day 8) (BaselinePRE: 1.01 ± 0.06 ; DAY 8: 1.05 ± 0.04 ; $T_{25} = -0.49$, $p = 0.63$) (Figure 5.7). This is consistent with previous research that has shown that gridness increases with increasing familiarity to the environment (Barry et al, 2007; 2012).

BaselinePRE TRIALS BCDE gridness vs DAY 8 TRIALS BCDE gridness

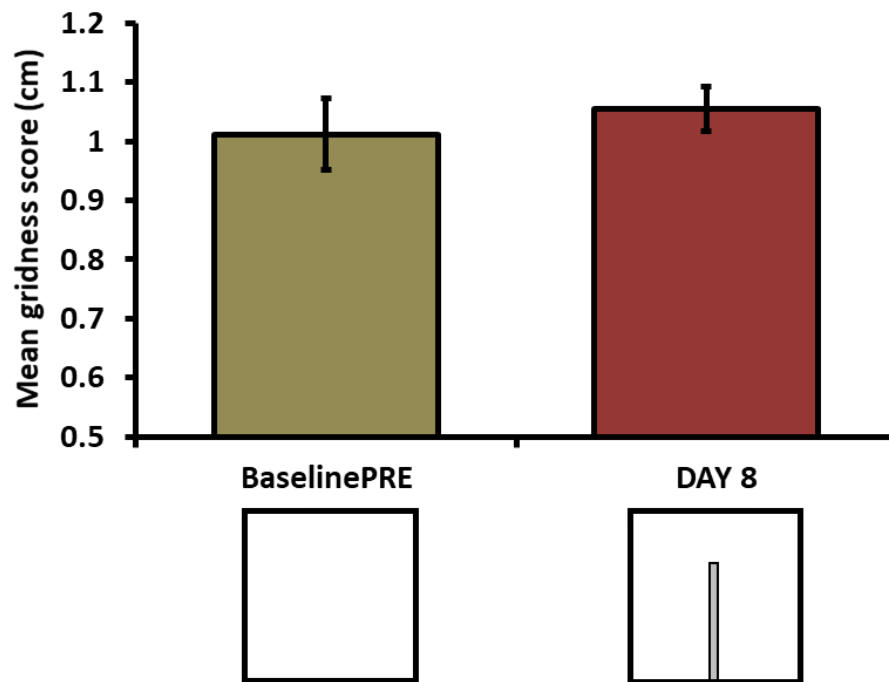


Figure 5.7 Gridness to baseline levels as the barrier becomes more familiar.

This bar graph shows that gridness observed during trials BCDE on BaselinePRE is similar to the gridness observed during trials BCDE (i.e. the barrier-in trials) on the last manipulation day (i.e. day 8).

5.2 Grid scale

A simulation run by Towse et al. (2014) showed that the optimal overall scale for a grid system represents a trade-off between maximizing precision (requiring small scales) and minimizing spatial uncertainty (requiring large scales). In another study by Hardcastle et al. (2015) they observed that grid cells accumulate error relative to the time and distance traveled and that this error is corrected by encountering environmental boundaries. Considering these two findings together, it seems that it might be the case that in environments where the average distance to boundaries is reduced, that there would be less error and less uncertainty about their location and thus grid scale would be smaller.

Here, I tested the specific hypothesis that due to lower uncertainty of spatial localization provided by the inserted barrier, grid scale would be smaller when the barrier was present compared to when it was not present.

5.2.1 As hypothesized, the barrier reduced grid scale

A 2x2 mixed-design ANOVA was used to examine the factors of barrier-state (BARRIER-OUT vs BARRIER-IN) and time-block (EARLY vs LATE) on grid scale. This revealed a significant main effect of barrier-state, $F(1, 88) = 16.38$, $p = 0.0001$, partial $\eta^2 = 0.157$, where grid scale was smaller when the barrier was present (BARRIER-IN: 37.32 ± 0.69 cm) compared to when it was not (BARRIER-OUT: 38.01 ± 0.69 cm) (Figure 5.8), supporting the hypothesis that we derive from our interpretation of the Towse et al. model, (2014).

BARRIER-OUT grid scale vs. BARRIER-IN grid scale: manipulation days 1-8

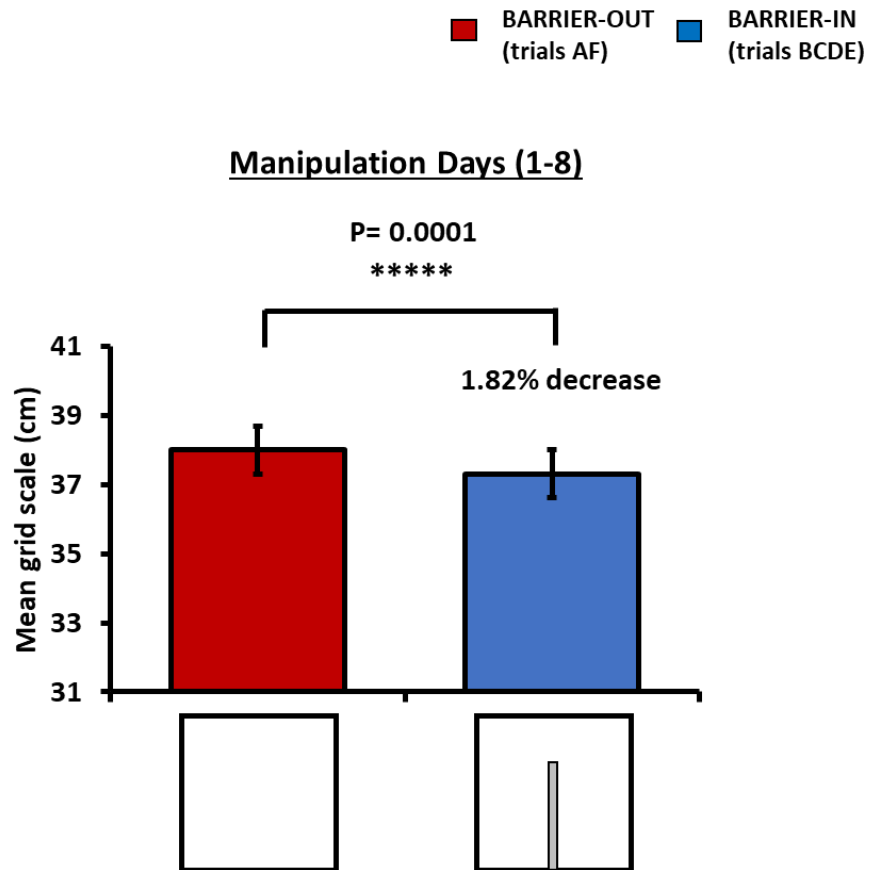


Figure 5.8 Grid scale decreased when the barrier was present.

This bar graph shows that when the barrier was present (i.e. trials BCDE) grid scale was smaller compared to when the barrier was not present (i.e. trials AF), supporting my hypothesis.

5.2.2 The barrier interacted with familiarization to further reduce the grid scale

There was not a significant main effect of time-block on grid scale $F(1, 88) = 1.11, p = 0.29, \text{partial } \eta^2 = (0.012)$. This goes against findings from previous research that have shown that familiarization to an environment causes grid scale to contract (Barry et al, 2007; 2012). However, it should be noted that although the barrier was initially novel in this experiment, the arena was already highly familiar following multiple habituation sessions and Experiment 1. Additionally, there was a significant interaction effect between time-block and barrier-state, $F(1, 88) = 14.55, p = 0.0003$,

partial $\eta^2 = 0.14$ (Figure 5.9; Figure 5.10). During the early time-block (days 1-4), there was not a significant difference in grid scale between barrier states (BARRIER-IN: $M=38.38$, $SEM=0.29$; BARRIER-OUT: $M=38.42$, $SEM=0.32$; $T_{49} = -0.61$, $p = 0.87$) (Figure 5.9A). However, during the late time-block (days 5-8), grid scale was smaller when the barrier was present, (BARRIER-IN: $M=36.24$, $SEM=0.37$), compared to when it was not present (BARRIER-OUT: $M=37.61$, $SEM=0.34$; $T_{39} = -6.04$, $p = 0.0000005$) (Figure 5.9B). This suggests that it is the space-defining properties of the barrier itself, not just familiarity, that is causing a decrease in grid scale, thus providing further support for my main hypothesis for Experiment 2, drawing upon Towse et al. (2014).

BARRIER-OUT grid scale vs. BARRIER-IN grid scale: early and late manipulation days

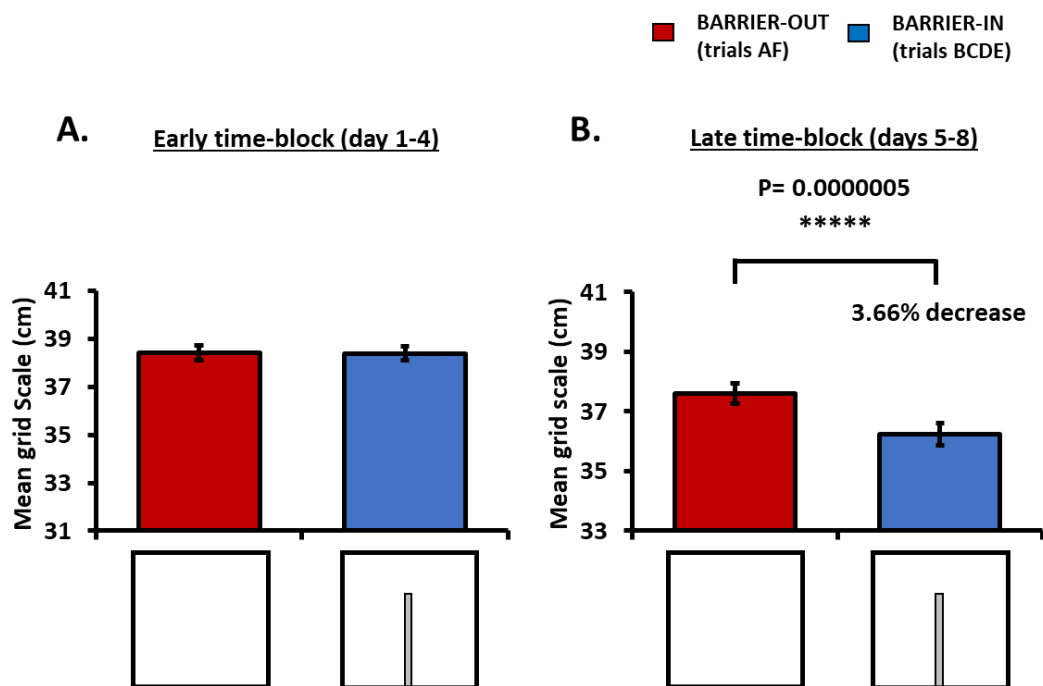


Figure 5.9 The barrier caused a reduction in grid scale during the late time-block, not the early time-block.

Within the late time-block, grid scale was significantly smaller when the barrier was present compared to when it was not present (B). Grid scale between barrier-states was similar during the early time-block (A).

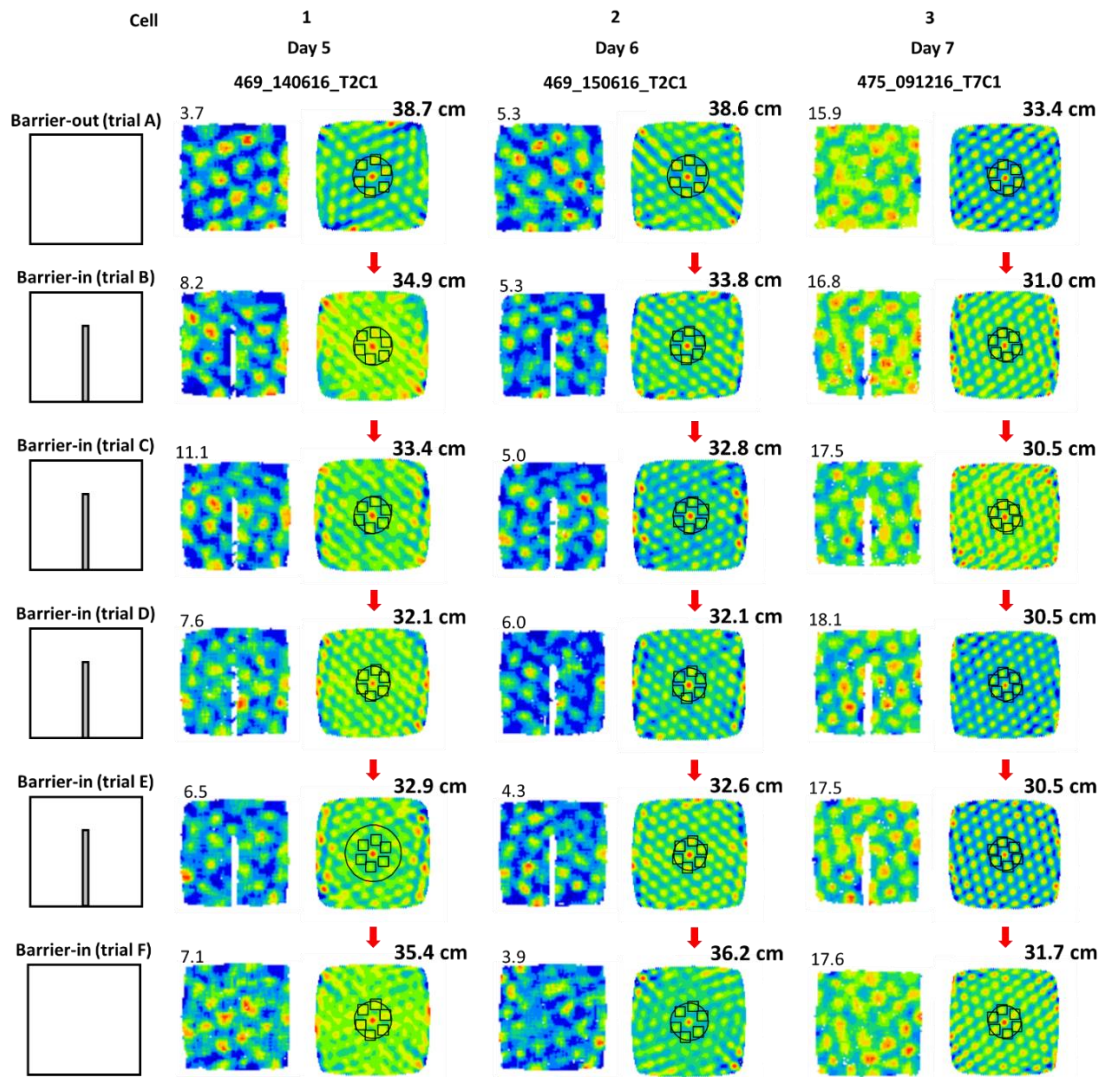


Figure 5.10 Grid scale becomes smaller when the barrier is present.

This figure shows the rate maps (left) and spatial autocorrelations (right) of three different grid cells across all 6 trials of a session from experiment 2. Grid scales (cm) are located at the top right of each autocorrelation, peak rates at the top left of each rate map.

As with *early-block gridness* reductions, this result that barrier-insertion elicited *late-block grid scale* reductions was not an artefact associated with trial order effects, in so much as there were no differences between trials AF and BCDE when the barrier was not present (BaselinePre) (TRIALS AF: 39.31 ± 1.18 cm; TRIALS BCDE: 39.11 ± 1.05 cm; $T_{16} = 0.77$, $p = 0.45$) (Figure 5.11A), (BaselinePOST) (TRIALS AF: 38.06 ± 2.39 cm; TRIALS BCDE: 38.09 ± 2.40 cm; $T_7 = -0.20$, $p = 0.85$) (Figure 5.11B).

TRIALS AF grid scale vs. TRIALS BCDE grid scale: baseline days

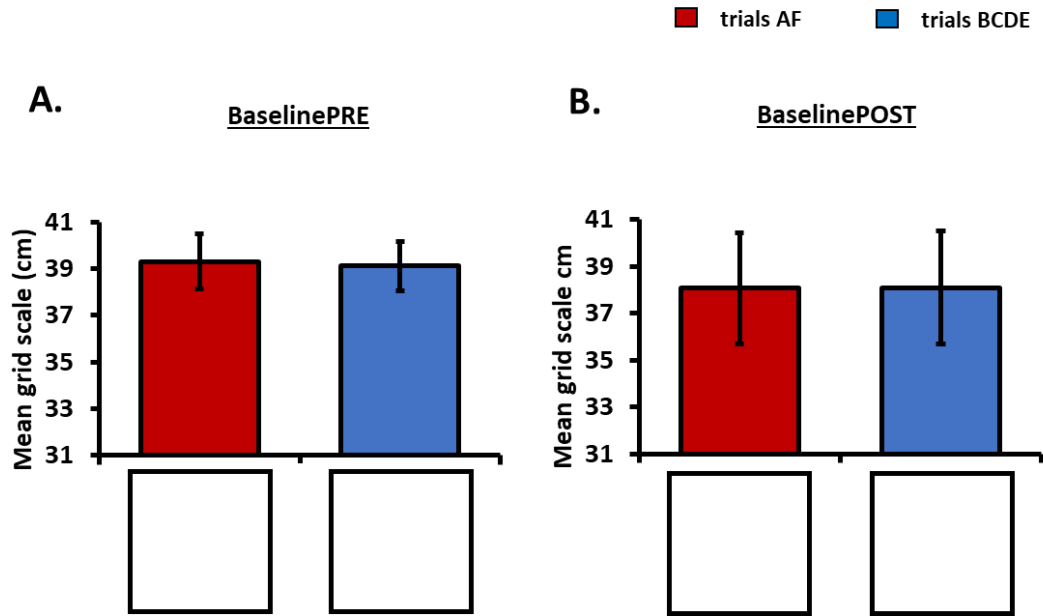


Figure 5.11 Grid scale does not decrease during trials BCDE when the barrier is absent in baseline trials before (A) and after (B) the manipulation period (days 1-8).

This figure shows that there is no significant difference in grid scale between trials AF and trials BCDE on BaselinePRE (A) and BaselinePOST (B) when the barrier is not present in any of the 6 trials.

5.2.3 First exposure to barrier insertion caused grid scale to expand

To see if grid scale *expansion* occurred when the rat *initially* experienced the barrier, I compared grid scale from the BaselinePRE day to grid scale of day 1. As mentioned in chapter 4, there is a possibility that a smaller grid scale could be attributed in some way to the trial sequencing instead of the barrier itself. To avoid interpreting this as an effect of novelty or familiarization, the ratio of grid scale from trials BCDE to grid scale from trials AF was used in the following analysis. Although the sample size is reduced for this comparison, as would be predicted by the results and theory of (Barry et al, 2012; Towse et al 2014), the grid scale did expand during these first exposures to the barrier (ratio of BCDE/AF trials: BaselinePRE: 1.00 ± 0.01 ; DAY 1:

1.03 ± 0.01; $T_{28} = -2.57$, $p = 0.02$) (Figure 5.12). This result offers two insights. First, it extends the Barry et al, 2012 finding by providing confirmatory evidence of grid scale expansion under novelty from a different kind of environmental novelty. Here, I introduced new geometry, while keeping context constant, whereas Barry et al introduced contextual novelty, while keeping environmental geometry constant. Both elicit immediate grid expansion. Second, it shows that the subsequent *reduction* in grid scale observed in the LATE period (Days 5-8) is not somehow a simple function of the physical properties of the environment in the BARRIER-IN configuration, related somehow to a slightly smaller environmental space (albeit the barrier is only 3cm thick).

BaselinePRE grid scale (BCDE/AF ratio) vs DAY 1 grid scale (BCDE/AF ratio)

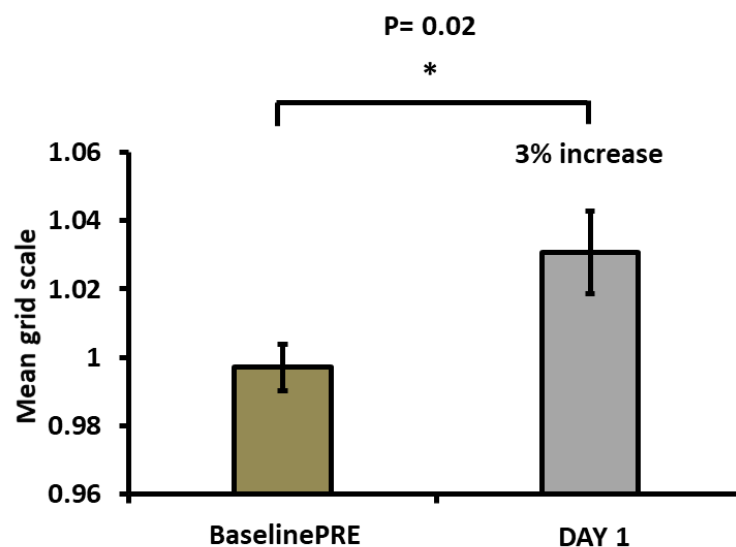


Figure 5.12 Grid scale expands when first introduced to the barrier.

The first day of exposure to the barrier (i.e. day 2) caused the grid scale to expand and become significantly larger than the grid scale seen the day before on the first baseline day (i.e. day 1).

5.2.4 The barrier, not just familiarity/repetition causes a reduction in grid scale

As we have seen, the results showed that there was a clear reduction in grid scale in the LATE period in the BARRIER-IN configuration, relative to the configuration without the barrier (BARRIER-OUT). This effect was statistically strong and was hypothesized. However, it is a reasonable question to ask if the smaller grid scale effect could be attributed specifically to the space-defining properties of the barrier itself. Could the smaller grid scale be attributed not to the barrier per se but in some way to the trial sequencing? The BARRIER-IN configuration occurred in trials BCDE. Thus, there were four trials in a row, and they were flanked by the bookending trials AF (BARRIER-OUT). Could the grid scale reducing causal factor be something associated with being these repeated inner trials? These four trials were conducted successively, there were four of them, and if there is something special about the first trial of the day, then obviously the BCDE sequence no such speciality. (I do of course remind the reader that I always ran a trial before the A sequence precisely to diminish any such novelty.)

In summary by this account, grid scale reduction could have arisen from a factor relating to repetition and/or relative familiarity embedded in the BCDE trial sequence. As it turns out, there are two clear strands of evidence against this trial sequence account.

Firstly, as we have already seen above (figure 5.12), on Day 1, relative to trials AF, grid scale actually increased in the BARRIER-IN condition, in the BCDE trial sequence.

Secondly, the trial sequence account makes a clear prediction about trials BCDE when there is no barrier, directly after the grid scale reduction effect appeared in the

LATE period; that the BCDE trials should have a smaller grid scale even though there is no barrier. This prediction is clearly undermined. As Figure 5.13 shows, relative to the AF trials, the BCDE trials had the same grid scale on the baseline day after day 8 when no barrier was present (BaselinePOST: 1.00 ± 0.01), but a reduced grid scale on day 8 when the barrier was present (DAY 8: 0.96 ± 0.02 ; $T_{16} = -2.28$, $p = 0.04$).

In summary, we can be confident that the grid scale reduction seen in the barrier condition was not due to the fact that the barrier condition occurred in the BCDE trials, but due specifically to the barrier's space-defining properties.

DAY 8 grid scale (BCDE/AF ratio) vs BaselinePOST grid scale (BCDE/AF ratio)

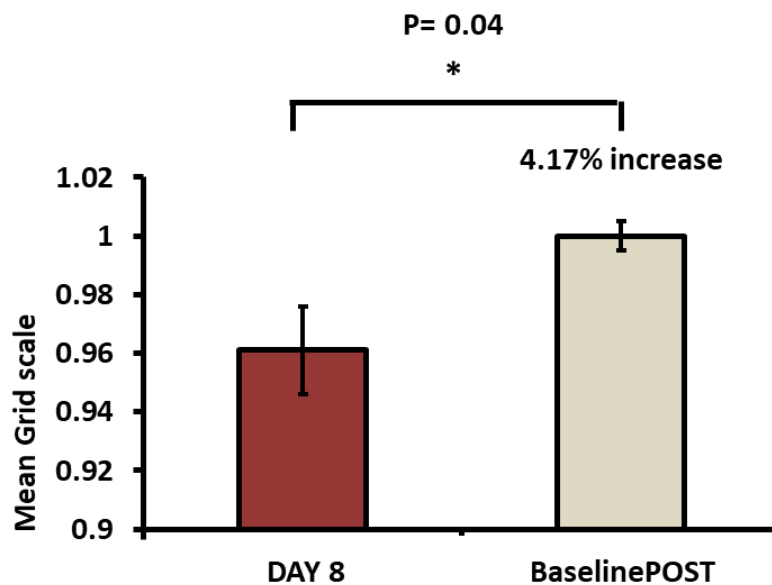


Figure 5.13 The presence of the barrier, not just familiarisation, causes grid scale to decrease.

This bar graph shows that grid scale from the final manipulation day (Day 8) is smaller than the grid scale seen on the baseline day that immediately follows (BaselinePOST). This suggests that the barrier, not just familiarization, is causing the grid scale to decrease.

5.3 Firing rates

5.3.1 Mean Rate

A 2x2 mixed-design ANOVA was used to examine the factors of barrier-state (BARRIER-OUT vs BARRIER-IN) and time-block (EARLY vs LATE) on mean rate.

There was not a significant main effect of barrier-state, $F(1, 88) = 0.114$, $p = 0.737$, $\text{partial } \eta^2 = (.00)$, or time-block, $F(1, 88) = 0.224$, $p = 0.637$, $\text{partial } \eta^2 = (.03)$, on mean rate during manipulation days (days 1-8). Nor was there a significant interaction between barrier-state and time-block $F(1, 88) = 1.209$, $p = 0.275$, $\text{partial } \eta^2 = (.01)$. In other words, neither the presence of the boundary, nor increasing familiarization had an effect on mean firing rates.

Table 5.1 There were no significant main effects of barrier-state or time-block during manipulation days (days 1-8).

			Mean Rate
A) BARRIER-STATE (n= 90)	Mean ± SEM	AF:	4.82 ± 0.38
		BCDE:	4.86 ± 0.40
	P value		0.74
B) TIME-BLOCK (n= 90)	Mean ± SEM	EARLY:	5.05 ± 0.64
		LATE:	4.66 ± 0.35
	P value		0.64

* $p < 0.05$ ** $p < 0.01$ *** $p < 0.005$ **** $p < 0.001$ ***** $p < 0.0005$

Similar results were found when analysing the effects of trial-group and baseline-day on mean rate during baseline days when the barrier was absent during all 6 trials, (TRIAL-GROUP: $F(1, 23) = 1.80$, $p = 0.193$, partial $\eta^2 = (.07)$; BASELINE-DAY: $F(1, 23) = .01$, $p = 0.93$, partial $\eta^2 = (.00)$; INTERACTION: $F(1, 23) = 0.37$, $p = 0.55$, partial $\eta^2 = (.02)$).

5.3.2 Peak Rate

A 2x2 mixed-design ANOVAs was used to examine the factors of barrier-state (BARRIER-OUT vs BARRIER-IN) and time-block (EARLY vs LATE) on peak rate.

There was a significant main effect of barrier-state, $F(1, 88) = 4.81$, $p = 0.03$, partial $\eta^2 = (.05)$, such that peak rate was higher when the barrier was present (BARRIER-IN trials BCDE: 11.00 ± 0.73) compared to when it was absent (BARRIER-OUT trials AF: 10.49 ± 0.68 ; $T_{89} = -2.35$, $p = 0.02$) on manipulation days (days 1-8) (Figure 5.2A).

Table 5.2 Barrier-state, but not time-block, had a significant main effect on peak rate.

			Peak Rate
A) BARRIER-STATE (n= 90)	Mean \pm SEM	AF:	10.46 ± 0.68
		BCDE:	11.00 ± 0.73
	P value		0.03*
B) TIME-BLOCK (n= 90)	Mean \pm SEM	EARLY:	10.64 ± 1.16
		LATE:	10.85 ± 0.68
	P value		0.88

* $p < 0.05$ ** $p < 0.01$ *** $p < 0.005$ **** $p < 0.001$ ***** $p < 0.0005$

There was not a significant main effect of time-block on peak rate, $F(1, 88) = 0.02$, $p = 0.88$, partial $\eta^2 = (.00)$ (Table 5.2B), nor was there a significant interaction between barrier-state and time-block $F(1, 88) = 2.00$, $p = 0.16$, partial $\eta^2 = (.02)$ suggesting that increasing familiarization does not have a significant effect on peak rate.

Similar results were found when analysing the effects of trial-group and baseline-day on peak rate during baseline days, (TRIAL-GROUP: $F(1, 23) = 1.12$, $p = 0.30$, partial $\eta^2 = (.05)$; BASELINE-DAY: $F(1, 23) = .01$, $p = 0.92$, partial $\eta^2 = (.00)$; Interaction: $F(1, 23) = 1.06$, $p = 0.31$, partial $\eta^2 = (.04)$).

5.4 Experiment 2 specific discussion

5.4.1 Summary of Results of Experiment 2

For experiment 2, I hypothesized that due to lower uncertainty of spatial localization provided by the barrier, grid scale would be smaller when the barrier was present compared to when it was not present. On the first baseline day (bPRE), before the barrier was introduced, grid scale was not significantly different between the middle trials (trials BCDE) and the bookending trials (trials A & F). Then, during early exposure to the barrier (Day 1), I observed that grid scale was larger during the BARRIER-IN trials (trials BCDE) when the barrier was present compared to the BARRIER-OUT trials (trials AF) when it was not present. The results then showed that during the early time-block (days 1-4), there were no significant differences in grid scale between the BARRIER-IN trials and the BARRIER-OUT trials. However, during the late time-block (days 5-8) grid scale became significantly smaller when the barrier was present compared to when it was absent. These results support previous findings showing that novelty causes grid scale to expand and that increasing familiarity- in this case, to the barrier- causes it to contract (Barry et al., 2012). It's possible that grid scale became smaller on the later days due to a continued increase in familiarity to the barrier. However, grid scale on the late days was significantly smaller when the barrier was present compared to when it was not present. This suggests that the barrier, not just familiarity, is causing a decrease in grid scale. Additionally, grid scale on the final manipulation day was smaller than grid scale on the baseline day that immediately followed. Not only do these results support my hypothesis, but they show a bidirectional modifiability of grid scale from the same manipulation that is surely due to plastic features of the grid cell representation of space.

As with grid scale, the barrier elicited an experience-dependent effect on gridness: gridness in the Barrier-IN condition was reduced relative to the Barrier-OUT condition during the early manipulation days and then increased back to baseline levels during the late manipulation days. It is unlikely that these results are artefacts associated with trial order effects as there were no differences in grid scale or gridness between trials AF and BCDE on the pre-experiment baseline day when the barrier was not present.

5.4.2 Models of spatial uncertainty and grid scale: grid scale is adaptive

Path integration is the process by which an animal is able to return to a goal site by relying exclusively on self-motion cues, such as vestibular input and proprioception. A long-standing idea in spatial research was that path integration accumulates error and therefore fixed external landmarks, such as boundaries, are needed to correct this. Following the discovery of head-direction cells, which act as an animal's internal compass, and place cells, whose firing fields represent an animal's location within an environment, researchers asserted that the hippocampus proper was a path integration device (McNaughton et al, 1996). The primary evidence for this claim came from the observation that place fields are largely preserved in darkness or when a landmark is removed (O'Keefe and Speakman, 1987; Muller and Kubie, 1987; Muller et al., 1987; McNaughton et al., 1989; Markus et al., 1994). The subsequent discovery of boundary cells, presumably representing the fixed landmarks, and grid cells, presumably performing path integration, lent more precision to this idea. This led researchers to suggest that entorhinal border cells would enable grid cells to correct any accumulated error in path integration (Solstad et al, 2008).

Since the discovery of border cells and grid cells, numerous theoretical and computational studies have proposed that environmental landmarks, such as boundaries, might correct accumulated grid error (Burak & Fiete, 2009; Hasselmo, 2008; Moser et al., 2008; Savelli et al., 2008). One interesting study that supports this proposal showed that error in mouse grid cells was positively correlated with the distance an animal had travelled since its last encounter with a wall-boundary (Hardcastle et al, 2015). The researchers recorded grid cell activity from mice as they made long trajectories across an open arena. The results showed that grid patterns were less precise and less stable when the rats were further away from the wall and that this kind of error increased by the amount of time that the animal spent away from the walls. When the rats reencountered the walls, the grid cells were able to recalibrate. The authors suggested that when the rats were in the interior of the arena, the grid-pattern was being maintained by self-motion cues, which accumulate error over time. When the rats were in contact with the walls the grid pattern was also being stabilised by environmental cues (i.e. boundaries). This suggests that boundaries act as an error correction mechanism. It should be noted that this study did not examine the effect of the animal's instantaneous Euclidean distance to boundaries, but was a study of the effects of path distance since wall contact. Moreover, (Hardcastle et al, 2015) was a purely observational study. They did not manipulate the boundary cues. However, the study strongly suggested the spatial coding enhancing effects of boundaries upon grid cells.

As discussed in Chapter 2, theoretical modeling has also suggested that grid scale is systematically linked to spatial uncertainty and that the temporary expansion of grid scale seen in novel environments may be the optimal response to spatial

uncertainty caused by the unfamiliarity of the new spatial cues (Towse et al., 2014). Towse et al (2014) also demonstrate that the optimal overall scale for a grid system represents a trade-off between minimizing spatial uncertainty (requiring large scales) and maximizing precision (requiring small scales). That is to say that, as spatial uncertainty increases, ambiguity errors are more likely to occur. Increasing the scale of a grid pattern can reduce these errors by: 1) reducing the size of spatial uncertainty relative to the grids; 2) increasing the range of the grid system so that the environment occupies less of the grids overall capacity. However, when there is lower spatial uncertainty within an environment, these errors are much less likely to occur. In this instance, increasing grid scale would only decrease spatial precision, and so smaller grid scales are more suitable.

5.4.3 Previous literature regarding grid scale and uncertainty

To my knowledge, there is relatively little work speaking directly to the relationship between grid scale and uncertainty, and all such work uses environmental novelty to elicit uncertainty. Barry et al. (2007) recorded grid cell activity from rats while they foraged in a rectangular environment with moveable walls. The rats were habituated to one of two configurations (100cm x 100cm or 70cm x 100cm) prior to recording. The first and fifth trials were in the familiar configuration. For trials 2-3, the environment was stretched/shortened along one or both axes. They observed that grid scale changed parametrically with novel changes to the size and shape of the environment and that this rescaling was correlated with environmental experience. That is, the grid scale reduced as the rats became more familiar with the new configurations. Barry et al. (2012) looked at the issue of grid scale and novelty in a much more direct manner. They recorded grid cell activity across five trials. The 1st and

5th trials took place in a familiar square arena. Trials 2-4 took place in novel arenas that were identical in shape and size to the familiar arena, but which differed in either their colour, material, scent or lighting (Barry et al., 2012). Scale expansion persisted across days, but reduced with experience. To some extent, grid scale could be investigated in experiments that have already been conducted. For instance, Wernle et al. (2018) looked at the effect of barrier removal, but to my knowledge reported no results regarding scale.

5.4.4 Grid scale can be bidirectionally modified by the same manipulation

The main purpose of this experiment 2 was to test the model of Towse et al. (2014) using a spatial uncertainty manipulation that was not novelty. The key hypothesis was that a barrier in the environment would reduce spatial uncertainty, and that this would reduce spatial scale. Spatial uncertainty would be reduced by the addition of an extra space-defining cue, (both visual and somatosensory) to guide distance judgements. The barrier increases spatial certainty within the environment by decreasing the average distance at any given time of the rat to boundaries, which correct accumulated path integration error. It is also possible that there is an important uncertainty reduction associated with reducing the symmetry within the environment. That is, when the barrier is not present the arena is an open 1.5m x 1.5m square. In this sort of set up, there is nothing within the arena to distinguish one corner, or wall, from another. However, when the barrier is present, the northern wall remains 1.5m long whereas the southern wall is divided into two 75cm segments. The western and eastern halves of the arena remain mirror images of each other, however the western half has a 1.5m wall to the left and the 1m barrier to the right, and the eastern half has a 1.5m wall to the right and a 1m barrier to the left. Additionally,

beyond the barrier itself being a landmark, 4 other landmarks are added to the environment when the barrier is present: the two large corners where the east and west sides of the barrier meet the southern wall, and the two smaller corners made by the barrier at its the northern end.

In saying the main aim was to test a non-novelty based manipulation, this is of course not to deny the manipulation involves novelty; at least initially, the inserted barrier cue would be presumed to increase uncertainty, because it is not predicted. Thus, it would be reasonable to predict that grid scale is not immediately smaller in the barrier-present condition, and is perhaps initially larger. However, with experience, grid scale is predicted to become smaller in the barrier-present condition compared to the barrier-absent condition.

Interestingly, I found that on the very first day of exposure to the barrier (Day 1, BARRIER-IN configuration), grid scale expanded compared to the BARRIER-OUT configuration. This result, albeit with a relatively small sample of cells (17 cells on BaselinePRE and 12 cells on Day 1) offers two insights.

First, it extends the Barry et al, 2012 finding by providing confirmatory evidence of novelty-elicited grid scale expansion but using a different kind of environmental novelty. Here, I introduced new geometry (barrier insertion), while keeping context constant, whereas Barry et al (2012) introduced contextual novelty, while keeping environmental geometry constant. Both these forms of environmental novelty (geometry and context) elicited immediate grid expansion in line with the Towse et al 2014 theoretical and computational model.

Second, it shows that the subsequent grid scale contraction observed when the barrier was present during the LATE time-block (Days 5-8) is not somehow a simple

function of the physical properties of the environment in the BARRIER-IN configuration. Although it might seem unlikely a causal factor, BARRIER-IN configuration offers a slightly smaller environmental space (albeit the barrier is only 3cm thick). However, as my results show, the same BARRIER-IN configuration elicits both an immediate expansion in grid scale (as observed on Day 1 BARRIER-IN configuration compared to the Baseline day's BARRIER-OUT configuration: across-cells statistics), and then a subsequent reduction in grid scale (as observed in LATE period Days 5- 8; within-cell BARRIER-IN vs BARRIER-OUT configuration statistics). This bidirectional modifiability of grid scale from the same manipulation is thus incompatible with a simple response to physical properties, but rather is surely due to plastic features of the grid cell representation of space.

5.4.5 Gridness returns to baseline levels following an initial novelty induced reduction

Though the key prediction to test in Experiment 2 was that grid scale would reduce as environmental uncertainty reduced, I also looked at gridness. Consistent with previous research, my results show that gridness increases with increasing familiarity to the environment (Barry et al, 2007; 2012; Carpenter et al., 2015). Importantly, unlike in Experiment 1, the manipulation in Experiment 2 manipulated the internal geometry, to some extent creating two compartments. Therefore, a reasonable expectation was, broadly similar to the Carpenter et al. (2015) study, that gridness would initially be reduced in the BARRIER-IN configuration relative to the BARRIER-OUT configuration, as the global coherence of the grid would be reduced in the BARRIER-IN configuration. Thus, overall gridness scores reflect the contributions not only from stable spatial coding but also from the disposition of the nodes across

the whole environment. However, with sufficient experience, the gridness was as high in the BARRIER-IN configuration as in the BARRIER-OUT configuration. A comparison of gridness from the Barrier-IN condition (trials BCDE) on the final manipulation day to gridness from trials BCDE on the pre-experiment baseline day (BaselinePRE) showed that gridness increased back to baseline levels following the reduction in gridness initially elicited by barrier insertion.

5.4.6 Peak rates might be linked to grid plasticity

While mean firing rates were relatively similar across the configurations, the BARRIER-IN configuration elicited a higher Peak rate. This co-occurred with an increase in gridness and a decrease in grid scale. Although other explanations are possible, this could suggest that the changes in peak rates were linked in some way to improved spatial coding across the whole environment.

5.4.7 Conclusion

One of the key ideas of the model in Towse et al. (2014) is that grid scale is adaptive. Expanding grid scale reduces the misalignments arising from unattainable precision when there is greater uncertainty about an environment and contracting grid scale increases precision regarding an animal's location when there is lower uncertainty about the environment. As mentioned above, I observed grid scale expansion when the barrier was novel and a subsequent contraction as the barrier became more familiar, which supports the idea that grid scale is adaptive. However, I also observed that grid scale recorded during the final manipulation day was smaller than the grid scale recorded on the baseline day that immediately followed. This suggests that the barrier itself, not just familiarity, is increasing certainty about the environment, thus causing a greater decrease in grid scale.

6 General discussion

6.1 Results overview

This thesis presents novel research showing that boundaries, not just familiarity, can have enhancing effects on established grid patterns. The aim of Experiment 1 was to investigate how a wall versus a drop-edge might enhance grid cell firing at distal locations. The results showed that the 4th wall increased gridness, not just at locations proximal to the manipulated boundary, but at locations distal to the manipulated boundary (out to 1.5 m). Additionally, the 4th wall, which was initially novel, increased gridness relative to the drop-edge, which was highly familiar. This experiment has also incidentally shed some light on interference between different representations within the same overall environmental context, which is discussed further in section 6.5. Experiment 2, focused on how uncertainty that is not novelty affects grid cell firing. This was accomplished by inserting a boundary into a familiar square arena, partially bisecting the southern 2/3 of the arena. Based on previous research (Hardcastle et al., 2015; Towse et al., 2014) I hypothesized that the barrier would reduce uncertainty of spatial localization within the environment and therefore reduce grid scale. The results supported this hypothesis: The results also demonstrated that the same manipulation can bidirectionally modify grid scale: the presence of the barrier caused grid scale to initially expand, becoming larger than grid scale recorded on the baseline day (no barrier present) occurring immediately before the first manipulation day, then contract, becoming smaller than grid scale recorded on the baseline day (no barrier present) immediately following the last manipulation day.

In the following sections, considerations based on findings from both experiments are discussed.

6.2 Similarities and differences in Experiments 1 & 2; how boundary cues enhance spatiality in the grid signal

Experiment 1 made an arguably subtle change to the materiality of the boundary at one side of the square, without affecting environmental geometry. Experiment 2 affected the internal environmental geometry, without changing the nature of the boundaries (all 50 cm high walls). The main insight that emerges from both of these experiments taken together is that changes to boundary cues have a broadly predictable/orderly enhancing effect upon already-established grid patterns in grid cells. Most simply put, boundariness is an important and positive factor in influencing grid cell firing. Importantly, though there is clearly an interaction with boundariness and familiarity, these experiments were at least partly able to tease apart the two factors of boundariness and familiarity, and show that enhancement effects were not simply driven by familiarity. In Experiment 1, gridness increased with experience being higher in the late block than the early block; a finding resonant with previous research that utilised environmental novelty (Barry et al., 2012). Interestingly, even during early exposure to the 4th wall, which was initially novel, gridness increased relative to the drop-edge condition, which was highly familiar to the rats. This is interesting because previous studies have shown that gridness reduces when an animal is exposed to environmental novelty (Barry et al., 2012). Another interesting finding from the early manipulation days of this experiment was that I did not observe grid scale expansion. This was a little unexpected as previous studies have reported grid scale expansion occurring when an animal is exposed to environmental novelty (Barry et al., 2012). One explanation for the above findings might be that walls provide much more certainty about the environment compared to drop-edges, and this

immediately counteracted the relatively subtle environmental novelty, which was certainly much more subtle than the context changes in Barry et al (2012). The 4th wall might increase certainty by providing a more definitive environmental boundary. That is, the 4th wall acts as a boundary to more sensory and idiothetic means of exploration than the drop-edge.

In Experiment 2, when the barrier was initially inserted into the arena it was novel, and this caused grid scale to expand. However, with experience, grid scale became smaller in the barrier-present condition compared to the barrier-absent condition. These results support previous findings showing that novelty causes grid scale to expand and that increasing familiarity causes it to contract (Barry et al., 2012). It's possible that grid scale in Experiment 2 became smaller in the later manipulation days due to a continued increase in familiarity to the whole arena. However, grid scale on day 8 (the final manipulation day) was smaller than grid scale on BaselinePOST, the baseline day immediately following day 8. This suggests that the barrier itself, not just familiarity, is causing a decrease in grid scale. This bidirectional modifiability of grid scale from the same manipulation clearly argues against a simple interpretation in terms of the physics of the different environment, and is surely best interpreted as genuine plasticity of the grid cell representation of space.

6.3 Relationship with previous work: manipulating spatial uncertainty in Experiments 1 and 2

Using computational modeling, Towse et al. (2014) demonstrated that the temporary expansion of grid scale seen in novel environments may be the optimal response to spatial uncertainty caused by the unfamiliarity of the new spatial cues. To my knowledge, there has been relatively little work speaking directly to the

relationship between grid scale and uncertainty, and all such work uses environmental novelty to elicit uncertainty (Barry et al., 2007; 2012).

In Experiment 2, I explored this relationship between grid scale and uncertainty by using a manipulation that was not novelty itself and that increased certainty of spatial localization within the environment beyond familiarisation. As mentioned above, this was accomplished by inserting a 1m long boundary into a familiar square arena. The findings from this experiment support the theory from Towse et al. (2014) and findings from Barry et al. (2007;2012): grid scale expanded during early experience of the barrier then contracted with increasing familiarity. However, immediately following the final manipulation day (Day 8), the rats completed a baseline day (no barrier present). A comparison of grid scale from these two days revealed that grid scale was smaller on the final manipulation day than on the following baseline day. This suggests that the barrier itself, not just familiarity, reduces environmental uncertainty, which reduces grid scale. These results also support Towse et al. (2014), which also demonstrates that grid scale is systematically linked to spatial uncertainty (i.e. larger scales reduce error when environmental uncertainty is high and smaller scales which increase precision are favoured when environmental uncertainty is low).

In Experiment 1, I did not observe grid scale expansion during early experience of the 4th wall. This was a little surprising under a narrow interpretation of the Towse model, considering that the drop-edge was highly familiar and the 4th wall was novel. As mentioned in section 6.2 one explanation might be that walls provide much more certainty about the environment compared to drop-edges, and this increased certainty immediately counteracted the relatively subtle environmental novelty. This result could also be seen to be potentially in contrast with a previous study which suggested

that novelty causes grid scale to expand (Barry, 2012). One explanation for this contrast might be that, although neither Barry et al. (2012) nor I manipulated environmental geometry, Barry et al. (2012) manipulated context (e.g. different rooms and different arenas of the same shape) whereas I kept context the same and manipulated the type of boundary located at one side of the testing arena. This ensured that any differences in gridness that occurred would be the result of attaching the 4th wall.

6.4 Relationship with previous work: how boundary cues enhance grid spatiality in distal space in Experiment 1

Where most previous research has focused on global or proximal effects of boundary manipulation on grid cells, I was able to show enhancing effects of boundaries on grid patterns distal to the manipulated boundary. This was accomplished by manipulating the type of boundary located at one side of the arena and analysing the grid pattern located in the distal half of the arena where a permanent wall was attached. This subtle manipulation revealed a clear increase in gridness, not only in the proximal space, but in distal space out to 1.5 metres away from the manipulated boundary. To my knowledge, such an effect has not been previously shown. Arguably, then, these results give us an important insight into how changes in boundary cues in one portion of an environment can exert relatively distal as well as proximal effects. They may for instance help to explain the results of Muessig et al (2015). Their study showed that place cells were less accurate, less stable, and less dense away from the boundaries (i.e. in the central portions of the environment) in pre-weanling rats compared older post-weanling and adult rats. Interestingly, the study also found that these characteristics in place cells became

adult-like in a step-like function, which occurred at the time of grid cell emergence. Thus, one plausible view to take from this work is that later-developing grid cells confer a 'gain of function' upon place cells. In other words, a key function of grid cells is to leverage the enhancement of spatial certainty that environmental boundaries provide, and extend this certainty into open space (Poulter et al, 2018).

6.5 Interference

Although understanding interference between different representations within the same overall environmental context was not an explicit research goal of these experiments, the results shed some light on this issue. The within-trial wall-state x arena-half interaction analysis of Experiment 1, kept the trial constant, and then focused upon whether, within a trial, there is an observable difference in gridness between the half of the environment that is often changing ('manipulated half') and the half of the environment that stays constant ('stable half'). This non-significant interaction showed that even when both halves of the arena are equally-walled, gridness is still significantly higher in the stable half. Here, arguably, the main gridness-affecting factor is not from the boundary-material per se, but from the fact that cues are often changing in one side of the environment, and that this is a potentially disruptive influence. Two useful hypotheses regarding cue change can be distinguished. The first hypothesis, termed the 'bistable no-interference' hypothesis, was that there is good memory for the two environmental configurations, each of which can be retrieved as appropriate. In which case, gridness will be similar across the stable and changing halves. The second hypothesis, termed the 'Non-bistable interference' hypothesis, was that the representation of one configuration interferes with the other configuration. In this instance we would predict that gridness is reduced

in the often-changing half ('manipulated half') compared to the stable half. The results favoured the second, 'non-bistable interference' hypothesis. That is to say, even when comparing two equally-walled halves of the environment in trials BCDE, gridness was significantly higher in the stable half than in the manipulated half of the arena. This could suggest some interference between representations of the environment with and without the fourth wall attached.

How this occurs might be explained by the newly discovered vector trace cells. These cells are found in the subiculum (Poulter et al., 2019), which projects heavily to the presubiculum (Amaral & Lavenex, 2007), and has been implicated in navigation, spatial memory, and imagery (Knierim et al., 2014; Bicanski et al., 2018; Poulter et al., 2019). Like boundary vector cells, vector trace cells generate a firing field at a specific distance and direction from an environmental boundary (Lever et al., 2009). However, unlike boundary vector cells, they continue to generate a firing field for hours after that boundary is removed (Poulter et al., 2019). These characteristics could potentially allow them to continue to fire in response to the edge of reachable space or to the lab wall, which are no longer perceivable when the 4th wall is attached. Conflicting input from these trace fields and input from other boundary responsive cells responding to the 4th wall might result in the lower gridness seen in the manipulated half of the environment. That is, they might be blurring where the environmental edge actually lies- at the present 4th wall/drop-edge or at one of the boundaries beyond. This also suggests that persistent lower gridness indicates memory for 1. multiple representations of the environment (wall-off and wall-on) and 2. memory for space beyond what can be perceived at the time.

6.6 Limitations

One limitation of this study is that I was not able to co-record any place cells or boundary cells along with the grid cells. It would have been interesting to see how these other two cell types behaved when presented with environmental uncertainty that was not novelty. For example, would the 4th wall in Experiment 1 and the boundary in Experiment 2 have had enhancing effects on place cells as they did with grid cells? In Experiment 1, would such a subtle manipulation have caused place field properties to alter in the half of the environment distal to the wall-vs-drop edge boundary? Would the boundary cells in Experiment 1 show thicker stripes along the drop-edge boundary (see Lever et al, 2009, Figure 3A, B) compared to the wall boundary, and would these stripes get thinner with experience, with gradually increasing certainty about spatial localisation? These are important questions for future research.

Another limitation is that I did not investigate more fine-scale spatial patches within the environment e.g. the $\frac{1}{8}$ of the environment nearest to the stable wall compared to the $\frac{1}{8}$ nearest to the drop-edge. This may not be possible as there would be few grid fields available for analysing grid scale and gridness. However, there is the possibility of comparing the firing rates of individual firing fields closest to the drop-edge/4th wall to the firing rates of the fields closest to the stable wall. The same could be done with the fields around the barrier in the second experiment. In a 2017 study, Ismakov et al found that individual firing fields have different firing rates to one another. Additionally, the firing rate ratios of the grid fields are maintained within sessions, across sessions, and during rescaling— but not during remapping. This suggests that grid cells encode local positional information. It would be interesting to

see what the firing rates of individual grid fields might look like along the manipulated boundary during the wall-off/wall-on manipulations Experiment 1, and along the lower 2/3 of the bisecting Y-axis during the barrier-in/barrier-out manipulations in Experiment 2. For example, might the firing rates of individual grid fields, or their firing rate ratios, immediately along the manipulated edge be higher or lower than that of the fields immediately along the stable wall? Such an analysis might offer some insight into why gridness continues to be lower in the manipulated half of the environment compared to the stable half of the environment during wall-attached trials. My current analyses of mean rate and peak rate do not offer any clear insights on this matter.

I also did not investigate correlations between behaviour (e.g. running speed and rearing) and grid properties. Multiple studies have demonstrated that changes in behaviour do not necessarily correlate with changes in the grid pattern (Derdikman et al., 2009; Krupic et al., 2015; Barry et al., 2007). For example, when Krupic et al (2015) recorded grid cells from rats in a trapezoid shaped environment, the rats running speed and directional headings differed between the broad end and the narrow end. However, there was no correlation between the extent of behavioural differences and differences in grid properties between the two ends.

One behaviour that would have been worth investigating is rearing— a behaviour that increases in response to novelty and has been hypothesised to be important for gathering spatial information (Lever et al., 2006; Barth et al., 2018). Additionally, when rearing frequency increases due to spatial novelty, the increase is hippocampus-dependent (Krupic et al., 2018; Burgess, 2008, Chen et al., 2016). One study investigating the relationship between rearing and hippocampal activity found that when mice reared within the firing field of a place cell, the cell's firing rate

decreased, while the firing rates of rearing-on cells increased (Barth et al., 2018). The authors suggest that the intra-place field firing reduction temporarily decouples the place cell activity from that of rearing related inputs. This could allow rearing to anchor a new map to external cues and prevent the formation of erroneous associations between a drifting map and incoming perceptual inputs. To my knowledge no one has directly investigated what effects rearing might have on grid cell properties.

In this thesis I treat gridness and grid scale as independent variables. It might be asked if this is justified, and argued that these variables are inversely correlated. In environmental novelty, for instance, gridness is typically reduced, while grid scale expands; in familiarity, gridness increases, while grid scale contracts (Barry et al, 2012). However, it is possible that our view of gridness and grid scale relationships is overly influenced by studies of novelty-familiarity. Chen et al. (2016) recorded grid cells in mice during dark and light trials and found that while gridness was reduced in the dark condition, grid scale improved, so to speak, becoming smaller at the 10s, 20s, and 30s timepoints. In another study by Chen et al (2018), grid cells were first recorded in a virtual environment followed by a real environment. While gridness scores were similar between the two, grid scale was smaller in the real environment compared to the virtual environment. It is possible that gridness and grid scale may be influenced by different allothetic and/or idiothetic information and may serve different, but complementary functions when coding for the spatial environment. Chen et al (2018) suggest that the differences they see between the virtual environment and the real environment are due to: 1. grid scale and theta frequency reflecting translational motion inferred from both virtual (visual and proprioceptive) and real (vestibular translation and extra-maze) cues and 2. firing rates and theta phase precession

reflecting only visual and proprioceptive cues. More research is needed on this matter. In summary, overall, there is no compelling reason to think that gridness and grid scale are intrinsically related, and some good evidence to think these measures lie on orthogonal dimensions.

References

- Allen, G.V., & Hopkins, D.A. (1989). Mamillary body in the rat: topography and synaptology of projections from the subicular complex, prefrontal cortex, and midbrain tegmentum. *Journal of Comparative Neurology*, 286(3), 311–336.
- Alme, C.B., Miao, C., Jezek, K., Treves, A., Moser, E.I., & Moser, M. (2014). Place cells in the hippocampus: Eleven maps for eleven rooms. *Proceedings of the National Academy of Sciences*, 111 (52) 18428-18435.
- Amaral, D.G., Dolorfo, C., & Alvarez-Royo, P. (1991). Organization of CA1 projections to the subiculum: a PHA-L analysis in the rat. *Hippocampus*, 1, 415-436.
- Amaral, D. G. & Lavenex, P. (2007). Hippocampal Neuroanatomy. In: Andersen, P., Morris, R., Amaral, D., Bliss, T., O'Keefe, J. (Eds.), *The Hippocampus Book*. Oxford: Oxford University Press.
- Amaral, D.G. & Witter, M.P. (1995). Hippocampal Formation. In: Paxinos, G (Ed), *The Rat Nervous System*. San Diego: Academic Press.
- Anderson, P., Bliss, T.V.P., & Skrede, K.K. (1971). Lamellar organization of hippocampal excitatory pathways. *Experimental Brain Research*, 13, 222-238.
- Bannerman, D.M., Rawlins, J.N., McHugh, S.B., Deacon, R.M., Yee, B.K., Bast, T., Zhang, W.N., Pothuizen, H.H., & Feldon, J. (2004). Regional dissociations within the hippocampus—memory and anxiety. *Neuroscience & Biobehavior Reviews*, 28 (3), 273–283.
- Barry, C., Ginzberg, L. L., O'Keefe, J., & Burgess, N. (2012). Grid cell firing patterns signal environmental novelty by expansion. *Proceedings of the National Academy of Sciences of the United States of America*, 109, 17687-17692.
- Barry, C., Hayman, R., Burgess, N., & Jeffery, K. J. (2007). Experience-dependent rescaling of entorhinal grids. *Nature Neuroscience*, 10, 682-684.
- Barry, C., Lever, C., Hayman, R., Hartley, T., Burton, S., O'Keefe, J., Jeffery, K., & Burgess, N. (2006). The boundary vector cell model of place cell firing and spatial memory. *Reviews in the Neurosciences*, 17(1-2), 71-97.
- Bender, F., Gorbati, M., Cadavieco, M.C., Denisova, N., Gao, X., Holman, C., Korotkova, T., & Ponomarenko, A. (2015). Theta oscillations regulate the speed of locomotion via a hippocampus to lateral septum pathway. *Nature Communications*, 6, 8521.
- Bicanski, A., Burgess, N. (2018). A neural model of spatial memory and imagery. *eLife*, 7, e33752.
- Bienkowski, M.S., Bowman, I., Song, M.Y., Gou, L., Ard, T., Cotter, K., Zhu, M., Benavidez, N.L., Yamashita, S., Abu-Jaber, J., Azam, S., Lo, D., Foster, N.N.,

- Tiryas, H.H., & Dong, H. (2018). Integration of gene expression and brain-wide connectivity reveals the multiscale organization of mouse hippocampal networks. *Nature Neuroscience*, 21, 1628–1643.
- Bjerknes, T.L., Langston, R.F., Krug, I.U., Moser, E.I., & Moser, M. (2015). Coherence among head direction cells before eye opening in rat pups. *Current Biology*, 25(1), 103-108.
- Bjerknes, T.L., Moser, E.I., & Moser, M. (2014). Representations of geometric borders in the developing rat. *Neuron*, 82(1), 71-78.
- Blair, H.T. & Sharp, P.E. (1996). Visual and vestibular influences on head-direction cells in the anterior thalamus of the rat. *Behavioral Neuroscience*, 110, 643–660.
- Bland, B.H., Oddie, S.D., & Colom, L.V. (1999). Mechanisms of neural synchrony in the septohippocampal pathways underlying hippocampal theta generation. *Journal of Neuroscience*, 19(8), 3223-3237.
- Boccarda, C. N., Sargolini, F., Thoresen, V. H., Solstad, T., Witter, M. P., Moser, E. I. et al. (2010). Grid cells in pre- and parasubiculum. *Nature Neuroscience*, 13, 987-994.
- Bonhoeffer, T. & Grinvald, A. (1991). Orientation columns in cat are organized in pinwheel like patterns. *Nature*, 353, 429–431.
- Bonnevie, T., Dunn, B., Fyhn, M., Hafting, T., Derdikman, D., Kubie, J. L. et al. (2013). Grid cells require excitatory drive from the hippocampus. *Nature Neuroscience*, 16, 309-317.
- Borhegyi, Z., Varga, V., Szilagy, N., Fabo, D., & Freund, T.F., (2004). Phase segregation of medial septal GABAergic neurons during hippocampal theta activity. *Journal of Neuroscience*, 24 (39), 8470–8479.
- Bostock, E., Muller, R.U., & Kubie, J.L. (1991). Experience-dependent modifications of hippocampal place cell firing. *Hippocampus*, 1(2), 193-205.
- Boyce, R., Glasgow, S.D., Williams, S., & Adamantidis, A. (2016). Causal evidence for the role of REM sleep theta rhythm in contextual memory consolidation. *Science*, 352 (6287), 812–816.
- Brandon, M.P., Bogaard, A.R., Libby, C.P., Connerney, M.A., Gupta, K., & Hasselmo, M.E. (2011). Reduction of theta rhythm dissociates grid cell spatial periodicity from directional tuning. *Science*, 332(6029), 595-599.
- Brandon, M.P., Koenig, J., Leutgeb, J.K., & Leutgeb, S. (2014). New and distinct hippocampal place codes are generated in a new environment during septal inactivation. *Neuron*, 82 (4), 789–796.

- Brun, V. H., Solstad, T., Kjelstrup, K. B., Fyhn, M., Witter, M. P., Moser, E. I. et al. (2008). Progressive increase in grid scale from dorsal to ventral medial entorhinal cortex. *Hippocampus*, 18, 1200-1212.
- Burak, Y. & Fiete, I. R. (2009). Accurate path integration in continuous attractor network models of grid cells. *PLOS Computational Biology*, 5, e1000291.
- Burgess, N., Cacucci, F., Lever, C., & O'Keefe, J. (2005). Characterizing multiple independent behavioral correlates of cell firing in freely moving animals. *Hippocampus*, 15, 149-153.
- Burwell, R.D., & Amaral, D.G. (1998a). Perirhinal and postrhinal cortices of the rat: interconnectivity and connections with the entorhinal cortex. *Journal of Comparative Neurology*, 391, 293-321.
- Burwell, R.D., & Amaral, D.G. (1998b). Cortical afferents of the perirhinal, postrhinal, and entorhinal cortices of the rat. *Journal of Comparative Neurology*, 398, 179-205.
- Bush, D., Barry, C., & Burgess, N. (2014). What do grid cells contribute to place cell firing? *Trends in Neuroscience*, 37(3), 136-45.
- Buzsaki, G., Leung, L.W., & Vanderwolf, C.H., (1983). Cellular bases of hippocampal EEG in the behaving rat. *Brain Research*, 287 (2), 139–171.
- Caballero-Bleda, M., & Witter, M.P. (1993). Regional and laminar organization of projections from the presubiculum and parasubiculum to the entorhinal cortex: an anterograde tracing study in the rat. *Journal of Comparative Neurology*, 328, 115-129.
- Canto, C.B., Koganezawa, N., Beed, P., Moser, E.I., & Witter, M.P. (2012) All layers of medial entorhinal cortex receive presubicular and parasubicular inputs. *Journal of Neuroscience*, 32(49), 17620-17631.
- Carpenter, F., Manson, D., Jeffery, K., Burgess, N., & Barry, C. (2015) Grid cells form a global representation of connected environments. *Current Biology*, 25, 1-7.
- Clark, B. J., & Taube, J. S. (2011). Intact landmark control and angular path integration by head direction cells in the anterodorsal thalamus after lesions of the medial entorhinal cortex. *Hippocampus*, 21, 767–782.
- Clark, B. J. & Taube, J. S. (2012). Vestibular and attractor network basis of the head direction cell signal in subcortical circuits. *Front. Neural Circuits*, 6(7).
- Chen, G., Manson, D., Cacucci, F., Wills, T.J. (2016). Absence of visual input results in the disruption of grid cell firing in the mouse. *Current Biology*, 26(17), 2335-2342.

- Chen, G., King, J.A., Lu, Y., Cacucci, F., Burgess, N. (2018). Spatial cell firing during virtual navigation of open arenas by head-restrained mice. *eLife*, 7, e34789.
- Colgin, L. L., Moser, E. I., & Moser, M.-B. (2008). Understanding memory through hippocampal remapping. *Trends in Neurosciences*, 31(9), 469-477.
- Czurkó, A., Hirase, H., Csicsvari, J., & Buzsáki, G. (1999). Sustained activation of hippocampal pyramidal cells by 'space clamping' in a running wheel. *European Journal of Neuroscience*, 11(1), 344-352.
- Dannenberg, H., Pabst, M., Braganza, O., Schoch, S., Niediek, J., Bayraktar, M., Mormann, F., & Beck, H., (2015). Synergy of direct and indirect cholinergic septo-hippocampal pathways coordinates firing in hippocampal networks. *Journal of Neuroscience*, 35, 8394–8410.
- Deller, T. (1998). The anatomical organization of the rat fascia dentate: new aspects of laminar organization as revealed by anterograde tracing with Phaseolus vulgaris-Leucoagglutinin (PHAL). *Anatomy and Embryology*, 197(2), 89-103.
- Doeller, C.F., Barry, C., & Burgess, N. (2010). Evidence for grid cells in a human memory network. *Nature*, 463(7281), 657-661.
- Dombeck, D.A., Harvey, C.D., Tian, L., Looger, L.L., & Tank, D.W. (2010). Functional imaging of hippocampal place cells at cellular resolution during virtual navigation. *Nature Neuroscience*, 13(11), 1433-4140.
- Felleman, D. J. & Van Essen, D. C. (1991). Distributed hierarchical processing in the primate cerebral cortex. *Cerebral Cortex*, 1, 1-47.
- Freund, T. F., Gulyas, A.I., Acsady, L., Gorcs, T., & Toth, K. (1990). Serotonergic control of the hippocampus via local inhibitory interneurons. *Proceedings of the National Academy of Sciences of the United States of America*, 87(21), 8501-8505.
- Fuhs, M. C. & Touretzky, D. S. (2006). A spin glass model of path integration in rat medial entorhinal cortex. *Journal of Neuroscience*, 26, 4266-4276.
- Fyhn, M., Hafting, T., Treves, A., Moser, M. B., & Moser, E. I. (2007). Hippocampal remapping and grid realignment in entorhinal cortex. *Nature*, 446, 190-194.
- Fyhn, M., Hafting, T., Witter, M.P., Moser, E.I., & Moser, M.B. (2008). Grid cells in mice. *Hippocampus*, 18(12), 1230-1238.
- Fyhn, M., Molden, S., Witter, M. P., Moser, E. I., & Moser, M. B. (2004). Spatial representation in the entorhinal cortex. *Science*, 305, 1258-1264.

- Georges-Francois, P., Rolls, E.T., & Robertson, R.G. (1999). Spatial view cells in the primate hippocampus: Allocentric view not head direction or eye position or place. *Cerebral Cortex*, 9(3), 197-212.
- Giocomo, L.M., Stensola, T., Bonnevie, T., Van Cauter, T., Moser, M.B., & Moser, E.I. (2014). Topography of head direction cells in medial entorhinal cortex. *Current Biology*, 24(3), 252-262.
- Goldowitz, D., White, W.F., Steward, O., Lynch, G., & Gotman, C. (1975). Anatomical evidence for a projection from the entorhinal cortex to the contralateral dentate gyrus of the rat. *Experimental Neurology*, 47(3), 433-441.
- Goodridge, J. P., Dudchenko, P. A., Worboys, K. A., Golob, E. J., & Taube, J. S. (1998). Cue control and head direction cells. *Behavioral Neuroscience*, 112(4), 749-761.
- Goodridge, J. P. & Taube, J. S. (1997). Interaction between the postsubiculum and anterior thalamus in the generation of head direction cell activity. *Journal of Neuroscience*, 17, 9315–9330.
- Gorchetchnikov, A. & Grossberg, S. (2007). Space, time and learning in the hippocampus: how fine spatial and temporal scales are expanded into population codes for behavioral control. *Neural Networks*, 20(2), 182-193.
- Goto, M., Swanson, L.W., & Canteras, N.S. (2001). Connections of the nucleus incertus. *Journal of Comparative Neurology*, 438 (1), 86–122.
- Graeff, F.G., Quintero, S., & Gray, J.A. (1980). Median raphe stimulation, hippocampal theta rhythm and threat-induced behavioral inhibition. *Physiology & Behavior*. 25 (2), 253–261.
- Guanella, A., Kiper, D., & Verschure, P. (2007). A model of grid cells based on a twisted torus topology. *International Journal of Neural Systems*, 17(4), 231-240.
- Hafting, T., Fyhn, M., Molden, S., Moser, M. B., & Moser, E. I. (2005). Microstructure of a spatial map in the entorhinal cortex. *Nature*, 436, 801-806.
- Hangya, B., Borhegyi, Z., Szilagyi, N., Freund, T.F., & Varga, V. (2009). GABAergic neurons of the medial septum lead the hippocampal network during theta activity. *Journal of Neuroscience*, 29 (25), 8094–8102.
- Hardcastle, K., Ganguli, S., & Giocomo., L.M. (2015). Environmental boundaries as an error correction mechanism for grid cells. *Neuron*, 86, 827-839.
- Harland, B., Grieves, R.M., Bett, D., Stentiford, R., Wood, E.R., & Dudchenko, P.A. (2017). Lesions of the Head Direction Cell System Increase Hippocampal Place Field Repetition. *Current Biology*, 27(17), 2706-2712.

- Harris, E., Witter, M. P., Weinstein, G., & Stewart, M. (2001). Intrinsic connectivity of the rat subiculum: I. Dendritic morphology and patterns of axonal arborization by pyramidal neurons. *Journal of Comparative Neurology*, 435, 490-505.
- Burgess, N., Jackson, A., Hartley, T., O'Keefe, J. (2000). Predictions derived from modelling the hippocampal role in navigation. *Biological Cybernetics*, 83(3), 301-312.
- Hartley, T., Burgess, N., Lever, C., Cacucci, F., & O'Keefe, J. (2000). Modeling place fields in terms of the cortical inputs to the hippocampus. *Hippocampus*, 10(4), 369-379.
- Hartley, T., Lever, C., Burgess, N., & O'Keefe, J. (2014). Space in the brain: how the hippocampal formation supports spatial cognition. *Philosophical Transactions of the Royal Society B: Biological Sciences*, 369(1635), 1-18.
- Hasselmo, M.E. (2008). Grid cell mechanisms and function: contributions of entorhinal persistent spiking and phase resetting. *Hippocampus*, 18 (12), 1213–1229.
- Hetherington, P. A. & Shapiro, M. L. (1997). Hippocampal place fields are altered by the removal of single visual cues in a distance-dependent manner. *Behavioral Neuroscience*, 111(1), 20-34.
- Hjorth-Simonsen, A., & Zimmer, J. (1975). Crossed pathways from the entorhinal area to the fascia dentate. *Journal of Comparative Neurology*, 161, 57-70.
- Hubel, D. H. & Wiesel, T. (1974). Sequence regularity and geometry of orientation columns in the monkey striate cortex. *Journal of Comparative Neurology*, 158, 267–293.
- Ishizuka, N., Weber, J., & Amaral, D.G. (1990). Organization of intrahippocampal projections originating from CA3 pyramidal cells in the rat. *Journal of Comparative Neurology*, 295(4), 580-623.
- Jackson, J., Amilhon, B., Goutagny, R., Bott, J., Manseau, F., Kortleven, C., Bressler, S.L., & Williams, S. (2014). Reversal of theta rhythm flow through intact hippocampal circuits. *Nature Neuroscience*, 17, 1362-1370.
- Jankowski, M.M. & O'Mara, S.M. (2015). Dynamics of place, boundary, and object encoding in rat anterior claustrum. *Frontiers in behavioural Neuroscience*, 9(250).
- Jankowski, M.M, Ronnqvist, K. C., Tsanov, M., Vann, S. D., Wright, N. F., Erichsen, J. T., et al. (2013). The anterior thalamus provides a subcortical circuit supporting memory and spatial navigation. *Frontiers in systems neuroscience*, 7(45).
- Jeffery, K. J. (2007). Integration of the sensory inputs to place cells: what, where, why, and how? *Hippocampus*, 17, 775-785.

- Jung, M. W., Wiener, S. I., & McNaughton, B. L. (1994). Comparison of spatial firing characteristics of units in dorsal and ventral hippocampus of the rat. *Journal of Neuroscience*, 14, 7347-7356.
- Kaitz, S.S. & Robertson, R.T. (1981). Thalamic connections with limbic cortex. II. Corticothalamic projections. *Journal of Comparative Neurology*, 195, 527-545.
- Killian, N.J., Jutras, M.J., & Buffalo, E.A. (2012). A map of visual space in the primate visual cortex. *Nature*, 491(7426), 761-764.
- Killian, N.J., Jutras, M.J., & Buffalo, E.A. (2015) Saccade direction encoding in the primate entorhinal cortex during visual exploration. *Proceedings of the National Academy of Sciences of the United States of America*, 112(51), 15743-15748.
- Kirk, I.J. & McNaughton, N. (1991). Supramammillary cell firing and hippocampal rhythmical slow activity. *Neuroreport*, 2, 723-725.
- Kjelstrup, K.B, Solstad, T., Brun, V.H, Hafting, T., Leutgeb, S., Witter, M.P., Moser, E.I., & Moser, M.B. (2008). Finite scale of spatial representation in the hippocampus. *Science*, 321(5885), 140-143.
- Knierim, J., Kudrimoti, H.S., & McNaughton, B.L. (1998) Interactions between idiothetic cues and external landmarks in the control of place cells and head direction cells. *Journal of Neuropsychology*, 80(1), 425-446.
- Knierim, J.J., Neunuebel, J.P., & Sachin, S.D. (2014). Functional correlates of the lateral and medial entorhinal cortex: objects, path integration and local-global reference frames. *Philosophical Transactions of the Royal Society B: Biological Sciences*, 369(1635), 20130369.
- Kocsis, B., & Vertes, R.P. (1997). Phase relations of rhythmic neuronal firing in the supramammillary nucleus and mammillary body to the hippocampal theta activity in urethane anesthetized rats. *Hippocampus*, 7 (2), 204-214.
- Koenig, J., Linder, A. N., Leutgeb, J. K., & Leutgeb, S. (2011). The spatial periodicity of grid cells is not sustained during reduced theta oscillations. *Science*, 332, 592-595.
- Kohler, C. (1985). Intrinsic projections of the retrohippocampal region in the rat brain. I. The subicular complex. *Journal of Comparative Neurology*, 236, 504-522.
- Korotkova, T., Ponomarenko, A., Monaghan, C.K., Poulter, S.L., Cacucci, F., Wills, T., Hasselmo, M.E., & Lever, C. (2018). Reconciling the different faces of hippocampal theta: The role of theta oscillations in cognitive, emotional and innate behaviors. *Neuroscience and Biobehavioral Reviews*, 85, 65-80.
- Kropff, E., Carmichael, J.E., Moser, M.B., & Moser, E.I. (2015). Speed cells in the medial entorhinal cortex. *Nature*, 523(7561), 419-424.

- Krupic, J., Bauza, M., Burton, S., Barry, C., & O'Keefe, J. (2015). Grid cell symmetry is shaped by environmental geometry. *Nature*, 518(7538), 232-235.
- Langston, R. F., Ainge, J. A., Couey, J. J., Canto, C. B., Bjerknes, T. L., Witter, M. P. et al. (2010). Development of the spatial representation system in the rat. *Science*, 328, 1576-1580.
- Laurberg, S. (1979). Commissural and intrinsic connections of the rat hippocampus, *Journal of Comparative Neurology*, 184, 685-708.
- Laurberg, S. & Sørensen, K.E. (1981). Associational commissural collaterals of neurons in the hippocampal formation (hilus fasciae dentate and subfield CA3). *Brain Research*, 212(2), 287-300.
- Leutgeb, J. K., Leutgeb, S., Moser, M.-B., & Moser, E. I. (2007). Pattern separation in the dentate gyrus and CA3 of the hippocampus. *Science*, 315(5814), 961-966.
- Leutgeb, S., Leutgeb, J. K., Barnes, C. A., Moser, E. I., McNaughton, B. L., & Moser, M.-B. (2005). Independent codes for spatial and episodic memory in hippocampal neuronal ensembles. *Science*, 309(5734), 619-623.
- Leutgeb, S., Ragozzino, K.E., & Mizumori, S.J. (2000). Convergence of head direction and place information in the CA1 region of hippocampus. *Neuroscience*, 100(1), 11-19.
- Lever, C., Burton, S., Jeewajee, A., O'Keefe, J., & Burgess, N. (2009). Boundary vector cells in the subiculum of the hippocampal formation. *Journal of Neuroscience*, 29, 9771-9777.
- Lever, C., Cacucci, F., Burgess, N., & O'Keefe, J. (1999). Squaring the circle: place cell firing patterns in environments which differ only geometrically are not unpredictable. *Society for Neuroscience Abstract*, 25, 1380.
- Lever, C., Caccuci, F., Wills, T., Burton, S., McClelland, A., Burgess, N., & O'Keefe, J. (2003). Spatial coding in the hippocampal formation: input, information type, plasticity and behaviour. In: K.J. Jeffery (Ed), *The Neurobiology of Spatial Behaviour*. Oxford: Oxford University Press.
- Ma, S. & Gundlach, A.L. (2015). Ascending control of arousal and motivation: role of nucleus incertus and its peptide neuromodulators in behavioural responses to stress. *Journal of Neuroendocrinology* 27, 457-467.
- Mamad, O., McNamara, H.M., Reilly, R.B., & Tsanov, M. (2015). Medial septum regulates the hippocampal spatial representation. *Frontiers in Behavioral Neuroscience*, 9, 166.

- Marcelin, B., Liu, Z., Chen, Y., Lewis, A. S., Becker, A., McClelland, S. et al. (2012). Dorsoventral differences in intrinsic properties in developing CA1 pyramidal cells. *Journal of Neuroscience*, 32, 3736-3747.
- Markus, E.J., Barnes, C.A., McNaughton, B.L., Gladden, V.L, & Skaggs, W.E. (1994). Spatial information content and reliability of hippocampal CA1 neurons: effects of visual input. *Hippocampus*, 4(4), 410-421.
- Maru, E., Takahashi, L.K., & Iwahara, S. (1979). Effects of median raphe nucleus lesions on hippocampal EEG in the freely moving rat. *Brain Research*, 163 (2), 223–234.
- Maurer, A. P., Vanrhoads, S. R., Sutherland, G. R., Lipa, P., & McNaughton, B. L. (2005). Self-motion and the origin of differential spatial scaling along the septo-temporal axis of the hippocampus. *Hippocampus*, 15, 841-852.
- McKenna, J.T. & Vertes, R.P. (2001). Collateral projections from the median raphe nucleus to the medial septum and hippocampus. *Brain Research Bulletin*, 54(6), 619-630.
- McNaughton, B. L., Barnes, C.A., & O'Keefe, J. (1983). The contributions of position, direction, and velocity to single unit activity in the hippocampus of freely-moving rats. *Experimental Brain Research*, 52(1), 41-49.
- McNaughton, B. L., Barnes, C. A., Gerrard, J. L., Gothard, K., Jung, M. W., Knierim, J. J. et al. (1996). Deciphering the hippocampal polyglot: the hippocampus as a path integration system. *Journal of Experimental Biology*, 199, 173-185.
- McNaughton, B. L., Battaglia, F. P., Jensen, O., Moser, E. I., & Moser, M. B. (2006a). Path integration and the neural basis of the 'cognitive map'. *Nature Reviews Neuroscience*, 7, 663-678.
- McNaughton, B.L., Leonard, B., & Chen, L. (1989). Cortical-hippocampal interactions and cognitive mapping: A hypothesis based on reintegration of the parietal and inferotemporal pathways for visual processing. *Psychobiology*, 17(3), 230-235.
- McNaughton, N., Ruan, M., & Woodnorth, M-A. (2006b). Restoring theta-like rhythmicity in rats restores initial learning in the morris water maze. *Hippocampus*, 16(12), 1102-1110.
- Miao, C., Cao, Q., Ito, H., Yamahachi, H., Witter., M.P, Moser, M., & Moser, E.I. (2015). Hippocampal remapping after partial inactivation of the medial entorhinal cortex. *Neuron*, 88(3), 590-603.
- Mizuseki, K., Diba, K., Pastalkova, E., & Buzsaki, G. (2011). Hippocampal CA1 pyramidal cells form functionally distinct sublayers. *Nature Neuroscience*, 14(9), 1174-1181.

- Moser, E.I., & Moser, M.B., (2008). A metric for space. *Hippocampus*, 18 (12), 1142–1156.
- Muessig, L., Hauser, J., Wills, T.J., & Cacucci, F. (2015). A developmental switch in place cell accuracy coincides with grid cell maturation. *Neuron*, 86, 1167–1173.
- Muller, R. (1996). A quarter of a century of place cells. *Neuron*, 17, 979-990.
- Muller, R.U., Bostock, E., Taube, J.S., & Kubie, J.L. (1994). On the directional firing properties of hippocampal place cells. *Journal of Neuroscience*, 14, 7235–7251.
- Muller, R. U., & Kubie, J. L. (1987). The effects of changes in the environment on the spatial firing of hippocampal complex-spike cells. *Journal of Neuroscience*, 7(7), 1951-1968.
- Muller, R. U. & Kubie, J. L. (1987). The effects of changes in the environment on the spatial firing of hippocampal complex-spike cells. *Journal of Neuroscience*. 7, 1951–1968.
- Ohki, K., Chung, S., Ch'ng, Y. H., Kara, P. & Reid, R. C. (2005) *Functional imaging with cellular resolution reveals precise micro-architecture in visual cortex*. *Nature*, 433, 597–603.
- Ohki, K., Chung, S., Hubener, M., Bonhoeffer, T., & Reid, R.C. (2006). *Highly ordered arrangement of single neurons in orientation pinwheels*. *Nature*, 442, 925–928.
- O'Keefe, J. (2007). Hippocampal neurophysiology in the behaving animal. In P. Andersen, Morris, R., Amaral, D., Bliss, T., O'Keefe, J. (Ed.), *The Hippocampus Book*. Oxford: Oxford University Press.
- O'Keefe, J. & Burgess, N. (1996). Geometric determinants of the place fields of hippocampal neurons. *Nature*, 381, 425-428.
- O'Keefe, J., Burgess, N., Donnett, J. G., Jeffery, K. J., & Maguire, E. A. (1998). Place cells, navigational accuracy, and the human hippocampus. *Philosophical Transactions of the Royal Society B: Biological Sciences*, 353(1373), 1333-1340.
- O'Keefe, J. & Dostrovsky, J. (1971). The hippocampus as a spatial map. Preliminary evidence from unit activity in the freely-moving rat. *Brain Research*, 34, 171-175.
- O'Keefe, J. & Speakman, A. (1987). Single unit activity in the rat hippocampus during a spatial memory task. *Experimental Brain Research*, 68(1), 1-27.
- O'Mara, S. (2005). The subiculum: what it does, what it might do, and what neuroanatomy has yet to tell us. *Journal of Anatomy*, 207(3), 271-282.

- O'Mara, S. M., Sanchez-Vives, M. V., Brotons-Mas, J. R., & O'Hare, E. (2009). Roles for the subiculum in spatial information processing, memory, motivation and the temporal control of behaviour. *Progress in Neuro-Psychopharmacology and Biological Psychiatry*, 33(5), 782-790.
- Ormond, J. & McNaughton, B.L. (2015). Place field expansion after focal MEC inactivations is consistent with loss of fourier components and path integrator gain reduction. *PNAS*, 112, 4116-4121.
- Pastoll, H., Solanka, L., van Rossum, M.C.W., & Nolan, M.F. (2013). Feedback inhibition enables theta-nested gamma oscillations and grid firing fields. *Neuron*, 77, 141-154.
- Paz-Villagran, V., Save, E., & Poucet, B. (2004). Independent coding of connected environments by place cells. *European Journal of Neuroscience*, 20, 1379-1390.
- Peng, Y., Barreda Tomas, F.J., Klisch, C., Vida, I., & Geiger, J.R.P. (2017). Layer specific organization of local excitatory and inhibitory synaptic connectivity in the rat presubiculum. *Cerebral Cortex*, 27, 2435-2452.
- Pikkarainen, M., Ronkko, S., Savander, V., Insausti, R., & Pitkanen, A. (1999). Projections from the lateral, basal, and accessory basal nuclei of the amygdala to the hippocampal formation of the rat. *Journal of Comparative Neurology* 403, 229-260.
- Pitkanen, A., Pikkarainen, M., Nurminen, N., & Ylinen, A. (2000). Reciprocal connections between the amygdala and hippocampal formation, perirhinal cortex and postrhinal cortex in the rat. *Annals of the New York Academy of Sciences*, New York, NY, US: New York Academy of Sciences, 911, 369-391.
- Poulter, S., Hartley, T., & Lever, C. (2018). The neurobiology of mammalian navigation. *Current Biology*, 28(17), 1023-1042.
- Preston-Ferrer, P., Coletta, S., Frey, M., & Burgalossi, A. (2016). Anatomical organization of presubicular head-direction circuits. *Elife*, 5 pii: e14592.
- Raudies, F., Brandon, M.P., Chapman, G.W., & Hasselmo, M.E. (2015). Head direction is coded more strongly than movement direction in a population of entorhinal neurons. *Brain Research*, 1621, 355-367.
- Rawlins, J.N., Feldon, J., & Gray, J.A. (1979). Septo-hippocampal connections and the hippocampal theta rhythm. *Exp. Brain Research*, 37 (1), 49-63.
- Rivard, B., Li, Y., Lenck-Santini, P. P., Poucet, B., & Muller, R. U. (2004). Representation of objects in space by two classes of hippocampal pyramidal cells. *Journal of General Physiology*, 124, 9-25.

- Robertson, R.T., & Kaitz, S.S. (1981). Thalamic connections with limbic cortex. I. Thalamocortical projections. *Journal of Comparative Neurology*, 195, 501-525.
- Sargolini, F., Fyhn, M., Hafting, T., McNaughton, B. L., Witter, M. P., Moser, M. B. et al. (2006). Conjunctive representation of position, direction, and velocity in entorhinal cortex. *Science*, 312, 758762.
- Savelli, F., Luck, J.D., & Knierim, J.J. (2017). Framing of grid cells within and beyond navigation boundaries. *eLife*, 6, (493).
- Savelli, F. & Knierim, J.J. (2019). Origin and role of path integration in the cognitive representations of the hippocampus: computational insights into open questions. *Journal of Experimental Biology*, 222.
- Savelli, F., Yoganarasimha, D., & Knierim, J. J. (2008). Influence of boundary removal on the spatial representations of the medial entorhinal cortex. *Hippocampus*, 18, 1270-1282.
- Scharfman, H. E., Witter, M. P., & Schwarcz, R. (2000). The parahippocampal region: Implications for neurological and psychiatric diseases. *Annals of the New York Academy of Sciences*, 911, ix-xiii, New York, NY, US: New York Academy of Sciences.
- Shapiro, M. L., Tanila, H., & Eichenbaum, H. (1997). Cues that hippocampal place cells encode: Dynamic and hierarchical representation of local and distal stimuli. *Hippocampus*, 7(6), 624-642.
- Shiple, M.T. (1975). The topographical and laminar organization of the presubiculum's projection to the ipsi- and contralateral entorhinal cortex of the guinea pig. *Journal of Comparative Neurology*, 160, 127-146.
- Solstad, T., Boccara, C. N., Kropff, E., Moser, M. B., & Moser, E. I. (2008). Representation of geometric borders in the entorhinal cortex. *Science*, 322, 1865-1868.
- Solstad, T., Moser, E.I., & Einevoll, G.T. (2006). From grid cells to place cells: a mathematical model. *Hippocampus*, 16, 1026-1031.
- Spiers, H.J., Hayman, R.M.A, Jovalekic, A., Marozzi, E., & Jeffery, K.J. (2015). Place field repetition and purely local remapping in a multicompartiment environment. *Cerebral Cortex*, 25(1), 10-25.
- Stackman, R.W., Golob, E.J., Bassett, J.P., & Taube, J.S. (2003). Passive transport disrupts directional path integration by rat head direction cells. *Journal of Neurophysiology*, 90(5), 2862-2874.
- Stemmler, M., Mathis, A., & Herz, A.V.M. (2015). Connecting multiple spatial scales to decode the population activity of grid cells. *Neuroscience*, 1(11), e1500816.

- Stensola, H., Stensola, T., Solstad, T., Froland, K., Moser, M. B., & Moser, E. I. (2012). The entorhinal grid map is discretized. *Nature*, 492, 72-78.
- Stensola, T., Stensola, H., Moser, M., & Moser, E.I. (2015). Shearing induced asymmetry in entorhinal grid cells. *Nature*, 518, 207-212.
- Stewart, S., Jeewajee, A., Wills, T.J., Burgess, N., & Lever, C. (2014). Boundary coding in the rat subiculum. *Philosophical Transactions of the Royal Society B: Biological Sciences*, 369(1635), 20120514.
- Strange, B.A., Witter, M.P., Lein, E.S., & Moser, E.I. (2014). Functional organization of the hippocampal longitudinal axis. *Nature Reviews Neuroscience*, 15(10), 655-69.
- Sun, Y., Nguyen, A.Q., Nguyen, J.P., Le, L., Saur, D., Choi, J., Callaway, E.M., & Xu, X. (2014). Cell-type-specific circuit connectivity of hippocampal CA1 revealed through Cre-dependent rabies tracing. *Cell Report*, 7, 269-280.
- Sun, Y., Nitz, D.A., Holmes, T.C., & Xu, X. (2018). Opposing and complementary topographic connectivity gradients revealed by quantitative analysis of canonical and non-canonical hippocampal CA1 inputs. *eNeuro* 5, e0322-17, 1-19.
- Tan, H.M., Bassett, J.P., & O'Keefe, J. (2015). The development of the head direction system before eye opening in the rat pup. *Current Biology*, 25, 479-483.
- Tang, Q., Burgalossi, A., Ebbesen, C.L., Ray, S., Naumann, R., Schmidt, H., Spicher, D., & Brecht, M. (2014). Pyramidal and stellate cell specificity of grid and border representations in layer 2 of medial entorhinal cortex. *Neuron*, 84, 1191-1197.
- Taube, J.S. (1998). Head direction cells and the neurophysiological basis for a sense of direction. *Progress in Neurobiology*, 55, 225-256.
- Taube, J. S. (2007). The head direction signal: origins and sensory-motor integration. *Annual Review of Neuroscience*, 30, 181-207.
- Taube, J. S. & Bassett, J. P. (2003). Persistent neural activity in head direction cells. *Cerebral Cortex*, 13, 1162-1172.
- Taube, J. S. & Muller, R. U. (1998). Comparisons of head direction cell activity in the postsubiculum and anterior thalamus of freely moving rats. *Hippocampus*, 8, 87-108.
- Taube, J.S., Muller, R.U., & Ranck, J.B. Jr. (1990a). Head-direction cells recorded from the postsubiculum in freely moving rats. I. Description and quantitative analysis. *Journal of Neuroscience* 10(2), 420-435.

- Taube J.S., Muller, R.U., & Ranck, J.B. Jr. (1990b). Head-direction cells recorded from the postsubiculum in freely moving rats. II. Effects of environmental manipulations. *Journal of Neuroscience*, 10(2), 436-447.
- Thompson, S.M., & Robertson, R.T. (1987). Organization of subcortical pathways for sensory projections to the limbic cortex. I. Subcortical projections to the medial limbic cortex in the rat. *Journal of Comparative Neurology*, 265, 175-188.
- Tocker, G., Barak, O., & Derdikman, D. (2015). Grid cells correlation structure suggests organized feedforward projections into superficial layers of the medial entorhinal cortex. *Hippocampus*, 25(12), 1599-1613.
- Towse, B.W., Barry, C., Bush, D., & Burgess, N. (2014). Optimal configurations of spatial scale for grid cell firing under noise and uncertainty. *Philosophical Transactions of the Royal Society B: Biological Sciences*, 369(1635), 20130290.
- Tsanov, M., Chah, E., Vann, S. D., Reilly, R. B., Erichsen, J. T., Aggleton, J. P., et al. (2011a). Theta-modulated head direction cells in the rat anterior thalamus. *Journal of Neuroscience*. 31, 9489–9502.
- van Groen. T. & Wyss, J. M. (1990). The connections of presubiculum and parasubiculum in the rat. *Brain Research*, 518, 227-243.
- van Groen, T. & Wyss, J.M. (1992). Connection of the retrosplenial dysgranular cortex in the rat. *Journal of Comparative Neurology*, 315, 200-216.
- van Strien, N.M., Cappaert, N.L., & Witter, M.P. (2009) The anatomy of memory: and interactive overview of the parahippocampal-hippocampal network. *Nature Reviews Neuroscience*, 10(4), 272-282.
- Vandecasteele, M., Varga, V., Berenyi, A., Papp, E., Bartho, P., Venance, L., Freund, T.F., & Buzsaki, G., (2014). Optogenetic activation of septal cholinergic neurons suppresses sharp wave ripples and enhances theta oscillations in the hippocampus. *Proceedings of the National Academy of Sciences of the United States of America*. 111 (37), 13535–13540.
- Verwer, R. W., Meijer, R. J., Van Uum, H. F., & Witter, M. P. (1997). Collateral projections from the rat hippocampal formation to the lateral and medial prefrontal cortex. *Hippocampus*, 7, 397-402.
- Wang, Y., Romani, S., Lustig, B., Leonardo, A., & Pastalkova, E. (2015). Theta sequences are essential for internally generated hippocampal firing fields. *Nature Neuroscience*, 18, 282-288.
- Wernle, T., Waaga, T., Morreaunet, M., Treves, A., Moser, M., & Moser, E.I. (2018). Integration of grid maps in merged environments. *Nature neuroscience*, 21, 92-101.

- Wiebe, S. P., Staubli, U. V., & Ambros-Ingerson, J. (1997). Short-term reverberant memory model of hippocampal field CA3. *Hippocampus*, 7, 656-665.
- Wills, T., Cacucci, F., Burgess, N., & O'Keefe, J. (2010). Development of the hippocampal cognitive map in the pre-weaning rats. *Science*, 328(5985), 1573-1576.
- Wills, T.J. Attractor dynamics in the hippocampal representation of the local environment. PhD thesis, 2005, University College London.
- Wills, T. J., Lever, C., Cacucci, F., Burgess, N., & O'Keefe, J. (2005). Attractor dynamics in the hippocampal representation of the local environment. *Science*, 308(5723), 873-876.
- Wilming, N., Konig, P., Konig, S., & Buffalo, E.A. (2018). Entorhinal cortex receptive fields are modulated by spatial attention, even without movement. *eLife*, 7, e31745.
- Wilson, M.A. & McNaughton, B.L. (1993). Dynamics of the hippocampal ensemble code for space. *Science*, 261(5124), 105-1058.
- Winter, S.S., Clark, B.J., & Taube, S.T. (2015). Disruption of the head direction cell network impairs the parahippocampal grid cell signal. *Science*, 347(6224), 870-874.
- Witter, M. (1993). Organization of the entorhinal-hippocampal system: a review of current anatomical data. *Hippocampus*, 3, 33-44.
- Witter, M.P. (2006). Connections of the subiculum of the rat: topography in relation to columnar and laminar organization. *Behavioural Brain Research*, 174(2), 251-264.
- Witter, M. P. & Moser, E. I. (2006). Spatial representation and the architecture of the entorhinal cortex. *Trends in Neuroscience*, 29, 671-678.
- Witter, M. P., Naber, P. A., van, H. T., Machielsen, W. C., Rombouts, S. A., Barkhof, F. et al. (2000). Cortico-hippocampal communication by way of parallel parahippocampal-subicular pathways. *Hippocampus*, 10, 398-410.
- Wouterlood, F. G., Saldana, E., & Witter, M. P. (1990). Projection from the nucleus reuniens thalami to the hippocampal region: light and electron microscopic tracing study in the rat with the anterograde tracer Phaseolus vulgaris-leucoagglutinin. *Journal of Comparative Neurology*, 296, 179-203.
- Wulff, P., Ponomarenko, A.A., Bartos, M., Korotkova, T.M., Fuchs, E.C., Bahner, F., Both, M., Tort, A.B., Kopell, N.J., Wisden, W., et al. (2009). Hippocampal theta rhythm and its coupling with gamma oscillations require fast inhibition onto

parvalbumin positive interneurons. *Proceedings of the National Academy of Sciences of the United States of America*. 106 (9), 3561–3566.

Wyss, J. M. & van Groen, T. (1992). Connections between the retrosplenial cortex and the hippocampal formation in the rat: a review. *Hippocampus*, 2, 1-11.

Yartsev, M. M., Witter, M. P., & Ulanovsky, N. (2011). Grid cells without theta oscillations in the entorhinal cortex of bats. *Nature*, 479, 103-107.

Zhang, S.J, Ye, J., Couey, J.J., Witter, M.P., Moser, E.I., & Moser, M. (2014). Functional connectivity of the entorhinal-hippocampal space circuit. *Philosophical Transactions of the Royal Society B: Biological Sciences*, 369, 20120516.

Zugaro, M. B., Arleo, A., Berthoz, A., & Wiener, S. I. (2003). Rapid spatial reorientation and head direction cells. *Journal of Neuroscience*, 23, 3478-3482.

Zugaro, M.B., Berthoz, A., & Wiener, S.I. (2001). Background, but not foreground, spatial cues are taken as references for head direction responses by rat anterodorsal thalamus neurons. *Journal of Neuroscience* 21, RC154.